Report Title: **"Final Technical Report for the Airborne, Optical Remote Sensing of Methane and Ethane for Natural Gas Pipeline Leak Detection"**

Type of Report: Final Technical

Reporting Period Start Date: October 14, 2003

Reporting Period End Date: March 31, 2005

Principal Author: Mr. Jerry Myers

Date Report Was Issued: April 15, 2005

DOE Award Number: DE-FC26-02NT41632

Name and Address of Submitting Organization:

Ophir Corporation

10184 W. Belleview Ave., Suite 200

Littleton, CO 80127

Disclaimer

Abstract

Ophir Corporation was awarded a contract by the U. S. Department of Energy, National Energy Technology Laboratory under the Project Title "Airborne, Optical Remote Sensing of Methane and Ethane for Natural Gas Pipeline Leak Detection" on October 14, 2002. The scope of the work involved designing and developing an airborne, optical remote sensor capable of sensing methane and, if possible, ethane for the detection of natural gas pipeline leaks.   Flight testing using a custom dual wavelength, high power fiber amplifier was initiated in February 2005. Ophir successfully demonstrated the airborne system, showing that it was capable of discerning small amounts of methane from a simulated pipeline leak. Leak rates as low as 150 standard cubic feet per hour (scf/h) were detected by the airborne sensor.

Table of Contents

List of Figures

List of Tables

1   Executive Summary

This final technical report provides a summary of the work accomplished throughout the co-funded airborne, optical remote sensor design and development project. The goal of this project was to demonstrate the feasibility of detecting natural gas pipeline leaks from an airborne platform, primarily through the sensing of methane gas, which is the primary constituent of natural gas. Ophir also believes that the sensing of ethane, a secondary constituent of natural gas, is important in order to discriminate natural gas from other sources of naturally occurring methane.

Ophir spent considerable time researching the absorption characteristics of methane and ethane through the review of existing data bases and through laboratory gas analysis. The overtone absorption band between 1600-1700 nm was chosen due to the availability of low noise non-cooled optical detectors, the increased likelihood of partnering with a high power, light source vendor, and the commercial availability of mid-infrared (IR) optics within the telecommunications L-Band.

The design and development of the high-power, light source proved to be the most challenging part of the overall airborne system design. The light source design had to incorporate three important concepts: first, it had to be able to output light at two different wavelengths in order to sense both methane and ethane; second, it needed to have a power output of approximately 1 watt (W); and lastly, the output spectral shape needed to be broadened from the normal laser diode linewidth to be useful in active gas correlation spectroscopy. The development effort for the light source was long and protracted; it incorporated a five-month delay due to vendor problems and some minor design specification changes. The light source, based upon an optical parametric amplifier fiber design, was finally incorporated into the airborne transceiver in December 2004.

Prior to receiving the dual output amplifier, Ophir conducted numerous laboratory and outdoor reflectance tests using an existing 1-W, 1555 nm Raman fiber amplifier. The airborne transceiver was tested out thoroughly as to the collection efficiency with different targets and the collimating properties of the light source transmitter optics. Much was learned about the effects of various surfaces at 150 m (500 ft) optical pathlength and target-to-receiver angular changes on signal return. The signal-to-noise of the system using the substitute light source was also verified against the predicted models.

The final system was mounted onto an airplane in February 2005, and numerous flight tests were performed over a controlled methane gas leak. The system demonstrated that it was capable of detecting a methane leak of 150 scf/h from an airplane altitude of 150 m and airspeed of 44 m/s (100 mph). The methane leak was confined to a small, low-lying ditch, and the weather conditions were ideal for most of the testing with light to variable winds.

Valuable information about the impacts of dynamically changing flight conditions on active gas correlation analysis was gathered. Issues that need to be resolved include learning more about the impacts of all kinds of surface terrain on the gas correlation ratio, determining the necessary wavelength stability of the amplifier to minimize drift in the

gas correlation ratio, and better discriminating between false positives and actual methane hits.

Given the results of the airborne methane gas sensing and the operational concerns of the amplifier, Ophir decided to not attempt to quantify the presence of ethane. In order to realistically sense ethane, which has a much smaller absorption line and is a much smaller constituent of natural gas, Ophir believed that it would need a much larger controlled leak source of a mixed-blend gas. Larger leaks were very difficult to create using existing commercially available gas cylinders, and at some time in the future, Ophir hopes that it can continue with sensing of ethane from the air using existing large simulated or real natural gas pipeline leaks.

2   Experimental

2.1   Laboratory Setup for Determining Methane and Ethane Atmospheric Absorption between 1600-1700 nm

Previously, Ophir spent a considerable amount of time reviewing the existing atmospheric transmission software, such as Air Force Geophysics Laboratory HITRAN, LOTRAN, and FASCODE for complete absorption spectra on methane and ethane. These software databases generally are regarded as quite extensive and inclusive of all absorbing molecules and wavelengths. It is logical to assume that methane and ethane have overtone absorption bands near 1.65 μm, since the fundamental absorption band occurs for both of these gases near 3.3 μm. Indeed, HITRAN showed that methane does exhibit overtone absorption between 1600 - 1700 nm, but there was no evidence in HITRAN that ethane showed similar bands. It was essential, if Ophir was to use a single light source to detect both methane and ethane, that ethane be shown to have either narrow or broadband absorption present. Several other databases were reviewed with similar inconclusive findings. Ophir determined that it would be necessary to perform absorption spectra testing at their facility to confirm ethane overtone absorption.

In the laboratory absorption setup, Ophir used a previously purchased Ando Corporation optical spectrum analyzer, several gas cells and a CVI Laser Fiber Optic Broadband Light Source. The optical spectrum analyzer was calibrated using a 1536.204 nm laser diode and a HP86120 multi-wavelength meter. Gas cells containing various methane and ethane gas concentrations were used in the optical path between the spectrum analyzer and the light source. The goal here was to produce absorption plots showing the existence of absorption lines for methane and ethane between 1600 and 1700 nm. While methane plots were available from several data sources showing absorption near this wavelength, Ophir was unable initially to locate ethane absorption scan data.

2.2   Methane and Ethane Absorption Measurements using a Super Luminescent Light Emitting Diode (SLED) Broadband Light Source at 1.63 μm and Balanced Detectors

While the industry had demonstrated that methane can be quantified using narrow band laser sources, no one had yet demonstrated that a single broadband light source can be

used to sense both methane and ethane. Ophir believed that although it has modeled the amount of expected absorption for methane and ethane and it has determined the optimal sensing wavelength, there is still enough uncertainty to justify experimentally verifying the modeled results.

The basic laboratory setup used in the proof of concept testing is shown in Figure 1.
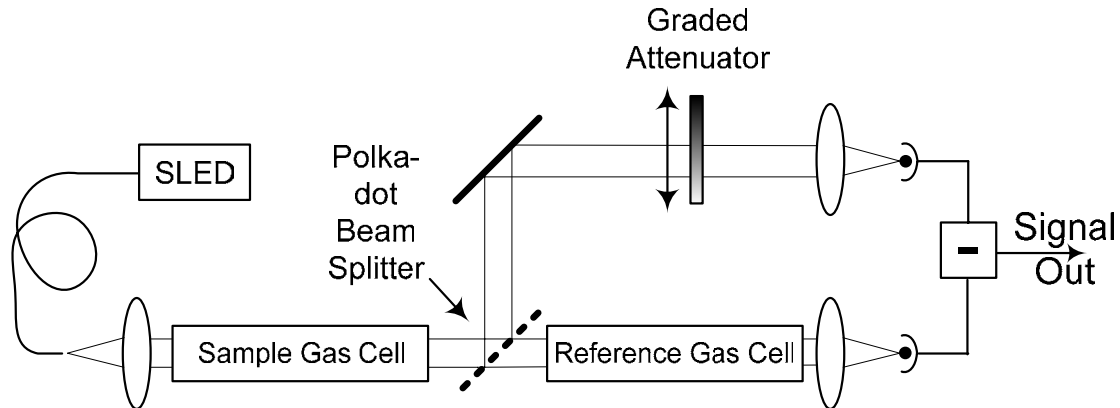
Figure 1. Proof of Concept Laboratory Setup

All of the items shown in Figure 1 were off-the-shelf with the exception of the sample and reference gas cells. The gas cells were built for the test of the Ophir fence-line monitoring system under an EPA-funded contract. These gas cells were 30 cm (1 ft) long, use 1-inch optics, and can be filled or evacuated with variable gas pressures. The approximate split ratio of the polka dot beam splitter was 1:1 or 50% transmission. The graded attenuator was a linear changing neutral-density filter optimized to near-IR wavelengths, and was used to balance the optical inputs into the balanced detector. The balanced detector from New Focus has detectors that were optimized for responses up to about 1620 nm and the signal response began to drop-off at wavelengths above 1620 nm. The signal output of the balanced detector was connected to a Tektronix digital oscilloscope and a Signal Technology lock-in amplifier.

The light source chosen for the experiment was a fiber coupled Super Luminescent Light Emitting Diode (SLED) that is centered near 1627 nm @T= 25 °C (or 1637 nm @T= 40°C) and has a Full Width Half Maximum (FWHM) of 45 nm. This particular SLED was capable of outputting up to 12 mW of power at a tuning temperature of 25°C and 4 mW at 40°C.

2.3 Gas Correlation Spectroscopy Using Narrowband Tunable Light Sources and Agilent Balanced Detector Configuration

2.3.1   Purposes for Demonstration of Using Narrowband Sources for Gas Absorption Studies

Up to this point in the project, Ophir had assumed that the best approach for sensing methane and ethane gases was to use a broadband light source to capture multiple absorption lines. The balanced detector configuration had been used basically with only two broadband light sources. The testing had shown that the noise reduction with the balanced circuit, using a broadband source, led to disappointing results in the area of noise reduction and lower signal-to-noise margins. Discrimination between varying levels of methane in the laboratory had been harder to accomplish, given the low absorption levels with the limited power levels and higher than expected noise. The existing gas cells, which have been used up to this time, have also shown etaloning effects due to internal gas pressures on the optical windows. It was becoming obvious that the gas cells to be used on the airborne sensor would need to be both rugged and impervious to internal pressure changes. The gas cells would most likely need to be a single rigid glass tube (with Brewster angled facets) surrounded by a protective metal fixture. Fiber optic inputs would also help to gather light more efficiently into the cells and eliminate some of the etaloning effects.

Another concern with using broadband light sources was that a great deal of the light energy falls outside the usable absorption bands for methane and ethane, whereas a relatively narrowband tunable source can be positioned to capture a single absorption line without the loss of out-of-band power. The search for high-power, broadband sources has shown that vendors have been slow to design and fabricate these sources in the methane and ethane-sensing bands. Both the Raman Amplifier and Spectrally Beam Combined broadband approaches suffered from a lack of available broadband seed sources. The other most promising approach was to use a Highly Non-Linear Fiber (HNLF) amplifier that does not require a seed source in the 1650-1700 nm range, but rather works on wavelength mixing to shift wavelengths. To achieve the necessary power output levels, a custom design will be required. These devices work more efficiently with narrowband light seed sources, so Ophir decided it would be prudent to perform balanced detection using narrowband light sensing.

2.3.2   Setup and Procedure for Conducting Methane Absorption Testing Through a Fiber Coupled Gas Cell Using Narrowband Tunable Light Sources

Given the available narrowband sources at Ophir (tunable sources up to 1640 nm), methane was the only feasible gas to perform absorption measurements, since ethane does not have absorption lines below 1665 nm. The setup shown in Figure 2 involved using an Agilent optical mainframe configured with a narrowband laser capable of being tuned to 1641 nm. According to the experimental data gathered by Ophir and through the Pacific Northwest National Laboratory database, there exists a triplet of methane absorption lines between 1637.5 and 1638.0 nm. Using the tunable laser source, it was

possible to scan the tunable source across this wavelength range and look at the absorption strength and location of the absorption lines. The laboratory setup utilized all optical fiber paths connecting the laser source to a fiber beam splitter, which passed collimated light through the methane gas cell in one path, and directly into the detector via the other path.

Critical to the procedure for acquiring data was the use of two detectors within an optical mainframe: (1) one detector was used to acquire light transmission data through the gas cell; and the (2) second detector was used to take a split-off portion of the blank output signal via a SMF cable. This formed a gas-to-blank detection ratio, which could be used to subtract common mode noise and DC current offsets, thus producing a pure absorption measurement across the absorption peak. This, in essence, provided for a balanced detection configuration, which is considered essential in beating down the overall noise level. It should also be noted that the detectors utilized in this test were some of the best detectors on the market and had noise levels down to the femtowatt (10^{-15} W) range. It was envisioned that these detectors would be used in the airborne configuration given their excellent sensitivity to very small optical signals.
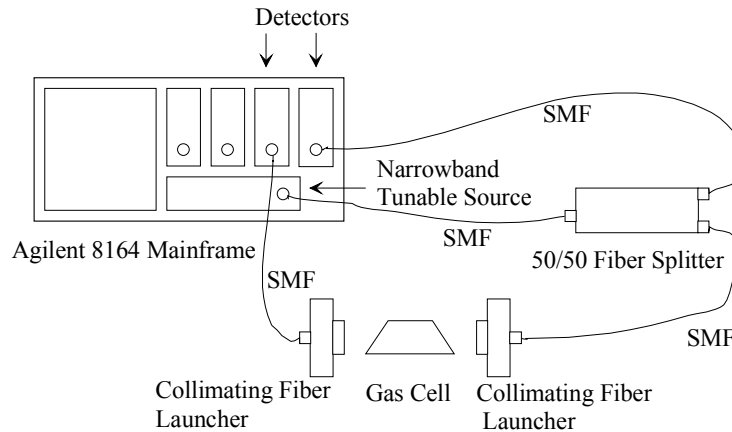
Parts List:

Agilent 8164A Optical Lightwave Mainframe

Agilent 81640A Tunable Light Source

Agilent 81634A/B InGaAs Power Sensor Modules (2)

Triad Technology Angled Glass Methane Gas Cell 7cm pathlength of pure methane (70,000 ppm-m of methane)

Single Mode Fiber Cables (SMF) 1 to 2 m in length

50/50 Fiber Splitter

Thor Labs F220F-C-1550 FC/APC Collimating Fiber Launcher (2) with Newport MM200-1A 2-Axis Adjustment Optics Holder

National Instrument Labview Software Drivers to Agilent Mainframe

Figure 2. Optical Circuit Used to Measure Etalon Drift through Reference Gas Cells

2.4 Short Optical Path Methane Absorption Testing Using a Narrowband Tunable Laser

This experiment was intended to replicate methane absorption measurements at an optical pathlength of 7.6 m (25 ft) one way, using the gas correlation software and a very narrowband tunable laser. The Agilent Model 81640A narrowband laser could be temperature tuned to reach 1640 nm in wavelength with a maximum output of less than 1 mW. The output power of the laser limited the experiment to very short optical pathlengths, and the wavelength limited the scan to only a few methane absorption lines (ethane absorption occurs at higher wavelengths).

The design setup for this experiment is shown in Figure 3.
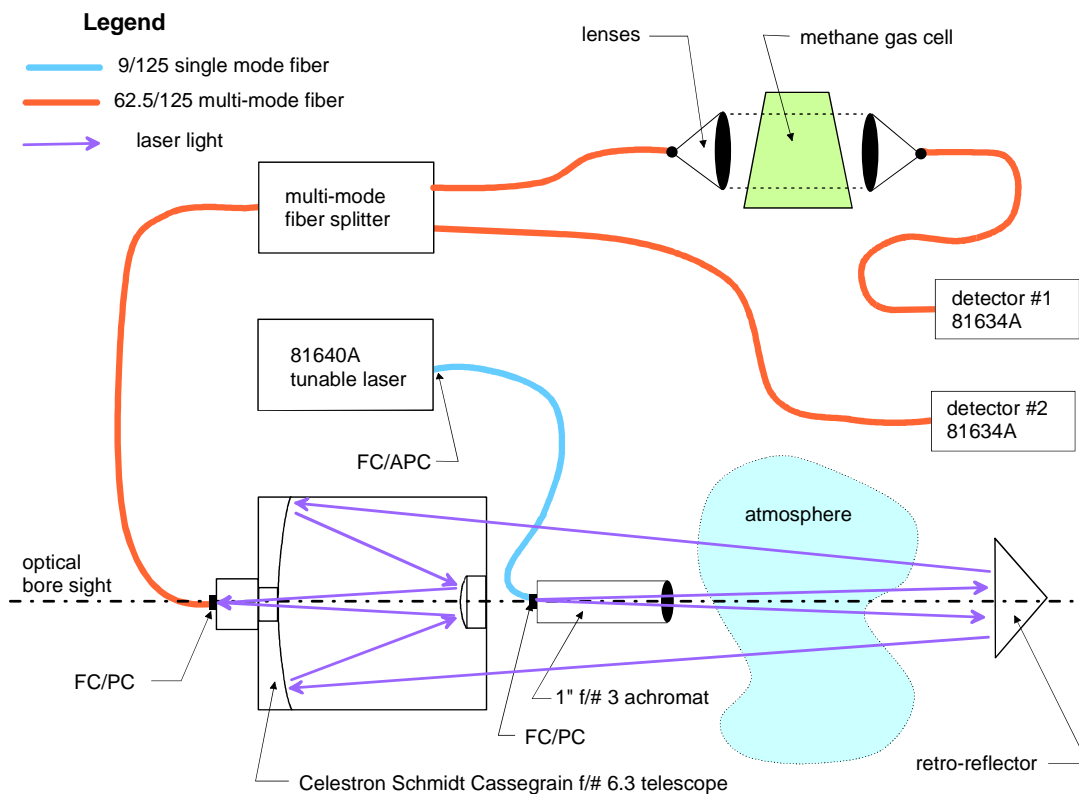
Figure 3. Experimental Setup for Short Optical Path Methane Absorption Measurements

2.5 Laboratory and Field Setup for Moderate to Long Path Target Reflectance Testing

2.5.1 First Target Reflectivity Tests Using Two-Inch Diameter Infrared Antireflection Coated Lenses for Laser Output and Detector Input Beam Forming

Signal-to-Noise (SNR) modeling for the airborne remote sensor configuration has shown that appreciable amounts of output power ($\cong 1$ W) will be needed to meet the system SNR requirements for long optical path targets. In addition, little data is available describing the overall signal reflectance that can be expected using an IR source against different background surfaces. Ophir has investigated the availability of high power sources in the IR wavelength of interest, and has determined that the design will definitely be custom in scope, meaning significantly more cost and risk to the project. To eliminate as much risk as possible, Ophir has taken the approach to minimize risk by performing certain key tests. The setup for the target reflectance tests when using an unmodulated light source and 2-inch receiver and transmitter optics was identical to that shown in Figure 3, which utilized a larger aperture telescope and a smaller transmitting optic.

The target reflectance tests were performed over a period of several weeks, with the first test performed in an Ophir downstairs laboratory at a distance of 10 m (33 ft). This was the basic proof-of-concept test to verify that the Ophir OSA and the fast response detector could capture a reflected signal from a 10 m target. Included in this test were reflectance measurements against numerous target surfaces, such as Spectralon, brick paver, potting soil, grass sod, cardboard, pine board, wet and dry paper towel, asphalt and concrete block. Reflectance measurements were also taken with the target positioned at multiple incident angles to the receiver optics.

A second test was performed, using the above setup, outside near the Ophir facility in indirect solar light. The goal of this test was to look at the contribution to the signal reflectance of the solar background against a perfect reflector. This test was done passively with no laser source. The range distance of this test was limited to around 4 m. The impact of solar background on the SNR can be devastating, if the solar contribution of the received signal is large in magnitude. While the gas correlation method will in fact remove much of the common mode solar contribution, the associated shot noise (random fluctuations) can not be removed. This noise component would reduce the system SNR. The results of this test were also used to determine whether a narrowband optical filter was required in the airborne sensor (to limit the broadband contribution of shot noise). This test also showed the polarization state of the passive solar light bounced off the Spectralon by rotating a 2-inch polarization filter in and out of the return.

These tests culminated with a final long-optical path range test out to 50 m. This test was performed at a remote site, free of any human contact that would allow for unimpeded testing of the high output 1 W 1555 nm Erbium Doped Fiber Amplifier (EDFA) output. Detector measurements were taken using Spectralon at a target range of between 10 and 50 m, with one test performed against a target consisting of a hilly background of extreme optical angle. The tests that were performed here included:

- Long optical path reflectance measurements
- Determination of solar noise contributions from "fully illuminated" sky
- Selection of optimum narrowband filter wavelength
- Light source modulation impact on receiver signal measurements
- Noise components induced by an all fiber-optic optical configuration

While the Ophir tests used 2-inch optics, the airborne sensor utilized a larger 14-inch receiver telescope. Given the amount of energy returned to the detector is proportional to (A_d / r^2), where A_d is equal to the receiver area and r^2 is equal to the range in meters squared, the distance scaling factor for these experiments is shown to be approximately 7. In other words, signal return data gathered at a range of 10 m using the 2-inch optics turns out to be equivalent to return data gathered by the airborne sensor at a distance of 70 m. Very quickly it can be seen that to reach a specified airborne range of 150 m (500 ft), a target range of 21 m (65 ft.) using the smaller optics is required. In fact, the experiments were done at multiple ranges all the way from 10 m to 50 m, more than covering the required airborne sensor range requirement.

2.5.2   Setup and Procedure for Conducting Target Reflectance Measurements with Large 14-inch Aperture Telescope and Using a 1555 nm EDFA

This series of tests was performed to expand upon the earlier target reflectance measurements using a 1 Watt (W) 1555 nm fiber amplifier, 2-inch receiver optics, and a Lambertian reflector. The new setup for these tests is shown in Figure 4 and shows the addition of a large 14-inch aperture Schmidt-Cassegrain Telescope (SCT) as the signal reflection receiver.   Many of the parts listed in Figure 4 were identical to those used during the previous target reflectance testing. A continuous, non-modulated current was used to drive the 1 W fiber amplifier.
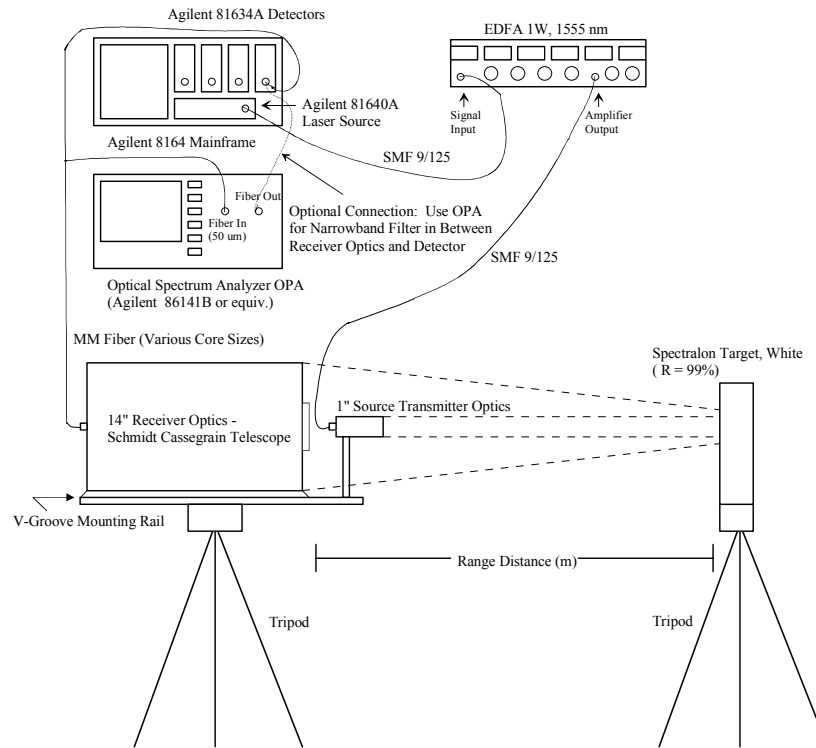
Figure 4. Setup for Target Reflectance Test Using Large 14-inch Aperture Telescope

The telescope was an F# 11 Schmidt-Cassegrain design, which included a large primary mirror and a secondary mirror that partially obscured the incoming light. The light path entered the opening and was gathered by the primary mirror, focused onto the secondary obscuring mirror, and then refocused through an opening in the primary onto a small spot. The main advantage of this type of telescope was that the optical pathlength is considerably shortened with the folded path, and this allowed for a much shorter overall length. The entire length of the telescope was 79 cm (31 in), which allowed Ophir to mount the telescope vertically within the airplane looking downward (the most efficient configuration). The focused light was gathered at the focal point of the telescope behind the rear-mounting flange onto multimode fiber; originally a fiber core size of 62.5 μm was used. As the testing progressed, larger core fiber was used as replacement receiver fiber.

All of the reflectance testing during this performance period was done without the use of the narrowband optical filter within the Optical Spectrum Analyzer. Most of the testing was performed during the evening hours, where background solar light was not an issue. Nighttime testing was the norm due to the inability to see the invisible near-IR 1555 nm light with Ophir's existing viewing equipment during the daytime, especially at longer optical pathlengths. Ophir did receive a loaner IR viewing camera from ElectroPhysics Inc., but the combination of the inability of the camera to display IR light within solar background and the limited battery life, made it useless in our test configuration. Ophir

decided to use a small (2 x 3 in) IR light-activated sensing card to locate the IR beam at night. As long as a visible light source was first used to locate and focus the output beam, the sensing card worked well. Unless otherwise stated, the output power of the 1555 nm fiber amplifier was limited to around 500 mW.

The optical range of the tests was set at 150 m (500 ft) one-way to simulate actual flight viewing conditions. The tests that were performed included the following:

- Using a co-aligned laser output and telescope receiver, measured the reflectance off a Lambertian target at 150 m with standard 62.5 µm core size receiver optical fiber.
- Reconfiguring the telescope as an F# 2 telescope, using the Faststar option, measured the back reflection into the 62.5 µm fiber coupled detector.
- Varied the field of view (FOV) spot size of the large telescope at the target to determine the impact on light collection. Likewise, varied the output laser spot size at the target to determine the impact on light gathering.
- Compared the performance of the large-aperture reflecting telescope to the 2-inch focusing optic (used in the previous tests).
- Determined the impact of the obscuration on the total light gathering capabilities of the large telescope by moving the light spot slightly off-center with the telescope FOV.
- Replaced the low-noise small active area detectors with the large (5 mm) diameter optical detectors, removed the fiber from the telescope focusing mount, and manually focused the light in free-space onto the detector. This test illustrated the impact of increasing the focus spot size on light gathering capabilities.
- Reconnected larger core fiber from the telescope to the large area detectors. Determine impact of using larger core fiber at the telescope focal point.

A photograph of the test setup, using the 2-inch laser source focusing optic, can be seen in Figure 5.

Figure 5. Photograph Showing Outdoor Test Setup of Co-Aligned Transceiver with 14-inch Telescope and 2-inch Laser Source Optic

3   Results and Discussion

3.1 Gas Industry Data Survey Results

Ophir Corporation believes it was important to have gas distribution industry input into the development and design requirements for an airborne, optical remote sensor of methane and ethane for natural gas pipeline leak detection. Ophir sent a list of informational questions to WBI Holdings, Inc. in Bismarck, ND and El Paso Pipeline Group in El Paso, TX. Attachment 1 shows the survey questions, a summary of the industry response to the questions, and the design impacts to the system.

3.2 Data Survey Results for Atmospheric Plume Dispersion of Natural Gas Pipeline Leaks

Concentration of natural gas within pipeline leaks is influenced by the size and location of the leak as well as by the environmental aspects surrounding the leak. An underground leak will dissipate the natural gas differently then an above-ground leak. Types of soil will also impact the flow of natural gas to the surface. A more porous soil such as sand can be assumed to produce a more diffuse leak than would be produced by a more compact soil such as clay. Furthermore, the gas plume exiting the ground surface is greatly impacted by the atmospheric stability and local winds. Ophir conducted a

literature search to better determine the natural gas plume dispersion and concentration and the impact on the pointing of the airborne optical, remote sensor.

When looking at three small hole diameters of 5.4 mm, 17 mm, and 54 mm in a pressurized pipeline of pressure 700 psi, Gopalsami [2002] determined experimentally that the plume size (diameter) with distance from the leak was not dependent upon the size of the leak hole. The plume diameter was determined to be 44 m (144 ft) at a leak distance of 100 m (328 ft) and the methane concentration was 100 ppm, for a 5.4 mm leak. The concentration of 100 ppm is well above the ambient methane levels of 1 – 2 ppm. More importantly, the plume diameter was well defined even at 100 m distance from the pipeline. This fact is especially important when flying over the pipeline with the airborne sensor. Digitizing a section of pipeline with GPS coordinates, and pre-programming the flight path to these coordinates, will allow the sensor to be pointed to within 20-30 m of the pipeline, well within the discernable methane concentration level.

In another study by Reichardt [2002], a preliminary modeling effort was performed looking at an axisymmetric plume derived from an exposed jet (no soil overburden) under quiescent conditions. More extensive modeling was then performed that took into account both soil effects and meteorology. Soil effects were taken across the extreme range of tightly compacted soil such as clay, to non-compacted soil such as sand. In either case, a single leak path to the surface was considered unlikely. Instead, multiple leak paths would develop and the degree of compaction was assumed to be inversely proportional to the number of leak paths to the surface. For the compact soil a source leak area of 1 m^2 was assumed, and at the other extreme for a non-compact soil type an area of 100 m^2 was assumed. Two methane leak rates, shown in Table 1, were taken from calculations involving realistic hole sizes and internal pipe pressures such as might be encountered in a transmission pipeline.

For estimation of the atmospheric dispersion of the plume, a simple Gaussian dispersion model was used. The degrees of atmospheric stability were categorized into stability classes A through F, where class A is highly unstable and class F is highly stable. Three plume sight paths were used in the modeling of the plume dispersion, but only two of these sight paths were relevant to the airborne sensor. Path 1 was looking down through the plume 5 m (16 ft) downwind at plume centerline, and path 2 was looking down through the plume 20 m (65 ft) downwind and 20 m off plume axis. Several of the following observations were made from the modeling results that will impact the airborne sensor pointing and subsequent detection capabilities:

- There was a huge difference in concentration between the center and the edge of the plume for all atmospheric stabilities and leak rates.
- For neutral and very stable environments, the edge of the plume at a distance of 20 m from the center showed negligible amounts of methane.
- The wind speed had a major impact on plume concentration. A wind speed of 10 m/s (22 mph) decreased the plume concentration by a factor of ten.
- While the leak area (related to soil type) impacted the concentration, it had much less impact then wind speed changes.
- A stable atmosphere led to less dispersion downwind from the leak, resulting in a higher concentration. This was due to the decrease in atmospheric mixing in the

vertical direction around the leak. Actually an airborne remote optical sensor measures total concentration along the optical path length between the air vehicle and the ground, and the vertical dispersion of the gas may not be as detrimental as with a horizontal-looking sensor.

It was very important that the airborne sensor be pointed downwind from the pipeline leak, and that the flight path is over the center of the plume (higher concentration seen for Path 1 scenario). A goal of flying within 20 m downwind of the pipeline can be met when using Global Positioning System (GPS) coordinated pipeline data. Several other plume-dispersion studies were discovered in the data search but most were related to power plant plumes, and were not relevant to natural gas pipeline leaks.

Leak Scenario	Leak Rate (scf/hr)
.0625 inch hole with 400 psi internal pressure	324
.125 inch hole with 1000 psi internal pressure	2088

Table 1. Leak Rates Considered for Calculations Reichardt [2002]

3.3 Selected Airborne, Optical Sensor Hardware Design Requirements

Based upon the natural gas company data survey and other research, Ophir selected the following design criteria for the airborne, optical remote sensor system:

- Light source centered on the overtone absorption band near 1650 - 1700 nm.
- A single light source shall be used to sense both methane and ethane.
- The light-sensitive photo detectors shall be large-area extended range InGaAs PIN photodiodes, with nearly uniform responsivity from 1400 – 1900 nm.
- Aircraft Airspeed $\Rightarrow$ 161 km/hr (100 mph)
- Aircraft Altitude $\Rightarrow$ 152.4 m (500 ft)
- Terrain reflectivity @1650 nm $\Rightarrow$ 20 % - 50%, Source: Wolfe [1985]
- Sensor Ground Spatial Resolution $\Rightarrow$ 0.5 m (1.5 ft)@100 Hz Update Rate [1]
- Weight $\Rightarrow$ <200 lbs
- Size $\Rightarrow$ 3 ft x 3 ft x 3 ft
- Minimal Detectable Concentration $\Rightarrow$ 500 ppm * m
- Input Power Requirements $\Rightarrow$ 500 W

---

[1] Although the airborne acquisition system will be capable of this resolution, the standard GPS locator resolution is limited to 10 – 15 m resolution.

Justification and rationale for the specification of some of these design parameters will be discussed more thoroughly later in this report. The minimal detectable concentration of the sensor may change depending upon the noise floor of the system. When comparing the modeling of plume concentration from Reichardt [2002] to the minimal detectable concentration of the Ophir sensor, one would expect to detect nearly all of the larger rate plumes but only some of the smaller rate plumes.

3.4 Results of Sensor Performance Modeling Under Operational Conditions

The airborne optical system SNR determines the minimum detectable change in reflected signal due to absorption by gas species of interest, therefore the minimum absorbance (ppm*m) of detectable trace gases. The detection scheme is designed to maximize signal to noise by reducing noise fluctuations inherent to optical remote gas-sensing techniques.

There are five major sources of noise. The first and most significant is extraneous light collected from the sun in the wavelength band of interest. Solar flux adds to the overall system shot noise by adding shot noise to the shot noise level from the probe light source. This situation is not fatal, however. Solar noise contribution is mitigated by modulating the probe light source and using phase-sensitive detection to detect the subtle changes in the probe intensity with trace gas concentration. The modulation separates signal photocurrent from the solar photocurrent and reduces the solar shot noise to an acceptable level. Alternately, instead of modulating the probe light source intensity, the trace gas source can be effectively modulated by holding the probe intensity a constant and spatially scanning the optical beam over the potential gas source. A trace gas absorption signal is obtained using phase-sensitive detection at the spatial scanning frequency as in the previous example. Spatially scanning the probe beam has the advantage that no light is lost due to intensity modulation, consequently there is no power penalty to the resulting signal to noise ratio.

The next three identified major noise sources are addressed by the balanced detection scheme. They are probe light-source intensity fluctuations, variations in the reflectivity of the earth's surface at the probe position, and fluctuations due to air turbulence.

Probe light-source fluctuations are due to the light generation process in the light source. As observed by Fast Fourier Transform (FFT), the spectral density of these fluctuations can be 15 decibels above the balanced detection minimum noise level. Additional noise is introduced as the probe beam moves across the earth's surface. The probe light reflectivity off the earth's surface varies as much as 50%, due to variations in vegetation, earth, and rock types. Finally, air turbulence creates additional noise by randomly modulating the optical path between the transmitter, earth's surface, and the receiver.

Fluctuations due to surface reflectivity and air turbulence required additional noise mitigation. Since the balanced detectors photodiodes quantum efficiency had a spatial dependence, any physical mechanism that moved the focused beam on the photodiodes will contribute to extraneous system noise. A solution to mitigate this problem was to include elements in the airborne optical system that would integrate the scene profile and remove high spatial frequency components.

As part of Ophir's research effort, an estimate was made of the best possible optical signal to noise achievable with an airborne Light Detection and Ranging (LIDAR) system. Included in this calculation was the shot noise from collected light, photodetector dark current shot noise, and estimated shot noise from solar flux assuming a worse case illumination scenario (sun at zenith). This calculation also included the radiometric aspects using an airborne system to transmit and collect light using a telescope with the largest practical aperture size (18 in diameter). We assumed that the aircraft would fly at 165 meters (500 ft) Above Ground Level (AGL) at a velocity of 100 mph and would project a diffraction-limited probe beam on the earth's surface. We also assumed that the detector footprint on the earth's surface exactly matches the probe beam spot size. This requirement eliminated excessive solar noise from the desired signal.

An estimate of the final optical signal to noise was determined by multiplying the light transmission factor times the probe beam intensity on the earth's surface, then referring to the Ophir signal to noise model curve produced in Figure 6. For a 1-Watt CW broadband transmitter with an overall minimum expected transmission of 0.01, the expected signal to noise achievable was 6×10^3. This number was based upon a broadband light source of sufficient bandwidth (30 nm) to overlap numerous absorption lines. As will be described later, a broadband source of such power and capable of spanning over both methane and ethane absorption lines was not available.
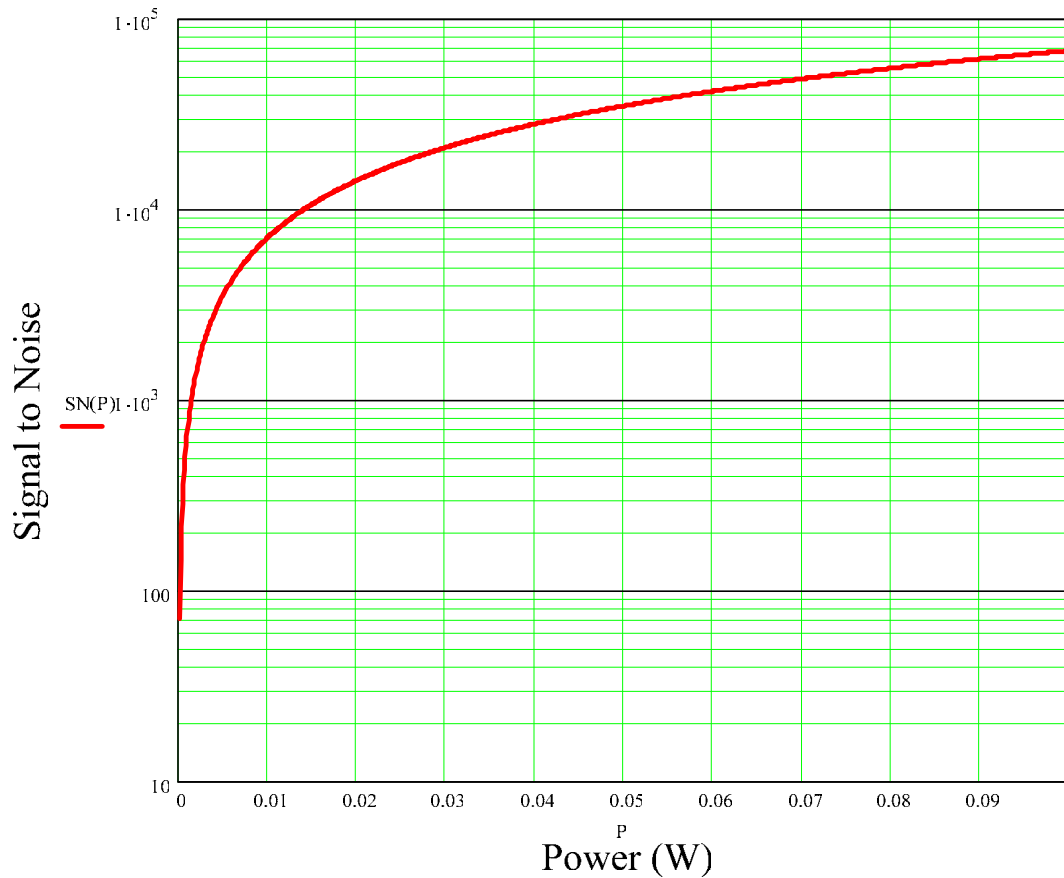
Figure 6. Maximum Achievable System Signal to Noise Ratio per Probe Power Intensity on the Earth's Surface

For the proprietary fiber amplifier, we calculated that assuming a shot noise plus 3 dB noise level we will be able to see down to 300 ppm*m ethane or methane. This is more sensitivity than is required for the application. The total optical path between the transmitter, the earth's surface, and back to the telescope receiver, was approximately 300 meters (1000 ft). Assuming a 1.5 ppm natural methane background concentration, the absorbance detection for the detection scheme need not be more sensitive than approximately 1.5 x 300 or 500 ppm*m.

3.5 Methane and Ethane Absorption Measurements Using Broadband Light Sources

3.5.1 Verification of Methane and Ethane Absorption Spectra within the 1600 – 1700 nm Wavelength Band

Using the setup described in section 2.1, with 100% methane introduced into the sample gas cell, the absorption spectra for the experiment for methane are shown in Figure 7. A similar test was performed using 100% ethane in the gas cell, and the results are shown in Figure 8 (the "flatter" line in both of the figures represented a reference transmission with only room air at ambient room pressure in the cell). As expected the methane showed definite absorption structure from 1620 – 1725 nm, thus confirming the other existing databases. More interestingly, the ethane showed substantial absorption structure between 1660 – 1720 nm. Some narrow band structure near 1685 nm was seen overlapping the fairly broadband component. It is thought that the fine structure on top of the broadband feature would also aid in discrimination between methane and ethane. At this time, a second confirming set of absorption data was found to exist in the Pacific Northwest National Laboratory (PNNL) database. Available on a subscription basis and maintained by Steve Sharpe, PNNL has absorption data for several hundred compounds. The signatures of both of these compounds agreed remarkably well with those produced by Ophir. In addition, an added benefit was seen where the PNNL spectral signatures for methane and ethane showed very little overlap with the existing atmospheric water vapor absorption lines.
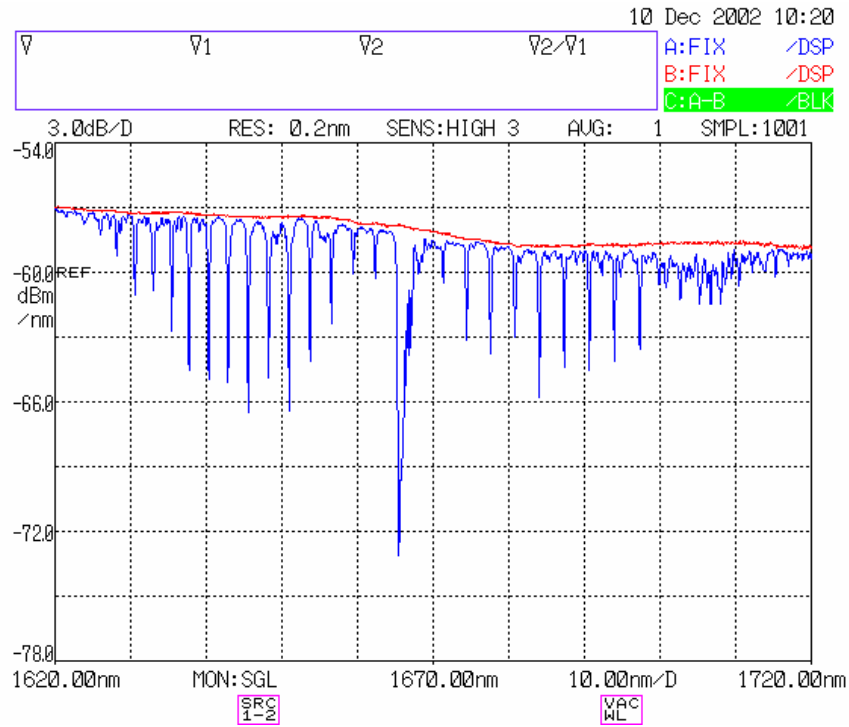
Figure 7. Ophir Experimental Observation of Methane Absorption Spectra Using 100% Methane
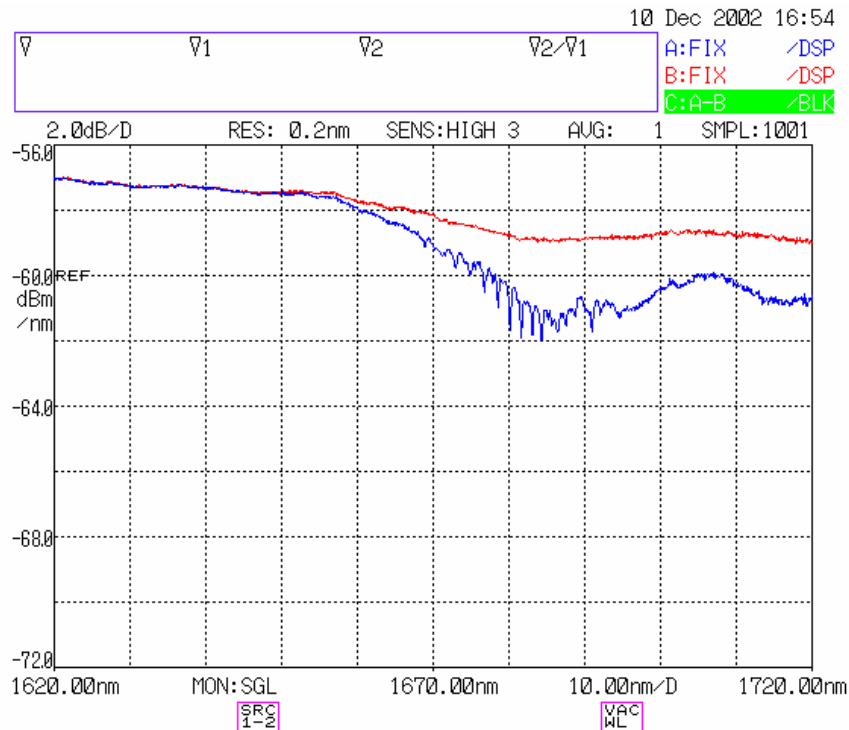
Figure 8. Ophir Experimental Observation of Ethane Absorption Spectra Using 100% Ethane

3.5.2 Methane and Ethane Absorption Measurements Using an SLED Broadband Light Source at 1.63 um and Balanced Detectors

3.5.2.1 Characterization of the SLED Light Source and Balanced Detector

The DC biased fiber-coupled SLED light source was directly coupled into an optical spectrum analyzer and the power density over wavelength was displayed. Ophir noted a very close agreement between the analyzer data output and the vendor-supplied output curves. Temperature tuning of the diode also showed similar close agreement. No unusual wavelength specific perturbations were seen in the analyzer display, which meant that the optics within the package was producing no non-linear artifacts. Initially, the SLED was driven only with a DC bias but in order to improve the noise characteristics, especially when using a lock-in amplifier, sine wave modulation was added.

Without any optical surfaces in the optical path and driving the diode current with a modulating waveform, the spectral waveform continued to resemble a well behaved Gaussian source. The next step was to determine the impact of adding the necessary optics in the beam path to allow for the diverging fiber-coupled output to be focused and guided onto the active areas of the two detectors, as shown in the setup in Figure 1. The immediate impacts on the beam output power, shape and spectral content can be summarized as follows:

- The spectral qualities of the beam were degraded from the Gaussian looking waveform due to the presence of unwanted back reflections. This departure from the ideal waveform introduced potential degradation of available energy at the detector, which will negatively impact the system SNR.
- Uncoated or non-optimally coated surfaces within the optical setup modified the light transmission through the optical circuit. Furthermore, it was observed that the degree of sensitivity to back reflections was dependent on the SLED drive current; the larger the drive current, the greater degree of back reflection sensitivity.
- The use of fiber optical isolators in the SLED optical setup did not sufficiently reduce the back reflections in the optical circuit.
- The gas cells were originally built with AR-coated windows, which were optimized for wavelengths near 3.3 μm. These windows worked poorly when transmitting light near 1.63 μm. The gas cells were disassembled and higher transmissive sapphire windows were installed. The transmission losses through all the window surfaces were reduced to 25%.
- Beam positioning was highly dependent on the pressure within the gas cells. For the balanced detector system to work properly over different gas concentrations, the beam spot could not wander across the detectors. Changing the pressure within the sample gas cell produced a slight movement in the beam, which changed the location of the beam spot on both of the detectors. This may have been caused from slight refractive index changes within the gas medium, or may have been due to slight bulging of the windows due to the pressure changes.

- Vibration within the setup was definitely a problem. Even slight movements in the optical fiber and the other optical components produced beam wander, which affected the split ratio into the balanced detectors.
- A gain adjustment on the balanced detector output was supposed to zero out any common mode noise or signal. We were unable to accomplish this and noted the presence of low amplitude second order harmonics on the output. The second order harmonics were not expected and may be the result of a slight phase shift between the two input optical signals and may be exaggerated by the broadband nature of the light source. Indeed modeling indicated that a small phase shift of 1° could account for the harmonics.

3.5.2.2 Methane and Ethane Gas Absorption Results

One major goal of the laboratory experiment was to provide quantitative data showing signal absorption for different methane and ethane gas concentrations using a broadband light source. Unfortunately, the SLED wavelength was less than optimal for both methane and especially ethane absorption. While methane showed measurable signal absorption, the absorption signal for ethane was very near the noise level of the system. A very small signal deflection was measured at the balanced detector, when a high concentration of ethane gas was introduced into the sample gas cell but varying the concentration produced no further changes in the signal (an indication that the signal was buried in the noise). These results compared favorably with the absorption model, which indicated little absorption at this wavelength.

Figure 9 showed a plot of the balanced detector signal vs. the methane absorbance in ppm*m using the laboratory setup with a 1.63 μm light source. The solid line showed the relationship between the approximate slope of the data and the noise floor. The noise floor was indicated by the dotted line and was measured at the detector output into a lock-in amplifier. This noise represented the minimal detector rms signal output produced when the optical paths were optimally balanced. Methane concentration in the cell was controlled starting with methane at an over-pressure of one atmosphere and then gradually reducing the pressure. It appeared that the thin gas cell window suddenly relaxed (in shape or flatness) at an absorbance near 27,000 ppm*m and caused a spatial shift in the optical beam to impact the ratio between the two optical detectors. The signal absorption data can be viewed as fairly linear with respect to varying methane concentration. Overall, this demonstration has shown that methane levels can be discerned and quantified by using a broadband source near 1.63 μm. Unfortunately, the power level of the broadband source will have to be orders of magnitude higher to account for the losses due to signal reflection from the surface. Ultimately, Ophir was unable to locate a vendor that could produce a high power light source covering both methane and ethane absorption lines, and this led to the abandonment of the broadband light source for the airborne sensor.

Signal Voltage vs Equivalent Absorbance
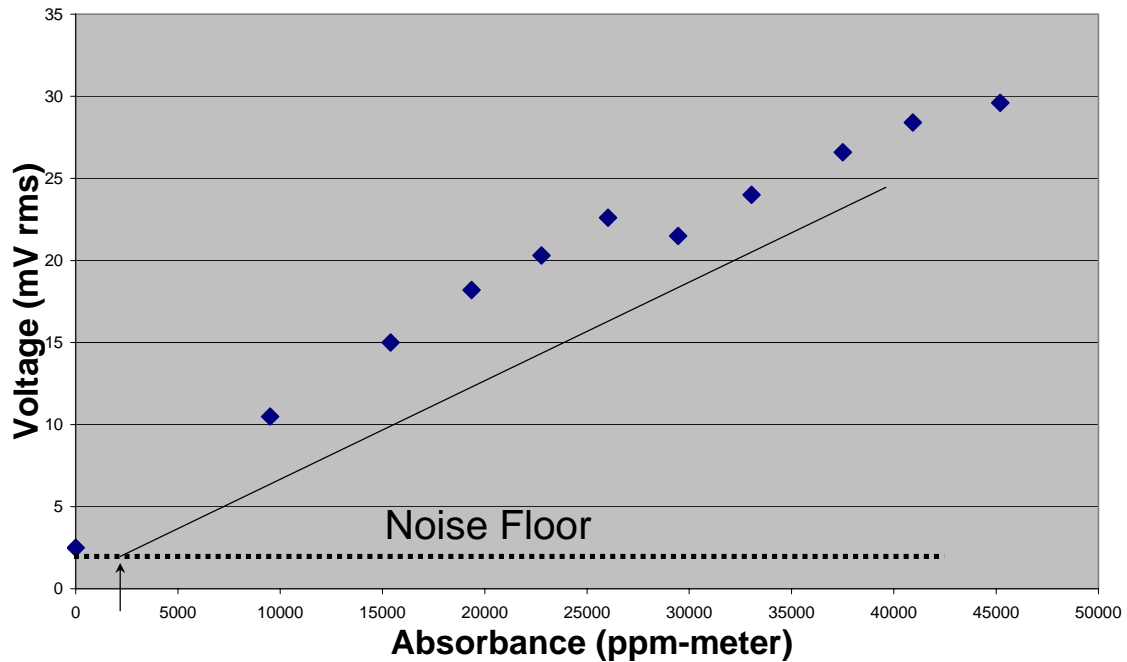
Figure 9. Methane Signal Absorption vs. Concentration Using 1.63 μm SLED Light Source

3.6 Methane Absorption Using Narrowband Tunable Light Source in Balanced Detector Configuration

3.6.1   Methane Absorption through an In-Line Gas Cell

Using the setup in Figure 2, Ophir performed a scan across several methane absorption lines near 1637.5 nm was performed. The scanning software incorporated by Ophir included the following functions:

- Tuning of the laser source from 1637.5 to 1638.0 nm in steps of approximately 0.003 nm at a rate of 20 nm/sec or 25 ms update rate.
- Balanced detector data sampling rate set to free run at 10 KHz.
- A detuning algorithm was utilized to adjust out the difference in signal strength through the gas cell and through the fiber. This detuning allowed the output trace to be zeroed out of any DC detector input signal mismatch.

The gas/blank linear detuned data for the methane scan is shown in Figure 10. The linewidth in wavelength (nm) is shown on the horizontal axis and the vertical axis is the triplet line depth in dB, from a two-channel gas-correlation ratio measurement. Notice the waveform has been scaled to 0 dB during the off absorption periods of the scan, indicative of the detuning software and the effectiveness of the balanced detection scheme. The methane absorption triplet was easily seen in figure. The exact absorption

depth and the Full Width Half Maximum (FWHM) of the individual peaks can't be
readily ascertained, as the overlapping peaks contributed to each other's overall
absorption and linewidth.   In order to isolate the individual peaks, existing LabView
software using Lorentzian theory was used.
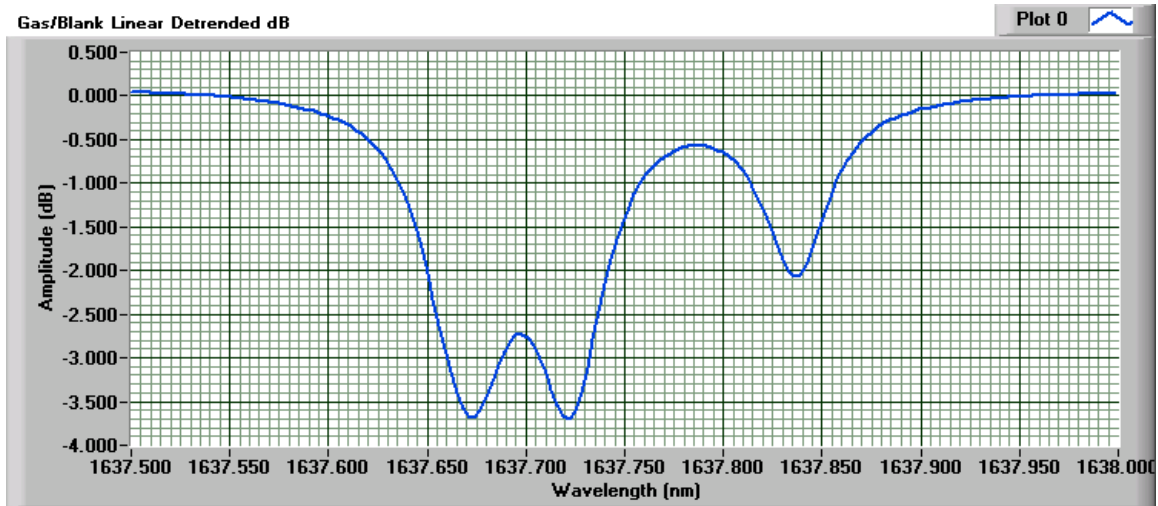
Figure 10. Methane Gas Absorption Scan Using Narrowband Tunable Laser

At the same time the airborne sensor was being developed, testing of the 3.3 µm fence-
line broadband monitoring system using the same gas correlation system was ongoing.
A series of tests using the ground-based system was conducted at a contractor's facility to
monitor the presence of natural gas leaks. The results showed the presence of natural
gas, but the concentration levels were way down from what was expected, given the
magnitude of the known leaks. It was suspected that some component of the system had
degraded over time, and an interesting test was performed using the Agilent narrowband
source to scan the fence line "calibrated" gas cell. The methane gas cell was scanned,
using the calibrated data gathered from the previous plot in Figure 10 and additional
Lorentzian theory to isolate the individual peaks was applied. The resulting waveform
scan is shown in Figure 11.
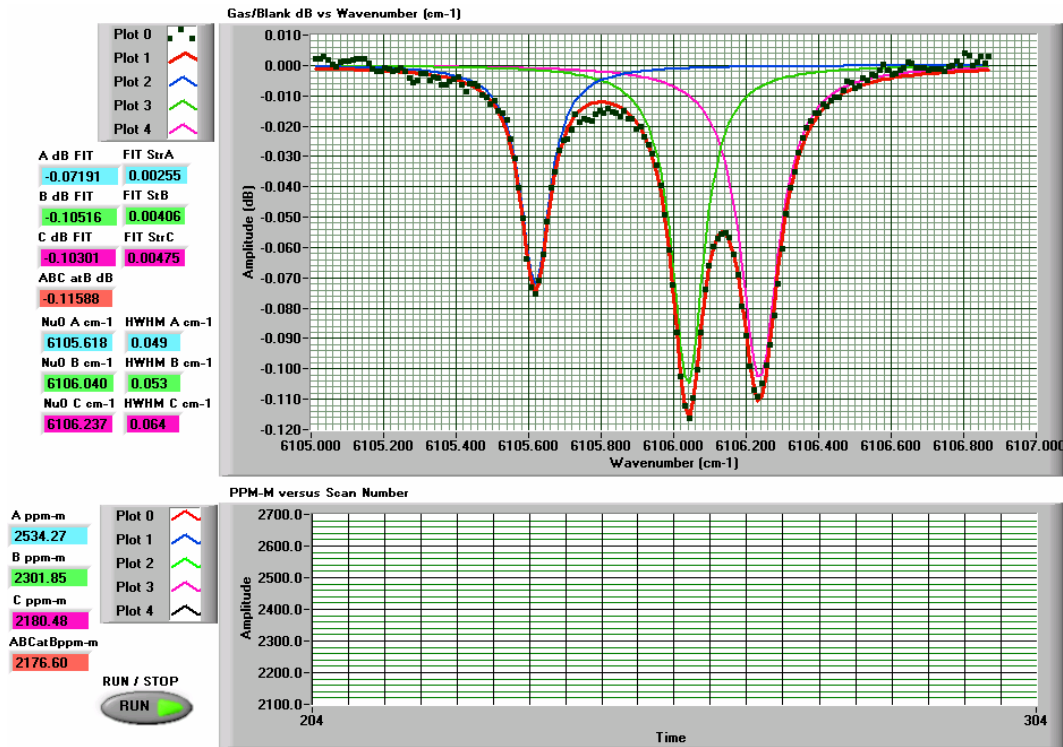
Figure 11. Gas Correlation Scan of Duothane Gas Cell Using Narrowband Tunable Laser and Balanced Detector Scheme

The raw scan points are shown as BLACK squares. The composite best-fit line of three Lorentz line shape functions to the data is the RED line. The three individual Lorentz lines fitted to the line triplet data are shown as BLUE, GREEN, and PURPLE. The experimental data set is of quite high quality, and the theoretical Lorentz line shapes fit very well. What did not fit well were the concentration levels of the "calibrated" gas cell shown in the lower left hand corner of the plot. These concentration numbers should have been close to 17,000 ppm*m, given the expected concentration and pathlength of the cell. This data indicated that cell was actually only 13% of the predicted gas concentration. When the gas cell was re-filled with 100% methane, a new scan was performed with the results very nearly matching the expected 17,000 ppm*m. These test results added credibility to the proposed use of a narrowband source with gas correlation to detect airborne natural gas leaks.

3.6.2 Short Optical Path Methane Absorption Testing Using Gas Correlation and a Narrowband Tunable Laser

The setup in Figure 3 was used to test the gas correlation technique in discriminating different levels of methane gas in the optical path. First, the telescope pair was removed from the setup, resulting in the laser output fiber source directly connected to the fiber splitter. A baseline laser scan was done across the methane absorption lines for the gas cell and blank (no gas) cell optical arms. The results of this scan are shown in Figure 12.
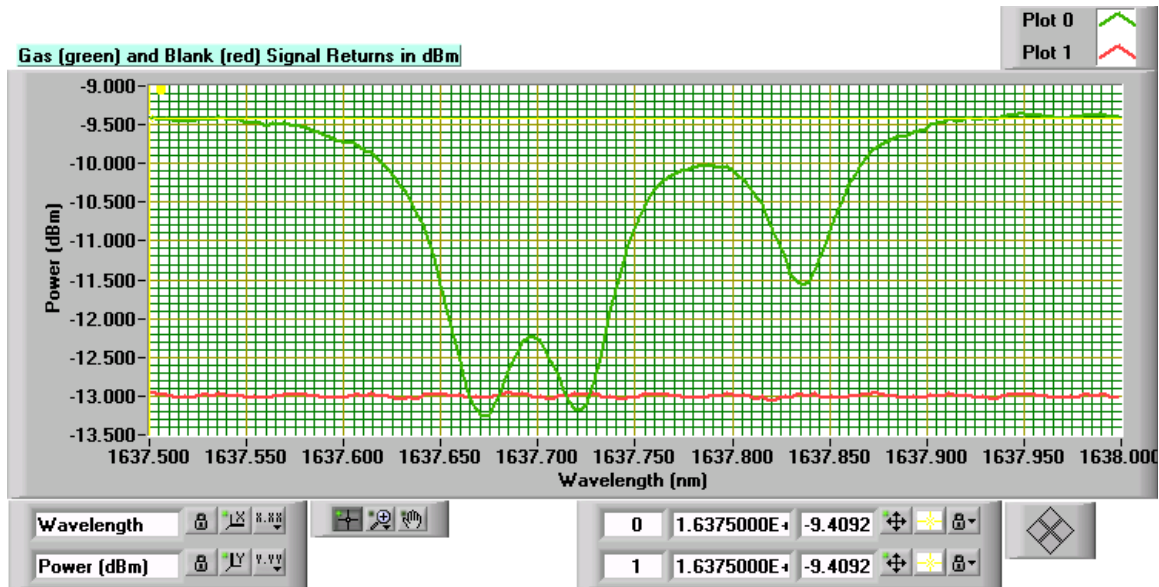
Figure 12. Baseline Laser Scan across Methane Absorption Lines - Green Trace is Raw Absorption Data from Gas Cell and Red Trace is from Blank Cell

Notice the flat absorption seen through the fiber channel with no methane (blank channel) in the path. Transforming the raw data shown in Figure 12 into methane gas concentration was done using the Ophir-generated gas correlation algorithms. The algorithm calculated the gas concentration of the cell to be 72,035 ppm * m and agreed closely with the real gas cell concentration of approximately 70,000 ppm * m (99.9 % methane over a 7 cm pathlength). Next, Ophir installed the telescope and receiver optics back into the configuration and measured the gas concentration of the gas cell plus any ambient level of methane to be 72, 621 ppm * m. Even though the signal levels were down by over 50 dB in the raw data (not shown), the gas cell concentration was recovered easily. The measured methane gas concentration was slightly higher than was expected, but it was surmised that this was due to the non-optimized noise level of the system. To test this hypothesis, Ophir next injected higher amounts of methane into the optical path.

The gas correlation software should have been able to discern background levels of injected methane from the very high gas cell concentration. This was not the case for these laboratory methane injection tests. There was no increase in the gas-to-blank ratio for the added methane, as has been seen for the previous developed broadband ground

based fence-line monitoring radiometer. Subsequent testing did not improve the test results. The differences between the two systems were noted to be the wavelength and the source linewidth, with the newer airborne system having a shorter wavelength and a much shorter linewidth. Optical modeling was initiated using the gas correlation software with a comparable, shorter linewidth, and true to the test results different levels of methane were not detected. It was clear, that the gas correlation modeling indicated that a broader linewidth, as well as a non-gaussian shape, was required to discriminate different methane gas concentration levels within the optical path.

This important finding helped to define the optical specifications for linewidth and spectral shape of the high-output light source. The light-source vendor has performed their own modeling to verify that they could safely reach the design output goals given the new input requirements, and they have indicated that they could.

3.7 Target Reflection Measurements at 150 m (500 ft) Optical Path Using a Co-Aligned Transceiver and a 1555 nm Erbium Doped Fiber Amplifier

3.7.1 Summary of Target Reflectance Measurements Using Co-Aligned 2-inch Receiving and Transmitting Optics and a 1555 nm Erbium Doped Fiber Amplifier

The Second Six-Month Technical Report summarized, in detail, the results of the extensive reflectance testing using the 1555 nm 1-W Erbium doped fiber amplifier (EDFA) and the small 2-in lens tube. These results indicated the following:

- Many surfaces that will be encountered by an airborne optical system reflected light similar in nature and magnitude to a true Lambertian surface (light is reflected back in all directions). Moist surfaces tended to limit the reflected light at 1555 nm.
- It was important to have the angle of incidence from the aircraft receiver to the ground at normal or 90 degrees. Large deviations from this produced reduced signal returns.
- With the 2-in receiver and the co-aligned fiber laser, the amount of reflected light from a true Lambertian surface at 50-m produced a return of 32 nW into a fairly small multimode 50 μm fiber cable. This amount of signal was at least three orders of magnitude greater than the advertised noise floor of the detectors.
- The use of narrowband filters helped to keep background solar noise below several tens of picowatts.
- There was significant light leakage through the fiber connectors. Serious attention needs to be placed upon limiting this leakage.
- Ophir measured surprisingly large (14.4 nW with a narrowband filter) reflected signals off of a grassy surface at a severe incidence angle at 50-m distance.
- A larger receiver optic of 14-in aperture (proposed airborne version) would theoretically yield equivalent light gathering power to the 2-in optic at an expanded optical distance of 350 m, exceeding the airborne goal of 150-m altitude.

3.7.2   Target Reflectance Measurements at 150 m (500 ft) Optical Distance Using Large 14-inch Aperture Schmidt-Cassegrain Telescope (SCT)

Previous reflection tests illustrated the need for larger receiving optics for the airborne sensor. This need was satisfied when Ophir purchased a Celestron commercial 14 –inch aperture telescope. The telescope has a single focusing knob used to move the primary mirror forward and backward, which enables the focal spot to move freely behind the telescope. Ophir spent some time getting familiar with the focusing capabilities of the telescope. It was determined that the minimum resolvable focus of the telescope was approximately 47 m (51 ft). The telescope should therefore work well at the airborne optical path distance of 150 m (500 ft).

The telescope was received with a single v-groove rail aligned lengthwise along the telescope. Mounting clamps were purchased separately that mated with the rail and secured the telescope to a flat tripod mount.

3.7.2.1 Reflection Measurements Using a Large Aperture Receiver Telescope Focused onto a 62.5-µm Fiber Core into an Optical Detector

The system was configured using the setup in Figure 4. The reflected signal was intercepted by the receiver, focused onto a multimode optical fiber and then directed into a fiber detector. The first series of tests was performed using a 62.5 µm fiber core, and the initial focus or FOV of the telescope was set to look at a spot 8 inches in diameter at the target (flooding the receiving fiber with a visible laser diode source, and then projecting the expanded FOV onto the target helped to set the desired telescope viewing spot size). The corresponding light source spot size was set to be around 3 inches at the target. Ophir laser radar (lidar) designs utilized at least a 2:1 FOV overlap with the laser source projection to insure that the laser return did not move out of the FOV due to vibrations or atmospheric perturbations. The two spots were aligned, using two visible laser diode sources, so that they were centered with respect to each other (additional experiments will be discussed later showing the impact of having the two spots off axis). The visible diode sources were removed from the setup and the near-IR source was connected to the output source fiber optic connector with an output $\approx$ 500 mW. Power at the detector was measured to be 20 pW, which was substantially less than expected. The power reflected back to the receiving optics was obviously much less than predicted based upon previous measurements.

In order to improve the signal return, Ophir experimented with the focus adjustment on the telescope speculating that the focus onto the fiber may have been slightly off. Finding the optimum focus onto the fiber increased the signal at the detector to just over 500 pW. While changing the telescope focus showed a large improvement, the overall signal return was still less than expected. Two areas of concern were seen by Ophir to be the most likely contributor to the lack of signal return; the first was the inability to focus the entire signal onto the small 62.5-µm fiber core and second, the impact of the telescope secondary mirror obscuration on the signal return.

The original optical modeling for the telescope was done using Zemax software and was based upon the premise that collimated light from an infinite distance was reflected back into the telescope. The software did not have the flexibility of changing the light characteristics from infinite to finite distances into the telescope. The Zemax calculations also included comparisons to the best-possible, diffraction-limited optical performance. While Ophir did not posses detailed information regarding the Celestron telescope design prescription, all SCTs have a number of optical elements in common as shown in Figure 13. This configuration closely approximates the Celestron SCT. The telescope prescription for the model was optimized to produce a diffraction-limited beam spot at the focal place for a single wavelength, at 550 nm. The performance of the optical system was then characterized by encircled energy calculations at the focal plane. The light wavelength was then shifted from 550 nm to 1650 nm and energy encircled calculations at focus were reproduced. At 1650 nm, the image plane from prime focus was moved and new encircled energy calculations were produced to get an idea of the light-coupling tolerance, hence potential vibration sensitivity, of light coupling into the multimode optical fiber. All of these calculations were based upon infinite focus or parallel light rays into the telescope.

Schmidt-Cassegrain Telescope configuration
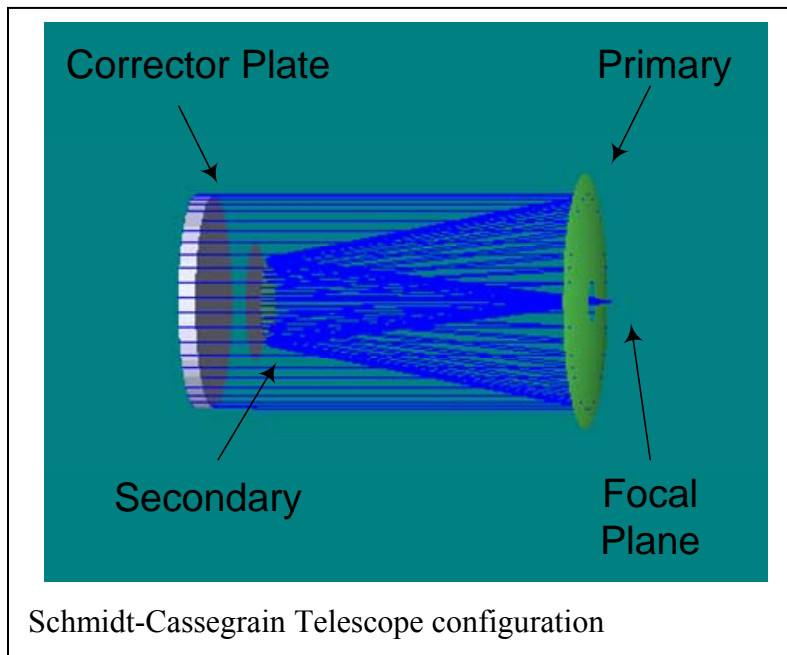
Figure 13. Schmidt-Cassegrain Telescope Configuration Used in Zemax Models

Encircled energy calculations at 1650 nm were completed and are shown in Figure 14.
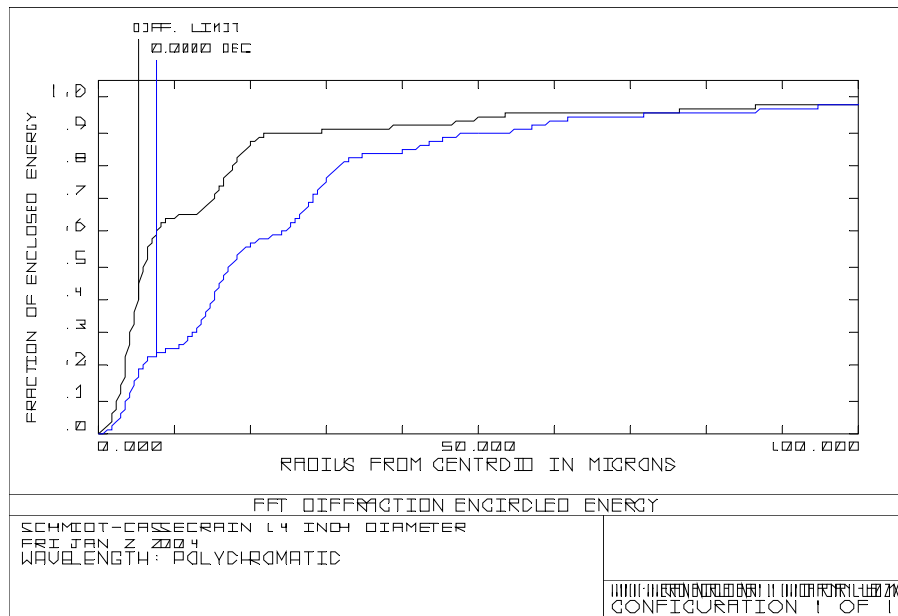
Figure 14. Encircled Energy Calculation at 1650 nm, Calculated at New Prime Focus Position

The new prime focus for the data shown in Figure 14 was 40 mm closer to the telescope primary mirror from the prime focus seen for the 550 nm light. The multimode fiber coupling efficiency was approximately 78% for the 1650 nm plot, therefore it would be expected in real life to be down in efficiency by about 10-12 %, when gathering near-IR light with the SCT. The Zemax models also helped Ophir understand the benefits of using the corrector. From Figure 14, it was evident that most of the received light was focused onto the 62.5 μm diameter fiber core.

3.7.2.1.1 Further Analysis of SCT Focusing Performance

The results of the initial target reflectance testing at 150 m were disappointing and did not agree well with the anticipated signal return. Previous signal reflection measurements done with smaller optics at shorter optical pathlengths indicated that the larger telescope would have a 7X increase in receiving power when adjusted for the signal return loss due to the $1/r^2$ rolloff, where r is the optical pathlength. In rough terms, the large telescope should have yielded slightly less power at 150 m as did the smaller optic at 50 m. This was clearly not the case with the large telescope, as it yielded only a few percent of anticipated signal return.

Ophir began to question the modeling analysis, as it did not explain the actual system performance. The modeling was performed using the assumption that the return light entered the telescope from an infinite focus distance or entered as parallel light rays (Zemax software was incapable of using any other object focus distance).   The fact that the light rays enter the telescope as non-parallel rays may have masked the problem with

focusing of the image. The lens equation is defined as equation (1); using it to evaluate the image and object sizes of the optical system may shed some insight into the lack of system performance.

$$1/s' = 1/s + 1/f \qquad (1)$$

where s′ is the image distance, s is the object distance and f is the focal distance.

In the test configuration, the object distance = 150 m, the focal distance of the telescope = 3.91 m and the image distance is unknown. Substituting these numbers into (1) and solving for s yielded s = 3.81218 m. The magnification of the system is defined by equation (2).

$$M = s' / s \qquad (2)$$

The magnification of our system is therefore 3.81218 / 150 or .0254. For a fiber with receiver core size of 62.5 μm, the maximum object size is only 62.5 μm / .0254 or 0.246 cm (0.1 in). In other words, the FOV of the telescope at 150 m is restricted to 0.246 cm when trying to focus the light onto a 62.5 μm fiber. This explained why only a small fraction of the available light energy striking the target was reflected back to the telescope (remembering that the light source was focused to a 10-cm (2-in) spot on the target). One way to compensate for this effect would be to shrink the light source spot size at the target, a second way would be to increase the fiber core size. For example, increasing the fiber core size to 1000 μm, increased the magnification by a factor of 16 which changed the acceptable object size to 4.1 cm (1.6 in). Results of incorporating these improvements into the test configuration will be discussed more later.

3.7.2.1.2 *Analysis of the Impact of Secondary Mirror Obscuration on Signal Return*

At an infinite distance, the secondary mirror obscuration will act to reduce the overall signal through the telescope by the ratio of the area of the obscuration (102.6 cm^2 or 15.9 in^2) to the area of the telescope aperture (993.1 cm^2 or 154 in^2) or by approximately 10%. As the optical distance decreases, the impact of the obscuration is more and more pronounced. In an attempt to further quantify the obscuration losses at 150 m, Ophir calculated theoretical losses due to the obscuration at 150 m using some existing laser radar (lidar) analysis software. This proprietary software had been used to calculate backscatter off aerosols at various optical distances, but was manipulated to determine the reflected signal off a hard target at 150 m. The output light source beam size was set to 5 cm (2 in), the center obscuration was 11.4 cm (4.5 in), and various fiber diameters were modeled. The output from this lidar return model is summarized in Figures 15 and 16, and shows the calculated signal return and the telescope to laser overlap, for 62.5 and 1000 μm optical fibers. In both of these Figures, it was obvious that the larger fiber saw the least impact in signal reduction from both relative return power and signal overlap. Signal overlap was the most impacted by the short optical pathlength, with very little of the signal getting back to the detector.
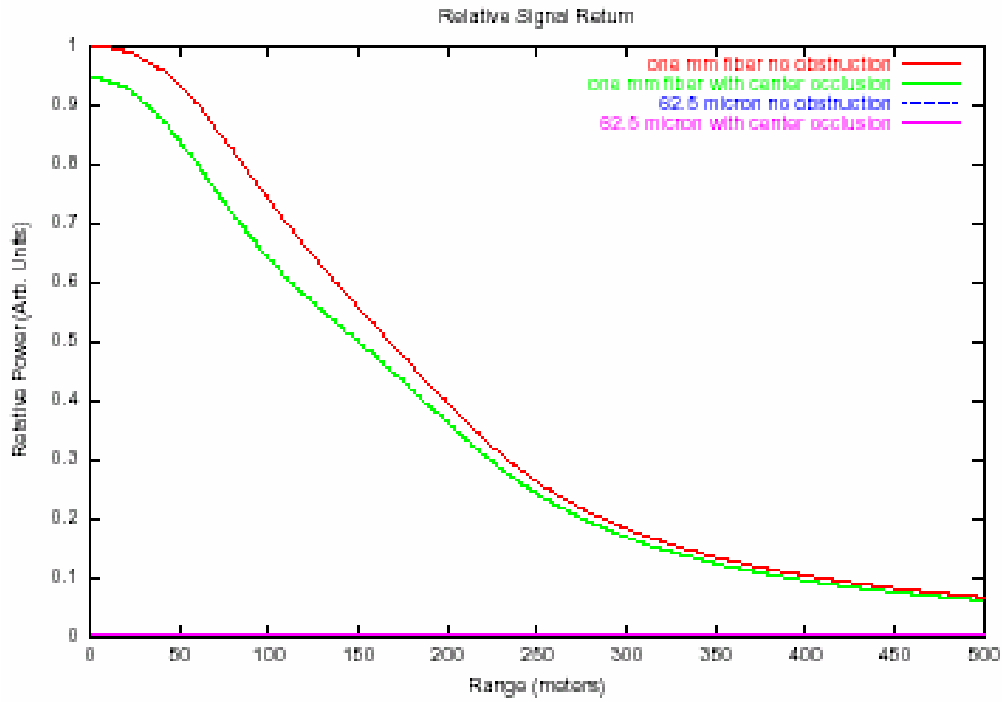
Figure 15. Modeled Signal Return for a 14-inch Telescope Using 62.5-micron and 1000-micron Optical Fiber Core with and without a Secondary Mirror Obstruction
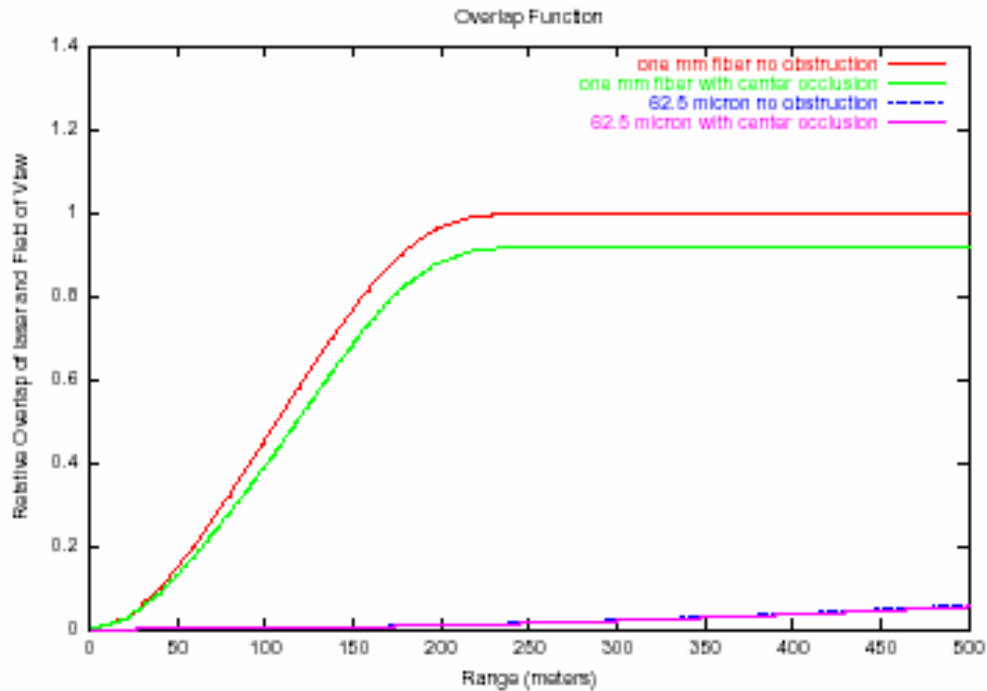
Figure 16. Modeled Signal Overlap of Laser and Telescope FOV Using 62.5-micron and 1000-micron Optical-Fiber Core with and without a Telescope Occlusion

3.7.2.2 Second Series of Target Reflectance Test at 150 m Decreasing the F# of the 14-inch SCT

The first goal of this test was to use a focal reducer of F# 3.3 in front of the optical fiber to reduce the focused spot size at the fiber by reducing the overall system F#. Classic radiometry stated that the energy back to a detector was inversely proportional to the square of the F#. Using this as a baseline, it can be seen that going from an F# 11 to an F# 3.3 would yield a tenfold order of magnitude gain in signal at the fiber. In reality, the gain in signal at the detector increased by a lesser amount or 3-4 times ($\cong 65$ pW). The focus through the reducer was optimized to obtain the maximum signal. This spot size at the target was approximately 1.25 cm (0.5 in), which agreed fairly well with the calculated spot size obtained from using equation (2) to find the optimum magnification. The focal reducer helped to show that indeed decreasing the focus spot aided in signal detection.

Given the much smaller than anticipated signal measurements, it was decided to perform a comparison of the airborne telescope to the smaller receiving optic with a smaller F#. The setup in Figure 4 was modified by replacing the 14-inch SCT with a smaller 2-in receiver, identical to the receiving optic used in the 50-m target reflectance test during the previous performance period. Standard multimode 62.5-μm core fiber cable was used. The receiver optic and the laser output optic were co-aligned and centered with the laser spot size set to 5 cm (2 in) in diameter. The receiver FOV was set to the smallest size possible at the target or 45 cm (18 in). The amount of signal at the detector was 135 pW or twice the energy captured by the larger telescope. Theoretically, the solid angle of the larger telescope should have contributed to larger signal return, unless there was some other factor limiting the signal collection *i.e.* limiting profile of optical fiber.   Even though the smaller optic worked at least as well at gathering return signal, the amount was still well under the signal required for sufficient signal-to-noise. It was becoming more obvious that the use of the small fiber with the larger F# telescope was the single largest limiting factor of the signal return at the detector.

3.7.2.3 Third Series of Target Reflectance Test at 150 m Using Large Core Optical Fiber

On April 27th, the third in a series of reflectance tests was performed. Most of the test data gathered was centered on using various larger-core optical fibers as the interface from the large telescope to the detector. In order to use the larger-core fiber, a larger area detector with an active diameter of 5 mm was used. The low-noise detectors used up to this time were restricted to an input fiber core diameter of less than 100 μm. The larger area detectors had an electro-optical noise floor of around 5 pW compared to less than 0.3 pW for the low-noise detectors. It was anticipated that although the large area detectors were "noisier" by an order of magnitude, the amount of signal gain would increase by several orders of magnitude.

3.7.2.3.1 Outdoor Target Reflectance Measurements Using Large-Core Optical Fibers and Large-Area Detector

The setup remained the same as shown in Figure 4 with the exception of the Agilent Model 88634A detector, which was replaced with a Model 81624A large area detector. The multimode 62.5-μm detector fiber was also eventually replaced with several fibers of larger core sizes. The large telescope was used as the receiver and the light source was focused with the 1-in transmitting optic with a focal length of 40 mm. The focus (FOV) of the telescope was adjusted to yield maximum signal at the detector.

The power output of the 1555 nm fiber amplifier was set at approximately 500 mW with the Pump #1 drive current set to 0.81 A and the Pump #2 drive current set to 0.56 A. These test conditions were held constant throughout the evening of testing. The Spectralon highly reflective Lambertian target was used for all of the reflective measurements.

It turned out that 1000-μm core fibers were the largest practical commercially available fiber on the market. Optical fibers larger than this were costly, inflexible and hard to use. The connector terminations were also limited. Ophir had chosen the FC/PC connectors due to their availability and ease of use, and FC/PC connectors were limited to core sizes of just slightly larger than 1000 μm.

Table 2 summarizes the signal reflection data taken for different large core fibers.

Optical Fiber Core Size, in μm	Core to Cladding Transition	Measured Power at Detector, in nW	Field-of-View Diameter at Target
100	Graded Index	1.5	Not Taken
105	Step Index	1.5	0.875 Inches
300	Step Index	12	0.625 Inches
600	Step Index	50	1~1.25 Inches
1000	Step Index	165	1.25~1.5 Inches

Table 2. Detector Power Measurements Taken with Target at 150-m Distance Using Large-Core Fibers

Increasing the fiber core definitely increased the amount of signal collected through the telescope and into the detector. A gain of hundred fold was seen when going from the 100-μm fiber to the 1000-μm fiber, which roughly corresponds to the ratio of the areas of the fiber core.

In order to determine the impact on signal return of varying the FOV of the telescope away from the optimal size, the FOV of the telescope during the 1000 μm was increased to 4 inches or roughly twice the size of the light source spot. The new power measurement at the detector was 38 nW, which was dramatically less than seen for

optimal focus. This further strengthened the argument to fix the telescope at minimum focus.

3.8 Transceiver Design Results

3.8.1 Development and Selection of the Transceiver Light Source

No component of the airborne, remote sensor has taken more thought, time, and effort to develop than the transceiver light source. Early in the project, Ophir had determined that the most favorable absorption wavelength band for sensing both methane and ethane was near the overtone band between 1650 – 1700 nm. This was due to the availability of very sensitive optical detectors, lower thermal noise, and the absence of water absorption lines for this wavelength. Unfortunately, the methane and ethane absorption bands were just outside commonly available telecommunication band light-source amplifiers.

From the absorption models performed by Ophir, the amount of power to achieve the necessary SNR would need to be 1 Watt or more over the appropriate bandwidth. Ophir spent a good deal of time contacting vendors who could develop high output sources in the mid-IR wavelength near 1600 – 1700 nm. Many of these companies were non-responsive, no longer in business, or not able to build to Ophir's light source specifications. Ophir was able to isolate three potential vendors, and of these vendors, only one continued to remain as a potential light-source vendor.

Initially, Raman fiber amplification was thought to be the source of choice, but Raman amplification required an optical seed source centered near the desired output wavelength, an optical pump source, and the fiber amplification medium. Unfortunately, there were no commercially available seed sources above 1640 nm, and a substantial amount of non-recurring engineering (NRE) cost would have been required to develop these sources. Ophir located one vendor that had proposed the development of a broadband seed source to be used with a Raman amplifier. Preliminary cost to develop this source exceeded $115,000, and when combined with the amplifier cost would have pushed the overall light source cost to over $170,000. To complicate the situation, the seed source vendor went bankrupt shortly after our discussions. Other issues that have plagued the use of Raman amplifiers for this application involved the high output power requirements and out of desired wavelength output emissions. Raman amplification depended upon the gain of a seed source power at a shifted wavelength above the pump wavelength. Higher output powers from these amplifiers included some emissions that were outside the seed source wavelength band, and can limit the available useful sensing power. If a narrow-band seed source was used instead of broadband source, additional non-linear effects can be seen such as Brillouin scattering. Brillouin scattering again limits the output power and can cause catastrophic failure of the amplifier.

 Other technologies that had been researched included spectrally beam-combined diodes, and HLNF amplifiers. The spectrally beam-combined diodes proved to have limitations that were similar to the Raman amplifiers, where seed-diode sources were required to be centered near the amplification output wavelengths. These seed sources did not exist at

the time. The remaining technology of HLNF amplification showed the greatest potential with the least amount of cost and associated risk.

 Ophir has made considerable progress in building a working relationship with the HNLF amplifier vendor. Both on-site meetings and teleconferences were conducted between Ophir and the amplifier vendor. A well-defined set of design specifications were created. Advantages of using these amplifiers for the airborne sensor included:

- Output wavelengths of 1650 –1700 nm can be tuned around seed laser sources that existed commercially within the C or L bands of the telecommunication industry.
- The seed sources for the amplifier can be either narrowband or broadband depending upon the application. Frequency modulation of the seed sources can be used to broaden the output.
- Output Modulation between two different gas sensing wavelengths at up to 1,000 Hz is possible.
- Power outputs of over 5 W have been demonstrated with this technology.
- An all-fiber design associated with the HLNF amplifier will have good immunity from vibration-induced problems. The amplifier will also have good performance over a wide temperature range.
- The fiber medium of the amplifier is a very small (6-7 μm) glass fiber that has very good spectral quality and a small numerical aperture, thus a well-collimated, confined light output.

There have been significant hurdles to overcome with the use of HLNF amplifiers in the remote sensing application, namely how to produce significant power output without introducing detrimental Brillouin scattering. Other issues were in selecting the seed wavelengths capable of detecting both methane and ethane, determining the optimal seed wavelength bandwidth, and agreeing on the overall interface between the amplifier and Ophir's test equipment. The initial broadband concepts of the amplifier were modified somewhat to accommodate the properties of the fairly narrowband absorption spectra (FWHM = 0.03 nm). Ophir has chosen to reduce the broadened output to a value that closely approximates a single absorption spectra width of methane. This allowed the amplifier to scan much more quickly and to position the wavelength directly over the absorption spectra over long periods of time, as long as the wavelength was tuned periodically to the methane and ethane spectra. This concept in reality used the best of both the broadband and the narrowband sensing approach. The strict gas spectroscopy method would have used a very narrow (less than 200 KHz) linewidth to scan back and forth across a single spectra, whereas Ophir used a much broader wavelength of 10 GHz linewidth. Using this broadening of the linewidth reduced the need for wavelength scanning and reduced problems due to Brillouin scattering.

The HLNF amplifier was received at Ophir at the end of November 2004, much later than the original specified date of June 26th. The late arrival date of the amplifier caused Ophir to miss an anticipated flight test, sponsored by the DOE NETL office, of the airborne system at the Rocky Mountain Oilfield Test Facility near Casper, Wyoming. Factors that impacted the delivery were: the custom nature of the design, the lack of coordination within the manufacturing facility located in Lannion, France and the research and development office in Virginia, a problem with drifting output power due to

polarization changes at the non-linear fiber, and heating problems within the amplifier. The amplifier was specified to be semi-ruggedized with the capability of operating in a single engine light aircraft. Unfortunately, once the unit arrived at Ophir it became obvious that it was designed to be primarily used only in the laboratory. The amplifier was returned twice for repair to Virginia; once for a heating issue on one of the C-Band laser pump diodes and next for a C-Band laser diode failure at a slightly lower operating temperature (18ºC). Other features such as the RS-232 communication interface to the C-Band quit working and the L-Band pump would not turn on at the lower temperature. All of these issues proved to be daunting when characterizing and checking out the amplifier.

The amplifier is a 19-inch rack mountable, 6U height format (11 inches) weighing under 50 lbs. A picture of the amplifier with the ruggedized laptop computer is shown in Figure 17.
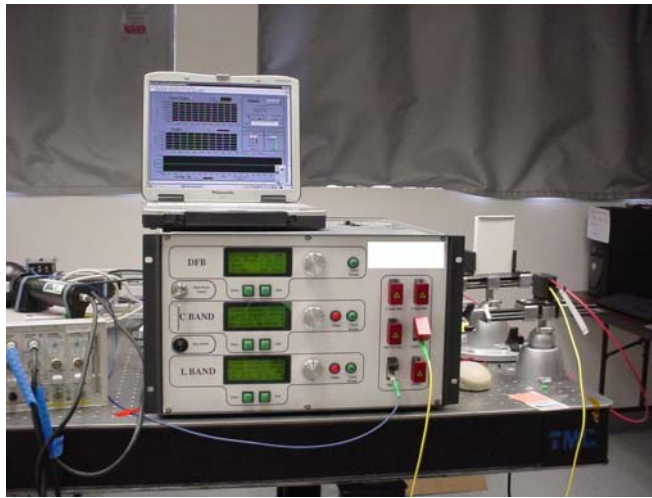
Figure 17. Photograph Showing Highly Non Linear Fiber Amplifier in Laboratory Test Setup

Characterization of the amplifier has shown the following specification requirements were met:

- Output capability of single wavelength or modulated dual wavelengths.
- Modulation of two wavelengths up to 1000 Hz.
- Wavelength tuning of ± 1 nm in 0.015-nm steps.
- Spectral output linewidth slightly broader than requirement of ≤ 0.03 nm.
- Maximum output power for methane band was 0.9 W and for ethane band was 0.7 W.
- Output power stability is 10%, more than the specified 5%.
- Light source can be controlled via front panel knobs or through three different RS-232 communication ports.

3.8.2   Methane and Ethane Gas Absorption Laboratory Measurements Using HNLF Amplifier

Gas correlation spectroscopy does not require rapid wavelength on-off tuning, but it still requires the amplifier to be wavelength stable and tunable. The amplifier vendor did not have an optical spectrum analyzer with the required resolution of 0.01 nm to verify the tuning stability. It was decided that to test this critical feature, a setup using methane and ethane gas cells, the HNLF amplifier, and high resolution optical detectors would be created. The goal of this test setup was to compare the amplifier scan of the gas cells with the PNNL generated gas absorption scans. If the Ophir generated scans compared well with the PNNL scans, then the amplifier tuning range and resolution was sufficient for gas correlation. The original methane and ethane gas cells were originally designed to be used in the gas correlation setup, where the gathered reflected light signal would pass through the cells and then be compared to the blank cells. The incorporation of larger optical fiber in the system rendered these cells useless as gas correlation cells, but they would still prove to be useful as calibration cells for setting the amplifier tuning wavelength. The cells were fiber coupled with FC/APC style connectors and 62.5 μm fiber, and had sealed gas cells of 7.5 cm (3 in) optical length filled with 99.9% gas. The gas cells were connected on one end to the low power (1%) output tap on the HNLF amplifier and the other end to the high resolution optical detector in the Agilent Optical Mainframe.

The amplifier wavelength was controlled through the RS-232 communications bus to the laptop PC. Ophir developed tuning software that would tune the seed diode wavelength from a start to stop temperature with resolution down to 0.01ºC. The desired output from this calibration routine was to obtain the temperature where the amplifier wavelength was slightly offset from the deepest absorption line. Next, the routine was run multiple times to ascertain if the same temperature was measured every time. The temperature scan was done from cold to hot and then back from hot to cold, using the same start and stop temperatures in order to note any hysteresis in the wavelength. Ample time was allowed for the diode temperature to achieve the setpoint change, prior to incrementing to the next temperature step. The results of the power-normalized methane scan can be seen in Figure 18. The diode temperature scan was done from 15-25ºC and then reversed. The temperature increment and decrement scan showed very close agreement in power through the gas cell. The lack of hysteresis made the wavelength tuning much easier to implement. Several more scans of the gas cell also showed very repeatable results, with the major absorption peak occurring at step 54 or T = 17.7ºC. Finally, Ophir performed a wavelength stability test by fixing the temperature to the deepest absorption line and monitoring the power to the detector. The power was monitored for 30 minutes and the power did not drift more than $\pm$ 2%, which indicated that the wavelength was not changing.

It was possible to verify the methane scans performed above to those that existed in the PNNL database. Figure 19 illustrates PNNL methane absorption data centered near the multiple absorption peaks near 1666 nm. Perhaps the easiest way of comparing the two methane plots was to count over the number of absorption peaks for methane from the flat response on the right hand side of the Ophir scan and the middle of the PNNL scan.

Remembering that the troughs were actually the absorption peaks, the number of troughs to the maximum depth (1666 nm) was six for both scans. This wavelength was also verified by measurements taken from an Ophir Optical Spectrum Analyzer (OSA), which measured the peak absorption to be at 1666 nm. One last observation was that the absorption lines on the right-hand side of Figure 19 showed less overall depth. This might be an artifact of the tuning step size being too large to accurately capture the entire peaks. There will be a trade-off on how small to make the calibration tuning steps, since smaller steps will extend the calibration time quite a bit. A good compromise was to use 0.05ºC for the step size.

The wavelength scan for ethane also revealed similar absorption peaks to those seen in the PNNL data base.
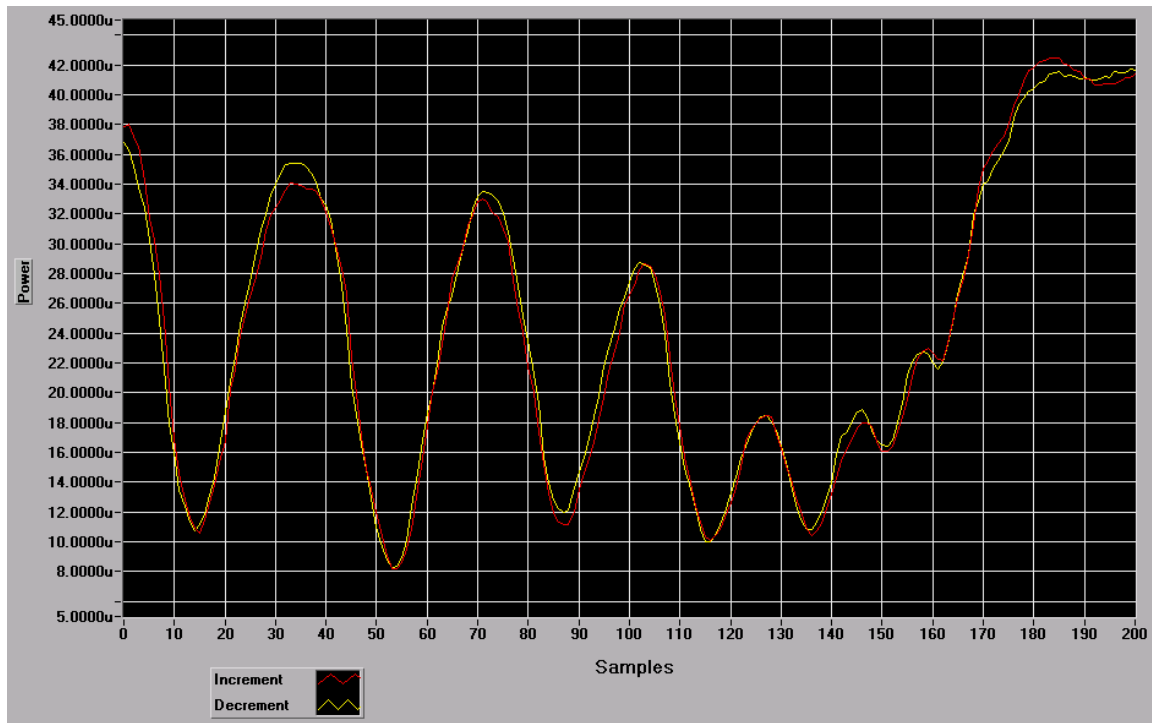
Figure 18. Normalized Wavelength Scan of Methane Gas Cell (Length = 7.5 cm) With 99.9% Methane. Vertical Scale Shown in µW of Power and Horizontal Scale Represented Temperature Steps of 0.05ºC
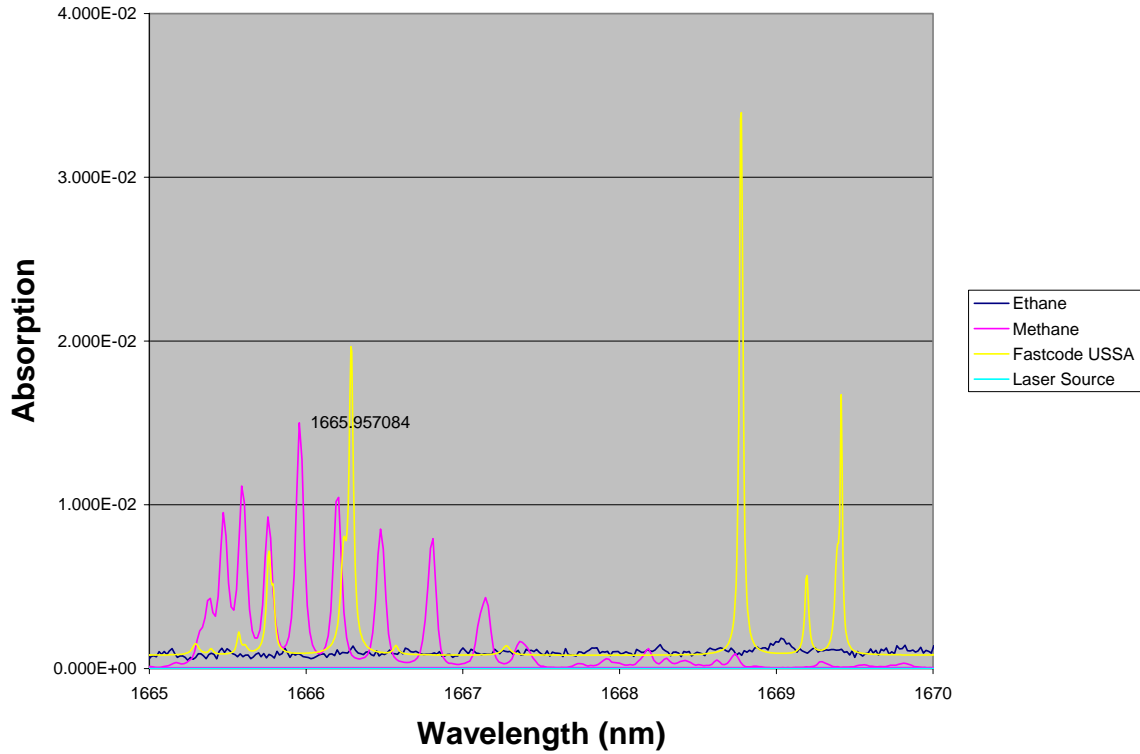
Figure 19. Composite Plot Showing PNNL Database and Fastcode Standard Atmosphere Water Vapor Content

One last plot which shows the modulated dual wavelength output feature of the HNLF is shown in Figure 20. The plot was taken from an OSA with a resolution of 0.05 nm and demonstrated the ability to modulate the amplifier between absorption wavelengths.
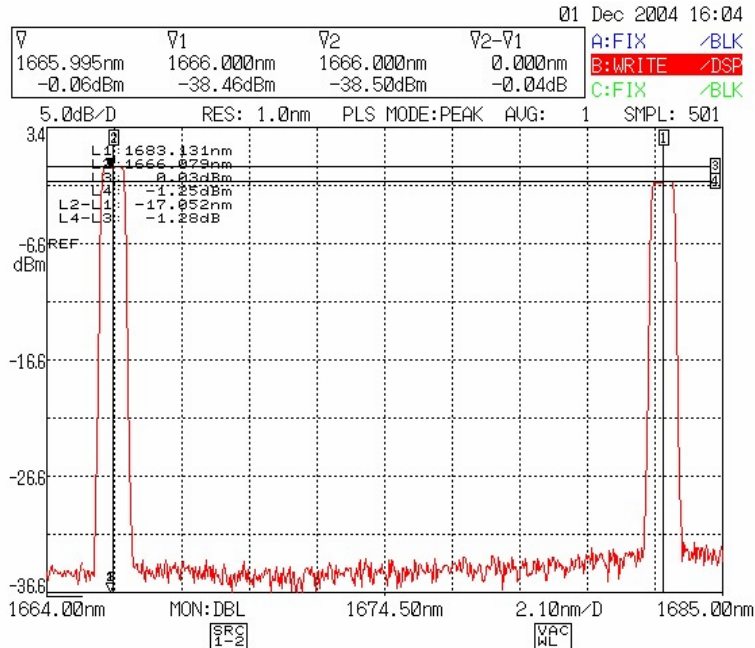
Figure 20.   Dual Output Wavelength from HNLF Amplifier Modulated at 1 KHz

3.8.3   Transceiver Design

3.8.3.1 Telescope Design

Target reflection measurements indicated that larger optics (> 2-in optics) would be required to meet the signal to noise requirements, when looking at the ground from an airborne system at 150-m altitude. The signal droped off inversely proportional to the square of the target distance. From 50 to 150 m, the signal to the detector is expected to decrease an order of magnitude or ten fold. At a minimum, Ophir determined that an 8-inch optic would be required to yield equivalent performance specifications at 150 m. Commercial telescopes were readily available with apertures of 8, 11 and 14 inches. The SCT had the advantage of a shorter optical focal length and was often the choice of astronomers for this reason. The airplanes that Ophir had access to for use as a flight platform all had height space restrictions in the cabin, so the SCT design was selected.

Ophir acquired a loaner 11-inch aperture telescope from Celestron to evaluate design concerns such as ruggedness and light transmission in the near-IR wavelength range. This model had the Starbright XLT coating, which was an upgrade and had slightly higher transmission. The XLT package had better coatings and a better corrector plate (made of white water glass). Directing a near-IR beam at 1555 nm into the telescope showed that the light transmission was 20% less than the advertised throughput for the visible wavelengths or about 60 % overall transmission. The visually clear corrector plate near the end of the telescope was probably the optic contributing to the highest transmission loss. Without the corrector plate, the telescope did not have the ability to focus the incoming light. It also acted to correct for spherical aberrations at the image plane.

As a result of the transmission testing through the loaner telescope, Ophir chose the larger 14-in. model with the XLT upgrade package. While the telescope may be somewhat larger than required, the large aperture should help to offset optical losses through the corrector plate. A picture of the telescope was shown previously in Figure 5.

3.8.3.2 Light Source Transmitter Optic

The fiber-coupled light source used an output SM fiber with a 9-µm fiber core that was fused onto a very short (1-2 mm) section of 40-µm core fiber. This fiber fusion technique is commonly used to produce a smaller power density across the fiber core, without impacting the overall fiber exit aperture angle. The fiber was coupled into a commercially available Thor Labs FC/PC fiber adapter fitted into a 1-in aluminum tube. The fiber output was focused using an anti-reflective (AR) coated 25.4 cm (1-in) diameter achromatic doublet lens with a focal length of 40 mm (1.6-in). The beam was focused to a minimum spot size of 5 cm (2 in) at 150 m (500 ft) distance. Toward the end of this project, Ophir located a vendor that manufactured custom large-diameter fiber collimators that were capable of focusing the fiber beam down to less than 1 inch diameter at 150 m distance. This should effectively increase the power density on the target, thus increasing the reflected signal. Although the collimators were normally built for the 1550 nm telecommunications band, they can be optimized to focus at 1640 nm using a narrowband tunable diode as the test source. Ophir placed an order for one of these collimators based upon the expected lead time of 8 weeks, which would have met our needs. Unfortunately, the lead time increased to 16 weeks and Ophir was forced to cancel the order. Future improvements to the system will most assuredly involve the use of such a collimator.

3.8.3.3 Transceiver Ruggedization for Airborne Use

It was hoped that the transceiver, consisting of the commercial telescope and the fiber coupled light source optic, with a few minor modifications could be made rugged enough to withstand the vibrations and shock of remote use in the field. The telescope had a movable primary mirror attached to a three-point fixture mounted onto a fixed-slide tube. The telescope focus was designed to allow lateral movement of the primary mirror along the slide tube using a fine threaded adjustment knob. Two other bolts were used to secure the primary mirror during shipment and following final focus. The holding bolts were modified to allow for locking nuts to be used against the rear surface of the telescope. The light source optic tube was mounted to a Thor Labs threaded kinematic mirror mount for 1-inch optics. A specially designed adapter plate was manufactured to attach the entire transmitter assembly to the center of the secondary mirror mount. The 1-in optic kinematic mount had three independent position adjusters with removable knobs for locking purposes. A weak point in this adjuster mount involved the use of springs to produce tension between the optic plate and the adjuster plate. Another source of movement was possible where the adjustment screws met the holder plate. The rounded point on the screw tip mated with the metal surface through three different methods, in an attempt to evenly distribute the screw contact surface. Movement was still observed when moderate sideways force was applied to the kinematic mount.

The procedure for aligning the transmitter and receiver optics was developed based upon Ophir's previous experience with lidar systems. The SCT configuration of the telescope consisted of a movable primary mirror and a somewhat fixed smaller secondary mirror. In actuality, the secondary mirror had three adjustment screws that could be used to adjust the collimation of the light into the primary. These screws were left at the factory adjusted collimation setting. The alignment procedure used was based upon the following steps:

- Illuminate the FOV of the telescope with a SM fiber-coupled visible light source (laser diode) through the rear fiber adapter. Position the illuminated spot upon the target at 150 m (500 ft) distance. Focus the FOV to the minimum resolvable focus.
- Illuminate the light-source optic with a SM fiber-coupled visible light source (laser diode) and position the spot on the target. Initially, the spot was focused down to approximately the minimum or 5 cm (2 in).
- Align the two light spots using the adjustments screws on the light source kinematic mount. Center the transmitter spot to the center of the telescope FOV.
- Replace the visible source into the transmitter optic with the near-IR (1550 nm) source and refocus the spot down to 5 cm (2 in).
- Remove the SM fiber from the telescope and connect the large core fiber from the telescope rear fiber adapter to the optical detector.
- Fine tune the alignment by monitoring the signal back into the optical detector.
- Test the alignment integrity by tapping on the telescope and the transmitter fixture. Rotate the telescope from horizontal looking to vertical looking and back again. Recheck the alignment.

Originally, the telescope alignment was meant to be done in the vertical orientation, which was how the telescope was mounted into the aircraft. To accomplish this, Ophir purchased a large 60-cm (24-in) square mirror to bend the optical path towards the ground target. The FOV spot of the telescope did not reflect well from the mirror and over some distance began to distort in shape. Ophir replaced the mirror with a higher optical mirror from a previous program with the same results. It is believed that the flatness of the mirror was not sufficient to evenly reflect the light over the large diameter of the telescope. The converging nature of the FOV also added to the distortion of the beam. The alignment procedure had to be changed to allow for the horizontal mounting of the telescope. A major concern was how the repositioning of the telescope vertically would impact the alignment. It didn't take long to determine that simple tapping and/or slight movement of the transceiver assembly caused unacceptable alignment changes.

Several design modifications were performed on both the telescope and the transmitter optic to finally meet the design goal. This entailed completely disassembling the telescope and adding features such as rigid tube mounting, and machining new locking hardware for the primary mounting bolts. Additional slots had to be machined into the telescope housing to allow for tightening of the locking hardware. The light source kinematic mount was also redesigned by removing the pressed fit adjuster screws and replacing with more positive locking-nut hardware. Opposing locking screws were also added to insure that the adjustment springs would stay in tension. The end result was a transceiver that was impervious to shock or vibration-induced alignment changes.

Photographs of the final ruggedized telescope and the light source transmitter are shown in Figures 21 and 22.
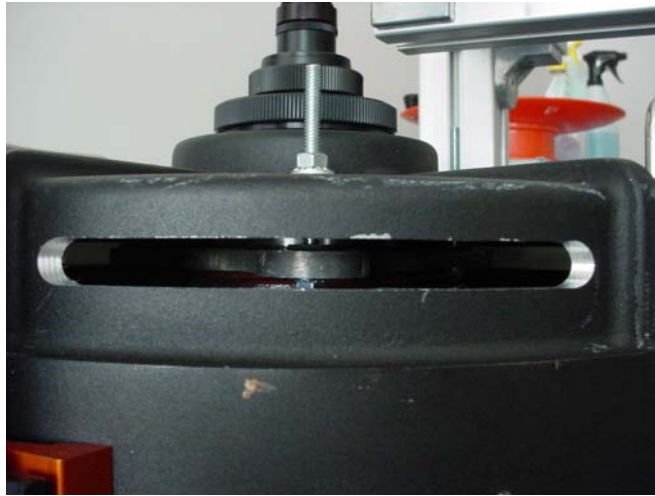
Figure 21. Rear of Telescope Showing Primary Mirror Locking Hardware and Adjustment Slot
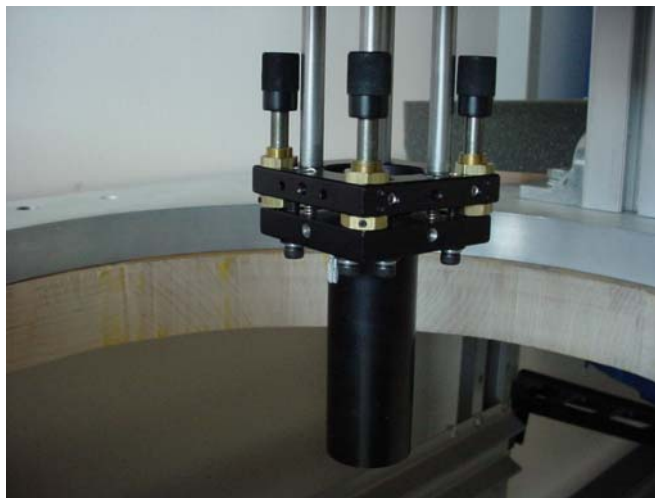
Figure 22. Light Source Adjustment Fixture

3.8.4   Airborne Transceiver Mounting Hardware Design

The telescope and the light source transmitting optics were co-aligned to a certain stare point or target. Optimally, the two should be aligned along the same axis, with the light source located at the exact center height of the primary and secondary mirrors of the telescope. The advantage to this design was that the telescope and the source optic could point at any target, regardless of the distance, and still be aligned with each other. Ophir adopted this configuration. The limiting dimension of this configuration was the overall length, since the optics were mounted in-line with each other. The length had to fall within the constraints of the cabin height of the small airplane chosen for the flight test.

Earlier in the project, Ophir had hoped to use the company-owned Beechcraft Bonanza as the airborne platform. Ophir intended to point the transceiver out the open side doors and to survey the pipelines at a non-normal angle. The reflection testing done in the laboratory showed that a downward-looking belly hole in the airplane was by far the best choice. Losses of 60-70 % of the reflected signal could be expected from a transceiver-target configuration mounted off-axis by 45°, as in the side exit Bonanza doors. The decision was made to locate possible lease aircraft in the Denver area with flight-test certified belly viewing holes. The most popular and most cost effective airplanes that met this requirement were the Cessna model(s) 206 and 207. The model 207 is a stretched version of the model 206 with a slightly larger engine and is capable of safely carrying more weight. They both have good control and performance at airspeeds below 100 mph, making them ideal for slow pipeline inspections.

Ophir worked out an arrangement with Aero Systems, Inc. of Erie, Colorado, reserving a Cessna model 207 on a monthly, weekly or daily basis beginning in July 2004. Aero Systems Inc. is actively flying a contractor-supplied lidar system on this airplane and was notified the company of our proposed flight schedule. Aero Systems, Inc. was helpful in supplying us with drawings of the cabin area showing the belly hole dimensions and mounting hardware.

The transceiver hardware consisted of the telescope, laser source focusing optic, telescope mounting rails, fiber-optic mounting adapters, mounting plate, and three vertical mounting rails. The vertical height of the rails is close to the maximum height of the cabin or 43 inches. These rails are made of extruded aluminum with lengthwise slots for attaching optical mounting hardware. The telescope is attached to two v-groove rails running lengthwise, which are mounted to four heavy-duty clamps that are bolted to the extruded rails. A third rail has been added to the mounting plate, which added stiffness to the rail assembly. The top of the rail assembly is stiffened by adding extruded bracing in order to prevent side-to-side motion of the telescope. The rail assembly was bolted to a large one-inch thick aluminum plate that was designed with mounting holes to mate to the existing shock mounts in the belly hole of the airplane. A picture of the transceiver assembly is shown in Figure 23.

Figure 23. Photograph of Airborne Transceiver Showing Mounting Hardware

3.9 Optical Breadboard Components

The optical breadboard contained the components necessary to accept the received fiber coupled light signal, filter the unwanted ambient light, split the light into two optical paths, perform a methane or ethane gas correlation using a fiber-coupled gas cell, and quantify the amount of signal present through the gas cell and the blank cell. The components were all designed to accept multimode 1000-µm core fiber with an NA = 0.22. Initially, smaller core fiber was proposed, but through reflection testing it was determined that much larger fiber was required to accept sufficient quantities of light. The tradeoff for using such fiber resulted in more complex and custom designs for the optical components. Much larger collimators were required to gather the fiber-coupled light than before, which also resulted in larger and longer optical assemblies.

3.9.1   Optical Detectors

Ophir has experimented with using large-core optical fibers (up to 1000 µm) in the receiver optical path, and has seen much better light coupling into the large area detector. The Agilent model 81624A large-area detector is very similar to the Agilent model 81634 detector described in previous setups. They interfaced with the Agilent optical mainframe, had similar data transfer characteristics, were sensitive over the same wavelength range, had the same averaging time of 100 µs, and operated over the same temperature range. The key differences resided in the type of fiber input they will accept and the noise levels. The large-area detector had the ability to accept large-core fiber,

whereas the 81634 detector was limited to fibers with cores up to 100 μm. The trade-off was in the area of noise levels. The large-area detector had a dark noise level that was roughly 25 times that of the 81634 detector or about 5 pW. Recent reflectance data has indicated that the amount of reflected light hitting the large core fiber was up to 100 times greater than with the standard multimode fiber, so the gain in signal should offset the gain in noise. Some of the earlier problems with light leakage into the fiber may become less of an issue, if the power received by the detector was many times higher than the observed leakage.

The optical detectors are located within a fiber-coupled external housing containing the sensing detector, biasing electronics and interface cable to the Agilent optical mainframe. They can be located up to 5 m (16 ft) away from the mainframe by using commercially available extension cables.

3.9.2   Optical Filters

The fabrication of the optical filters was a two-stage process, involving two different vendors. The optical filter substrates were ordered and delivered to Ophir by Barr Associates. One filter had been built with the methane-sensing wavelength as the center transmission wavelength and the other with the ethane-sensing wavelength as the center. The full width half maximum (FWHM) for the filters was 5.0 nm. The average transmission through the filters was between 75-80 %. Both of these filters were designed to highly reject the other center wavelength with 30 dB of rejection typical, guaranteeing complete independent discrimination of methane and ethane. The filters also had very good blocking characteristics of all visible light or in particular solar background light, adding to optical noise rejection.

Oz Optics was chosen to package the filter substrate into a large-fiber core coupled package. The fiber-coupled filters were a standard product line, but the fiber size and the collimators made them a custom design. The collimators within the package were again AR coated to minimize reflection loss. The overall length of the fiber coupled package was 5 cm (2 in).

3.9.3   Optical Splitters

Originally, the system design was developed using standard multimode 62.5-μm fiber core; and the corresponding 1:1 splitters were easy to obtain. The transition to larger fiber pushed us into a more custom design. Oz Optics was chosen to develop and design the splitters. The design specifications for the splitters were:

- Split ratio of 1:1 where the two outputs are equal in signal strength.
- Collimators optimized to focus light wavelength between 1650-1700 nm and accept and focus to 1000-μm fiber.
- Beam cube within splitter should be optimized to transmit and split light at 1620 nm (highest wavelength available to Oz Optics). There will be slight ratio difference for higher wavelength.
- Polarization changes in input shall not cause split ratio to change.
- Transmission losses through the splitter outputs shall be minimized.

The beam cube splitters used in the first design attempt were polarization sensitive, meaning that they would transmit one axis of polarized light better in one direction than another. It was assumed that reflections from the ground surface would be non-polarized since most research has shown that Lambertian surfaces tend to reflect light in such a manner. With totally non-polarized light, the beam splitters should divide the input evenly and consistently. Prior to using the splitters to collect and split light from distant targets, Ophir conducted numerous indoor tests using close-in targets. The collecting optic for these tests was the large 1000-µm tapered fiber itself. The reflective tests were done using several light sources of different wavelengths and linewidths focused onto a small reflective target and captured by the large-core fiber. These tests indicated that the type of target, the distance of the target, the light-source optical characteristics all contributed to varying split ratios. The split ratio from input broadband white light differed greatly from that of a narrowband 1555 nm source and similar findings were determined for different surfaces. This split ratio anomaly became even more apparent when two splitters were combined in series, which is required for sensing both methane and ethane at the same time. The first beam splitter actually had outputs that contained highly polarized light and when the polarized light entered the second beam splitter, the split ratio was changed radically. The first splitter usually approximated a 1:1 split, but the second splitter was anywhere from a 1:5 to 1:10 split. This caused great concern, since gas correlation by nature required only a ratio change in the event of changing ambient gas levels, not due to any other variables.

After communication with Oz Optics, it was decided to rebuild the splitters using completely polarization insensitive beam splitters. The transmission losses were slightly greater than the previous measurements, but additional testing showed that the ratios were unchanging regardless of the reflective target material or the target distance. The series connection of the beam splitters yielded similar findings. There was still some ratio change depending upon the wavelength of the light source, but the changes were much smaller than before at only a couple of percent. When the narrowband filters were put into the path (eliminating all but a single narrowband wavelength), the ratio differences were much less. Additional testing at longer optical pathlengths up to 150 m showed that the split ratios were the same as that seen at the shorter distance. This is an important result, since the altitude of the airborne remote sensor could vary over several hundred feet.

3.9.4   Optical Breadboard Assembly

The optical components that made up the gas correlation detection system had one thing in common; they were meant to accept and send out light via multimode 1000-µm core, NA = 0.22 optical fiber. The large-core fiber acted very much like a large light pipe, and like large pipe did not bend easily. Ophir could have used longer coiled up fibers, but some of the reflection testing indicated that any movement in the adjoining fibers caused some changes in the ratio. In order to minimize the overall size of the breadboard fixture and to minimize movement in the adjoining fibers, Ophir decided to use short custom length optical fibers to connect each of the components. These short runs of fiber were very stiff and required that the components be precisely positioned and at the same height. To accommodate these positioning requirements, Ophir utilized the same type of

extruded aluminum (smaller cross section) used to mount the transceiver. The sliding groove in the extruded railing provided flexibility when mounting the components. Spacers were used underneath the components to achieve the proper matching height. A photograph of the completed assembly (mounted to the transceiver) is shown in Figure 24.   The optical breadboard is connected to the receiver telescope by the long red optical fiber.   The overall dimensions of the optical breadboard assembly were 100 cm x 71 cm (40 in x 28 in). The first beam splitter used to split the methane and ethane gas channels is shown in the upper left hand corner. The beam splitter outputs were connected to the methane and ethane narrowband filters, which filter unwanted extraneous bands of light. The two splitters that follow the filters were used to further split the signal into a gas cell (yellow anodized fixture) and a blank channel. The signals are finally directed to the two large area detectors (long black cylinder) to be processed by the optical mainframe.
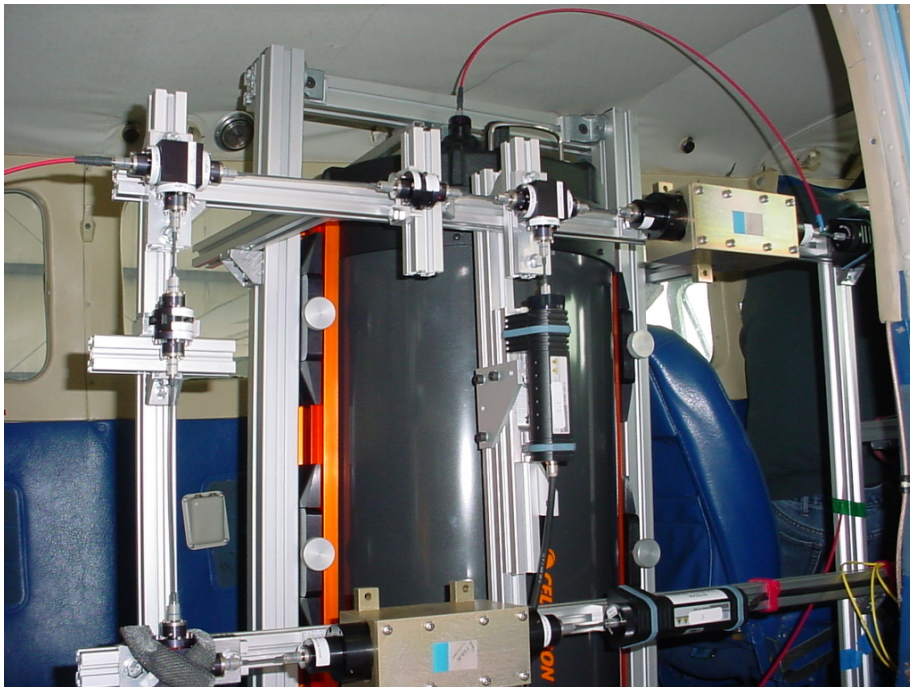
Figure 24. Optical Breadboard Assembly Shown with Transceiver (Ethane Blank Channel Detector Not Shown)

3.10 Airborne Remote Sensor Electronics Rack

Ophir has chosen an aircraft-qualified 19-inch electronics rack to house the system power inverter, fiber amplifier, optical data processing mainframe, and ruggedized laptop computer. This particular design was equivalent to an earlier FAA-qualified design utilized by Aero Systems. The rack was very lightweight and rugged with aluminum angle cross members on the sides. Weight of the rack and the contents totaled 160 # (pounds), with the transceiver and optical breadboard adding another 150 #, for a total system weight of 310 #. The entire rack assembly was shock mounted to a floor base plate that was attached to the seat rails with flight-qualified rail clamps (identical to the

clamps used for mounting the seats). A low center of gravity was utilized for mounting, while at the same time insuring operator ease of use. During this phase of the project, the operator was responsible for manually tuning of the amplifier and for maintaining the flight data acquisition software through the laptop computer user interface. The laptop computer was mounted to the top of a small shelf that jutted out from the front of the rack and was turned towards the user for ease of use. Some minor initial setup of the optical mainframe such as detector zeroing and wavelength selection was also required of the operator.

Onboard aircraft power was supplied through a 28 VDC alternator and inverted using a 1800 VA aircraft inverter. The total power requirements of the Ophir system were approximately 700 VA. A photograph of the electronics rack is shown in Figure 42. The assembly order of the electronics from top to bottom was the fiber amplifier, the laptop computer, the optical mainframe, and then the inverter was mounted to the bottom plate.

3.11 System Software Design

Software development for the airborne system can be categorized into the following four functions:

- Data processing algorithms for producing gas pathlength concentration values. Most of the data algorithms for retrieving gas concentration data from the raw collected data were derived from earlier software development for the ground-based gas radiometry system.
- Graphical User's Interface (GUI) to enable operator to setup data averaging times and display update rates, and to view delayed real-time data including raw signal, ratio signal, gas concentration, global positioning system data, and probable gas "hits" based upon threshold data.
- GUI interface to the fiber amplifier that allows operator to monitor and control amplifier operation.
- Post processing software for analyzing gas monitoring data results.

The operator of the airborne optical sensor was responsible for choosing the averaging times and data display rates, setting up the fiber amplifier to output the proper wavelength and power, and for setting up and zeroing out the optical detectors.   An example display of the data acquisition and display software is shown in Figure 25.
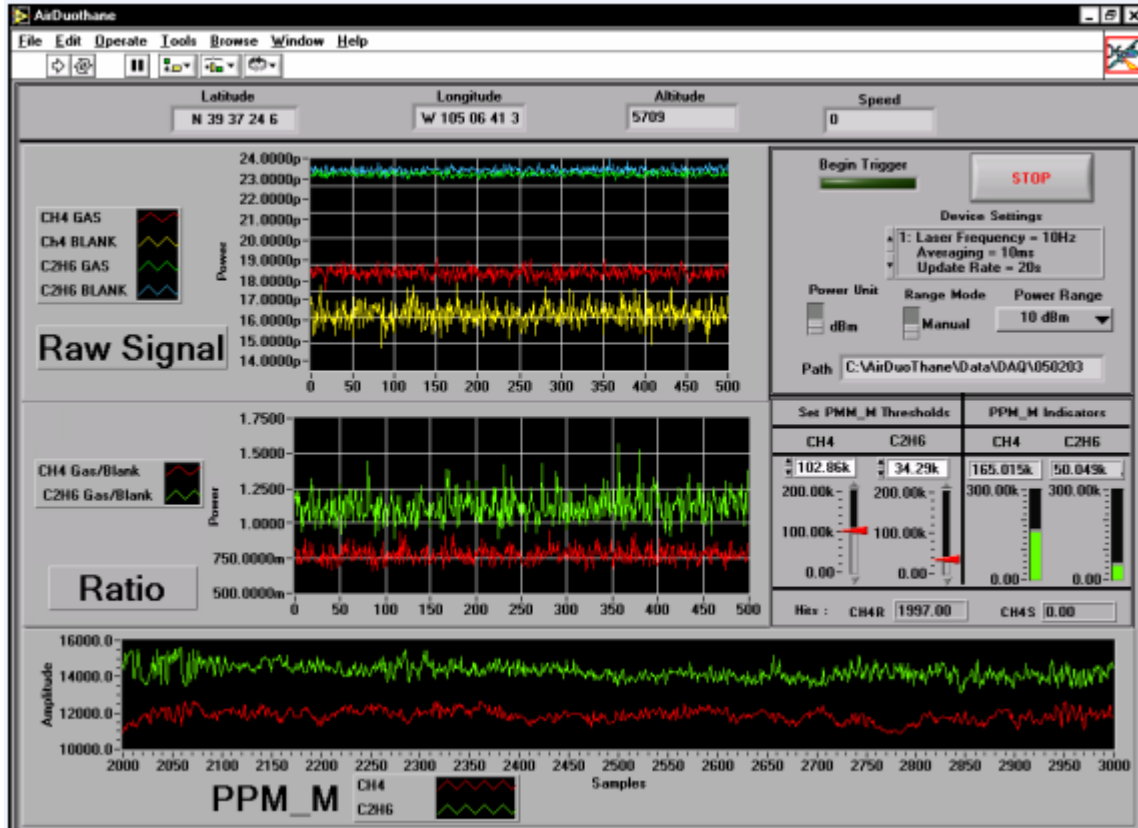
Figure 25. User's Software Interface for the Airborne Optical, Remote Sensor

The display contained information on the raw detector data after it had been processed to separate methane and ethane data from the multiplexed data buffers. The display also showed the ratio of the retrieved gas cell over blank cell data, normalized to subtract out all common mode signals. Finally, the gas concentration data was displayed in ppm * m over the intended flight path. The gas raw data, ratio data and concentration data are updated on the computer display at a user-selected rate, with a typical value being 20 seconds. The update rate was dependent upon the averaging time selected for the optical detector multiplied times the number of buffer memory samples. The larger the buffer memory, the longer it took to dump the optical data to the laptop controller. Unfortunately, the optical mainframe can not dump data and acquire data at the same time, so the update rate is usually optimized to both minimize the downtime and to see data results quickly. The Global Positioning System (GPS) data was gathered and displayed at a 1-Hz data rate. A separate display can be toggled on that will display the actual GPS route against the programmed route, identifying any deviations. High amounts of methane and ethane concentration are automatically displayed and stored into a data file. The user can dynamically change the thresholds for the high concentration "hits" during the flight test. This data file can be accessed at any time during the flight to allow the pilot to initiate repeat passes over suspected natural gas leaks.

The operation of the amplifier was performed using a combination of software driven commands and manual tuning through front panel knobs. Ophir driven design

specifications for the amplifier included the capability to completely control the amplifier with computer commands over three separate serial RS-232 communication buses: one for the seed source control, one for the C-Band pump control and one for the L-Band pump control. Manual control of the amplifier was also part of the design specifications. Test software delivered with the amplifier enabled Ophir to perform some low level testing. Ophir originally intended to control the amplifier totally through the computer serial interface and had developed software interfaces using the vendor supplied serial commands, but due to the lateness of the amplifier delivery and the complexity of the amplifier design it was decided to rely mostly on the manual operation features. One area where Ophir did use this software interface was in controlling the temperature of the seed sources, which controlled the output wavelength. A calibration of the system was performed daily and the resulting tuned temperature was input into the temperature tuning interface.

The function of the wavelength calibration software was to control the amplifier to a pre-determined wavelength that would yield a known calibrated gas ratio based upon background atmospheric methane. Any deviation from the expected gas ratio would severely impact the calculated gas concentration values. The major factor contributing to a gas ratio discrepancy was the position of the amplifier wavelength to the gas absorption line of interest. Any drift in this wavelength would produce immediate changes in the gas/blank ratio from the calibrated data, producing erroneous concentration data. Ophir wrote software that tested the overall stability of the wavelength, utilized a normalized routine to account for slight power drifts, and has documented the results.

Sample results from the wavelength calibration software routine are shown in Figure 26. The graphical display shows the absorption plot when incrementing and decrementing the seed diode source temperature. It was important to look at temperature control in either direction to make sure that the diode was not showing signs of temperature hysteresis. The plots clearly show the absence of hysteresis. The display also showed calculated values of the optimum tuning temperature based upon previous gas correlation data. So far, the calculated temperature for numerous calibration cycles has remained the same at 17.3 ºC, indicating a stable and predictable amplifier output.
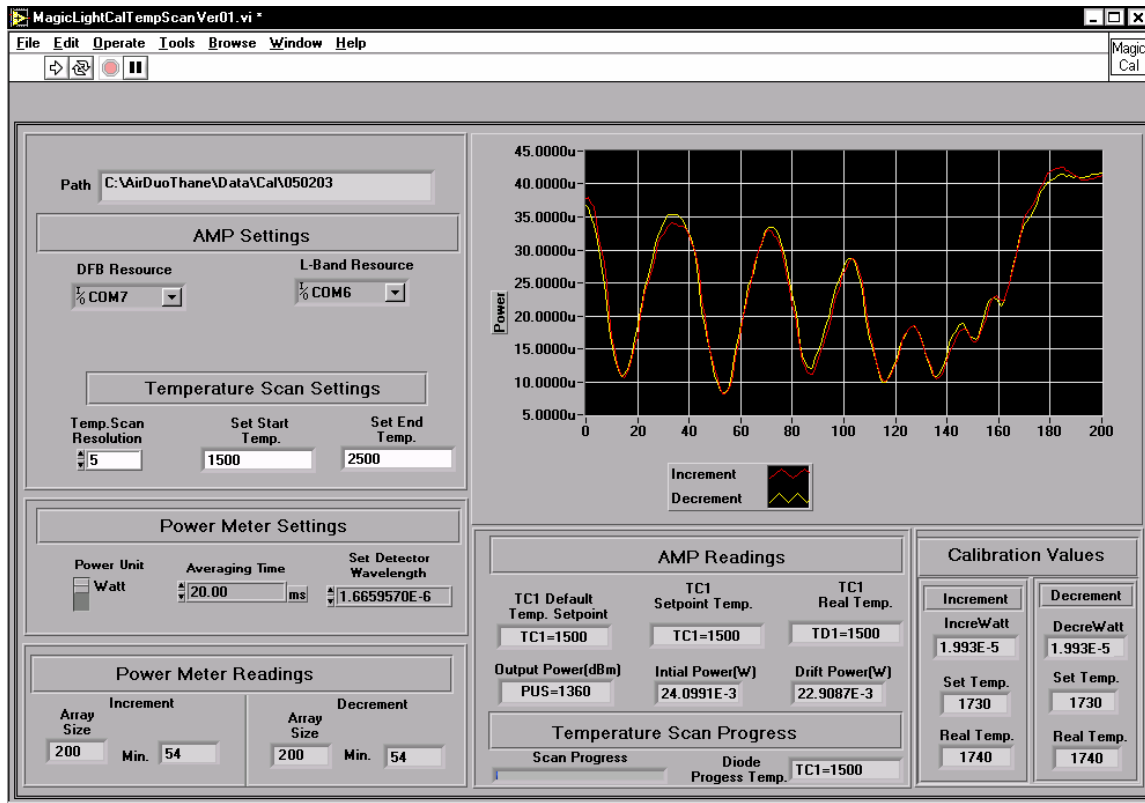
Figure 26. User's Interface for Obtaining Optimum Amplifier Tuning Temperature

3.12 Flight Test Results

3.12.1   Flight Test Results Using Airborne System with 1555 nm, 1-W EDFA Light Source

Prior to receiving the 1666 nm fiber amplifier, Ophir conducted several flight tests using the 1555 nm, 1 W EDFA light source operated in a continuous wave mode, to identify airborne configuration related problems. The presence of methane or ethane could not be detected with this light source. The configuration of the optical breadboard used in these flights was shown previously in the photograph in Figure 24. This configuration included monitoring of four channels; two for the methane gas and blank and two for the ethane gas and blank. Large 1000-µm core, low-aperture optical fiber was used for transmitting the collected light to the different optical components. It should be noted here that the narrow bandpass filter substrates centered on the methane and ethane absorption bands at 1666 nm and 1683 nm were not installed into the filter holders during these flights, since the filters would have blocked the 1555 nm laser light. Based upon ground testing, Ophir expected to measure laser return well in excess of the background return.

The optical mainframe unit was configured to take 100-µs detector samples, average them over a 20-ms period, download the averaged data to the detector memory buffer until the buffer contained a user selectable 20 or 40-second time period, and then display the data.   The trigger for the mainframe is user selectable, and can be set to automatically

retrigger after the buffer has been displayed or can be set to manually trigger. The plots were initially displayed to the user with the vertical scale automatically adjusted to units of Watts and the horizontal scale representing memory buffer location. Post processing of the data allowed Ophir to convert the horizontal scale to a time-of-day value, if desired.

The first flight of interest occurred on September 23, 2004 at 02:00 PM with clear to partly cloudy skies. The flight scenario was to capture the reflected light from the ground surface approximately 150 m (500 ft) away with the laser source first turned off, then capture the signal with the laser source turned on. The output power of the laser was between 600-700 mW. Airborne data snapshots showing raw and ratio data with the laser off are shown in Figures 27 and 28, respectfully and with the laser on are shown in Figures 29 and 30. The expected increase in the signal baselines were absent in Figure 29 and 30, indicating the laser spot on the ground was probably misaligned with the receiver FOV and the detectors were only sensing background solar light (the system had been aligned to a 150-m target on the ground the evening before, but was only aligned with the transceiver pointing horizontally at the target). The level of the solar background signal was very close to those observed during most of the previous ground testing. During the flight the amount of solar background signal was clearly proportional to the amount of cloud cover and the time of day. The later part of this flight was done closer to sunset with broken skies, and the detector return was lower.

When looking at the ratio data in Figures 28 and 30, it can be seen that the ratio noise for methane was substantially less than for ethane. It should be noted that the ratio vertical scales were different for these plots, and the ratio absolute values were actually the same. The difference in noise between the plots was indicative of the type of detectors used. For the methane channels a dual input module using the same trigger input was used, whereas for the ethane channels two single input modules were used. The time-stamped data for the gas and blank detectors were blended to create a ratio. The single-input modules appeared to have a slight delay associated with the trigger inputs, creating misaligned time stamps of the data. When flying over varying terrain, even a slight time misalignment added to the ratio noise. A second dual input module was purchased for the optical mainframe to insure that the ratio data results were absent of any time skew generated noise. An interesting spike in the signal and ratio data was seen. More flight testing began to shed light on these unusually high ratio anomalies. These anomalies correlated nearly every time with the presence of water. Water acted as an absorber of light in two ways; first, water vapor acted to physically absorb the light and second, the light tended to penetrate the water below the surface causing a reduced return. Therefore, the signal data showed a much reduced signal back to the detectors over water and a much higher ratio of the data, meaning the blank channel was reduced more than the gas channel.
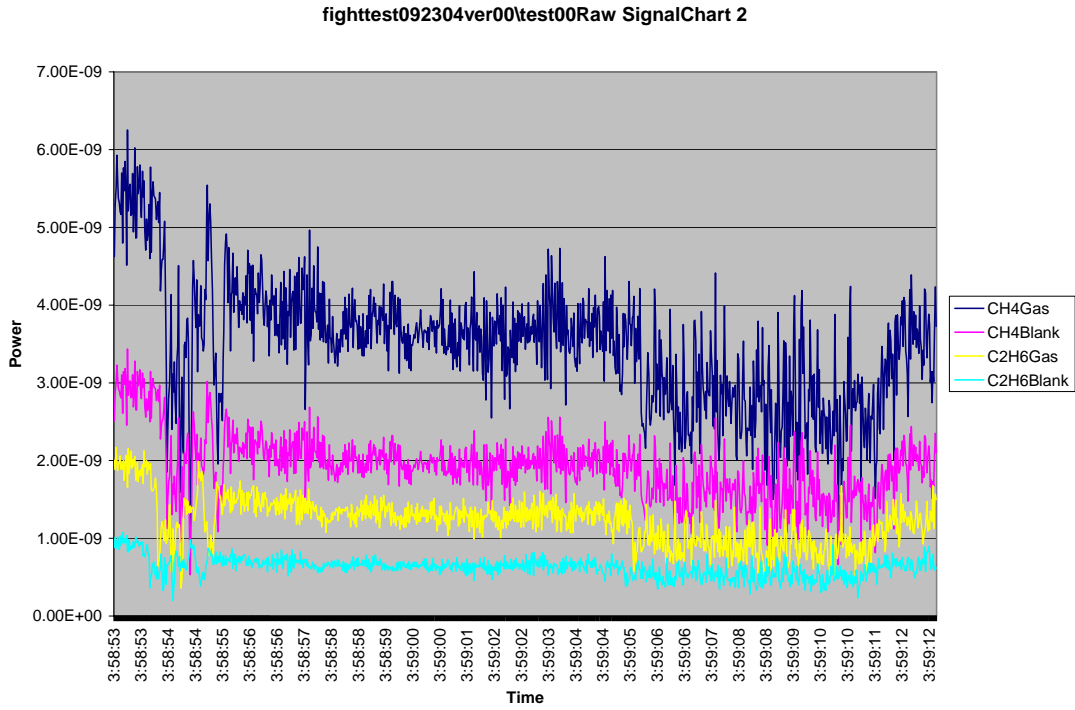
Figure 27. Raw Detector Flight Data with Laser Off Taken on September 23, 2004 Showing Power in Units of Watts for Methane and Ethane Gas and Blank Channels
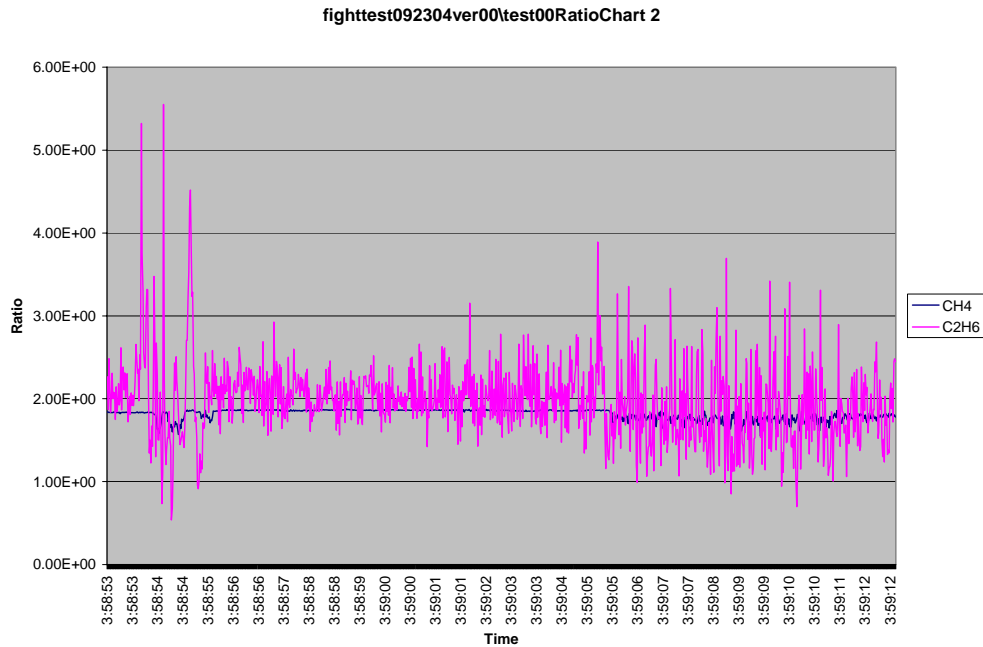
Figure 28. Ratio of Gas to Blank Channels for Methane and Ethane with Laser Off for Flight on September 23, 2004
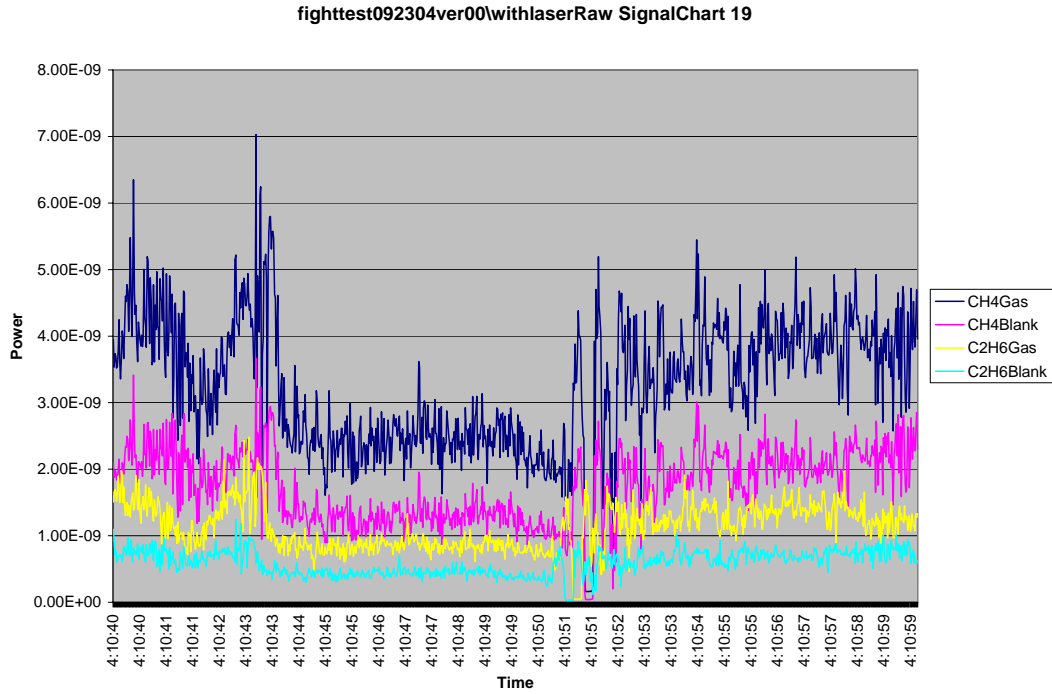
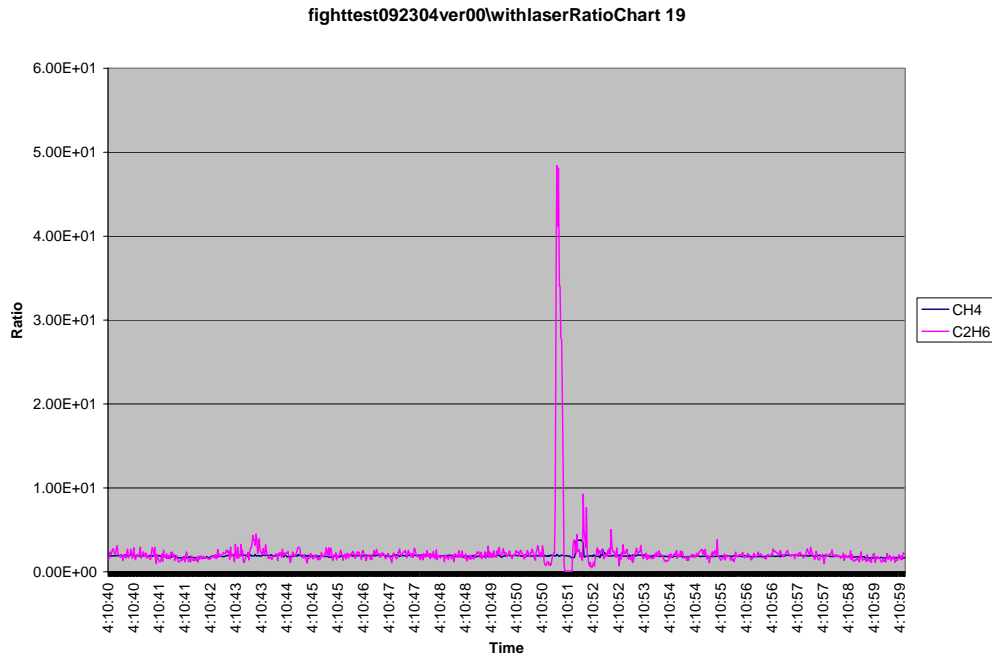**Figure 29. Raw Detector Flight Data with Laser On Taken on September 23, 2004 Showing Power in Units of Watts for Methane and Ethane Gas and Blank Channels**

Figure 30. Ratio of Gas to Blank Channels for Methane and Ethane with Laser On for Flight on September 23, 2004

Ideally, the transceiver would have been aligned on the ground mounted vertically as in the airplane, pointed at a folding mirror and focused onto the target. Normally, with fixed, locked optics it wouldn't have even mattered how the system was aligned, but the flight data indicated a flaw in the alignment procedure masking a slight movement in the optics. Ophir attempted many times to align the transceiver in the vertically upright mode to no avail. A perfectly collimated telescope would have yielded better results, but the airborne receiver was focused down from a 14-inch spot size to an ideal spot size of 2-3 cm (1 in) at 150 m pathlength. During ground testing this yielded the optimum signal return onto the large core fiber. Ultimately, the converging nature of the telescope FOV defeated the use of the large area folding path mirror. Extreme warping and beam wrap-around of the receiver FOV spot at the target was seen. Even a high quality, very expensive optical-grade mirror did not improve the results. Ophir clearly needed to determine the location and the extent of the movement within the transceiver optics, prior to performing any additional flight tests.

A realignment of the transceiver was performed, paying particular attention to the procedure for locking of the optics assembly hardware. Some minor vibration and shock testing of the transceiver showed still some small alignment movement. A second attempt to gather flight data on September 28th, yielded the same results as before, primarily the absence of any laser return. Quite of bit of redesign and testing was devoted to ruggedizing the airborne transceiver at this point.

After redesigning the transmitting optic assembly and providing better locking hardware for the telescope primary mirror, vibration and shock testing was performed on the transceiver to assure the transmitter and receiver stayed within alignment on a 150-m target. The transceiver assembly was subjected to minor high frequency vibrations by tapping the housing with metallic tools and shock tested with minor drops onto a table. These tests were performed on the transceiver while it was in an upright position and in a horizontal position, in order to identify any small movements due to different gravity effects on the optics. A change was also made to the focusing procedure of the telescope onto the target at 150 m. The goal here was to allow for some additional tolerance in optics alignment between the laser spot and the telescope FOV. The FOV of the telescope was increased to 10-11 cm (4-5 in) while the laser spot size was left at approximately 5 cm (2 in). The signal return at the detectors were reduced in magnitude, but were still high enough to yield acceptable signal-to-noise levels. The ground test results of the redesign were quite good and a flight was performed on November 20th to test the alignment.

The configuration for the November 20th flight test included removing the ethane gas and blank detectors from the optical breadboard. The original polarization sensitive optical beam splitters were the same as used in previous tests, except that only one splitter was required due to the absence of the ethane detectors. It was thought that the ratio variability seen when using the two beam splitters in series would become more predictable with just a single splitter. Previous testing had shown that variables such as terrain surfaces, optical fiber bend radius, and wavelength, all produced both changing and different split ratios out of the two outputs (a huge negative in gas correlation spectroscopy). For example, solar background produced a different ratio split than did 1555 nm laser light. This proved troublesome, especially in the absence of the

narrowband filters which limited the wavelength through the optical breadboard. Unfortunately, ground and flight testing showed that although the split ratio was less impacted, the single splitter still showed some dependence on the variables listed above.

Figure 31 shows a typical data snapshot of the methane gas and blank detector signal returns with the 1550 nm laser powered off and on. The background terrain was a mixture of plowed fields and crop stubble, and the laser output power was roughly the same as seen in previous flights. The horizontal scale was not correlated to time of day, as the GPS recording software was not working correctly for this flight. It was clearly seen that the signal level increased an order of magnitude when the laser was turned on, verifying proper alignment of the transceiver. The choppy transition between the off and on times was a result of the gradual turn on of the laser. Subsequent signal data plots showed much smoother levels of elevated return for the laser-on mode. This was the first flight where laser return was in fact measured from the airborne platform. The corresponding gas correlation ratio plot for the same time period is shown in Figure 32. One can see the ratio change fairly substantially as the laser return increased, indicating a continued dependence of the splitters on small polarization and wavelength changes. Numerous other important findings determined during this flight included:

- Increasing the altitude of the airplane above the ground from 150 m (500 ft) to 300 m (1000 ft) decreased the overall signal return by nearly 70%, but the return was still significantly above the acceptable signal-to-noise threshold.
- There was very little return seen by the detectors when flying over water. The gas correlation ratio jumped significantly as well over water. This proved to be useful when performing later methane scans, in order to help correlate positions of known leaks to known water sources.
- A scheduled stop at a nearby airport allowed Ophir to insert the 1666 nm narrowband filter into the optical breadboard. The background light dropped from 3-5 nW to less than 270 pW for the methane gas channel under similar solar background conditions (clear sky). In the absence of direct sun (due to clouds) at the end of the flight, the signal return was less than 20 pW.
- Gas correlation ratios still showed a higher dependence on target surfaces and altitudes than desired. Fluctuations of 20 % were common in the ratio data. This will increase the level of false alarms for methane detection, if not corrected.

The constantly changing gas ratio seen in the previous flight data sent up a red flag when using the optical beam splitters. It was originally assumed that the return from a lambertian reflector, such as the ground, would be diffuse and unpolarized. This assumption did not appear to be correct given the ratio data gathered during this last flight. Ophir corroborated these findings by performing laboratory testing using different surfaces. Ophir determined that in order to produce more stable ratio data, polarization insensitive beam splitters would be required. At this time, the vendor was instructed to design and build just such optical splitters. These splitters were received in early January 2005.

flightr1Raw SignalChart 62
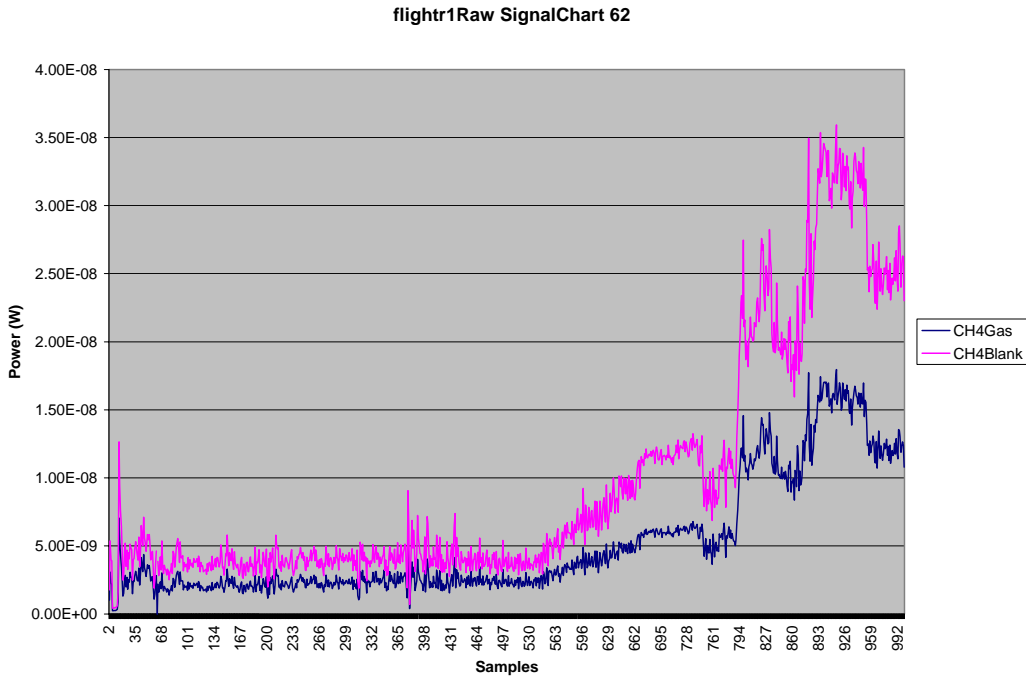
Figure 31. Data Snapshot for November 20th Flight Showing Methane Signal Return for Laser Powered Off and On (Time of Flight 02:40 - 03:53 PM)

flightr1RatioChart 62
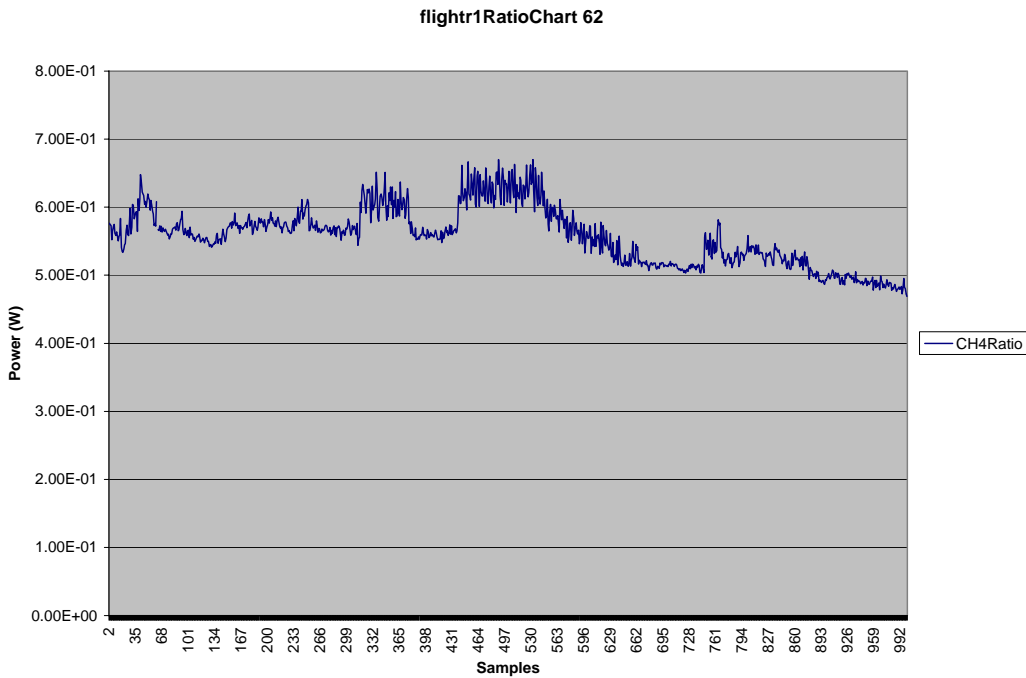
Figure 32. Corresponding Data Snapshot for November 20th Flight Showing the Methane Gas Correlation Ratio

## 3.12.2   Long Path Ground Test Results Using Airborne System with HNLF Methane and Ethane Light Source

The ultimate goal of the airborne system was to detect the presence of methane and ethane gas, commonly associated with natural gas pipeline leaks, but the flight testing that has been described to this point was done using a light source incapable of sensing either gas. Ophir finally received the long awaited light source capable of outputting two different wavelengths that overlap methane and ethane absorption lines in early December 2004. The amplifier experienced operational problems throughout the first two months, requiring three separate repair cycles back to the amplifier vendor. Finally, the amplifier performance issues were resolved and beginning in February 2005, Ophir was able to collect methane absorption data at long optical paths.

The first series of ground testing in February involved calibration of the airborne sensor against known concentrations of methane gas. Variable concentration, ranging from 0% to 99.9% methane, gas cells 3.651 cm (1.44 in) in length were placed into the light source beam path and signal return from the 150-m remote target was measured. A photograph of the setup used for this test is shown in Figure 33. The polarization independent beam splitter was also incorporated into the absorption setup along with the narrowband 1666 nm filter. Note the small gas cell positioned on the angled mount located in front of the light source transmitting optic. These tests proved to be inconclusive due to the impact of the glass surfaces of the gas cells on the gas-to-blank ratio. When a glass cell with no methane was placed into the path, a shift in the ratio was observed, making it hard to discriminate the ratio increase due to methane versus that due to the glass windows of the cells. To make matters worse, the ratio difference was highly dependent on the angle of the glass surface, which in the field was hard to control.

Figure 33. Photograph of Outdoor Test on February 14th Determining Gas Correlation Ratio Changes Due to Variable Gas Concentration Gas Cells in Optical Path

To continue on with the calibration testing, Ophir elected to switch from the closed gas cells to open gas cells consisting of open sections of 7 cm (3 in) diameter PVC tubing with a single methane inlet tube. The methane concentration within the tube was varied by switching tanks of variable concentration levels. The sample averaging time for the optical mainframe detectors was set at 20 msec and the data snapshot duration was 20 seconds. This absorption test although not as well controlled as the closed-gas cells, provided the first real indication of ratio changes due entirely to the presence of methane. Figures 34 and 35 illustrated the impact of injecting 99.9% methane into the open tube on the gas correlation ratio. Figures 34 and 35 showed the initial opening of the gas cylinder valve, and Figures 36 and 37 showed the ratio and signals the next data snapshot, where the methane has been on for awhile. The large short duration initial jump in the ratio was due to the initial opening of the valve, where a short sudden methane burst into the tube was evident. The surface winds were also along the direction of the tube at 5-10 mph and quickly dissipated the methane from the tube. Once the valve has been opened for awhile, the ratio level stayed well above the baseline level. Closing the valve on the bottle yielded the ratio and signals seen in Figures 38 and 39, and, closely matched the baseline measurements taken before the methane release.

2005-02-14\Night1740_100PercentRatioChart 2
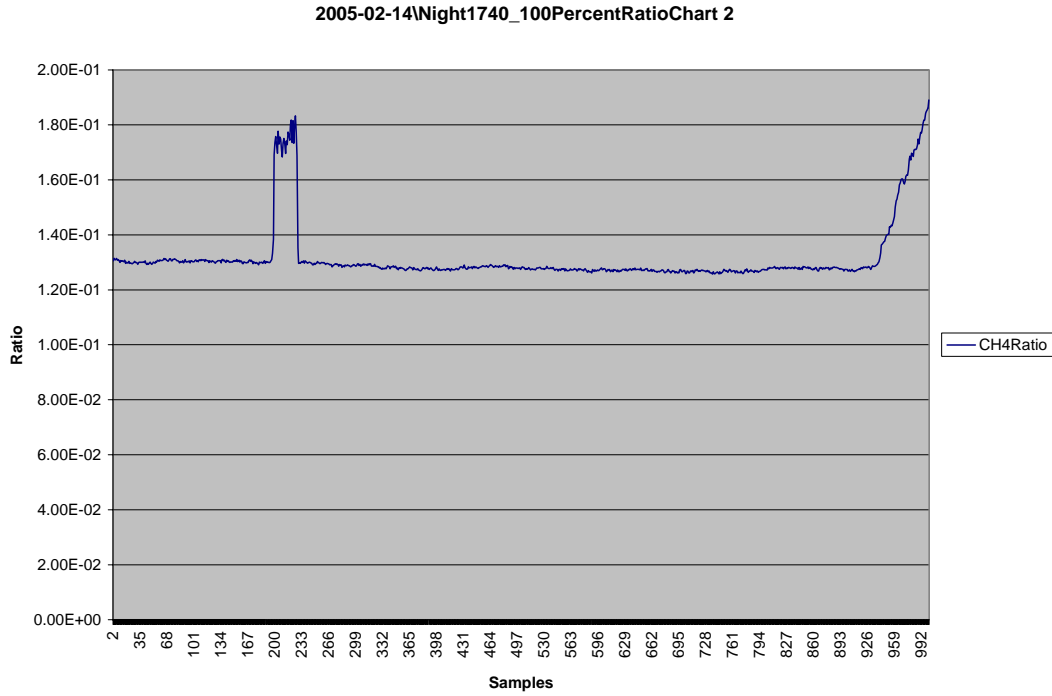
Figure 34. Outdoor Evening Test on February 14th Showing Gas Correlation Ratio Changes Due to Injected 99.9% Methane into Optical Path

2005-02-14\Night1740_100PercentRaw SignalChart 2
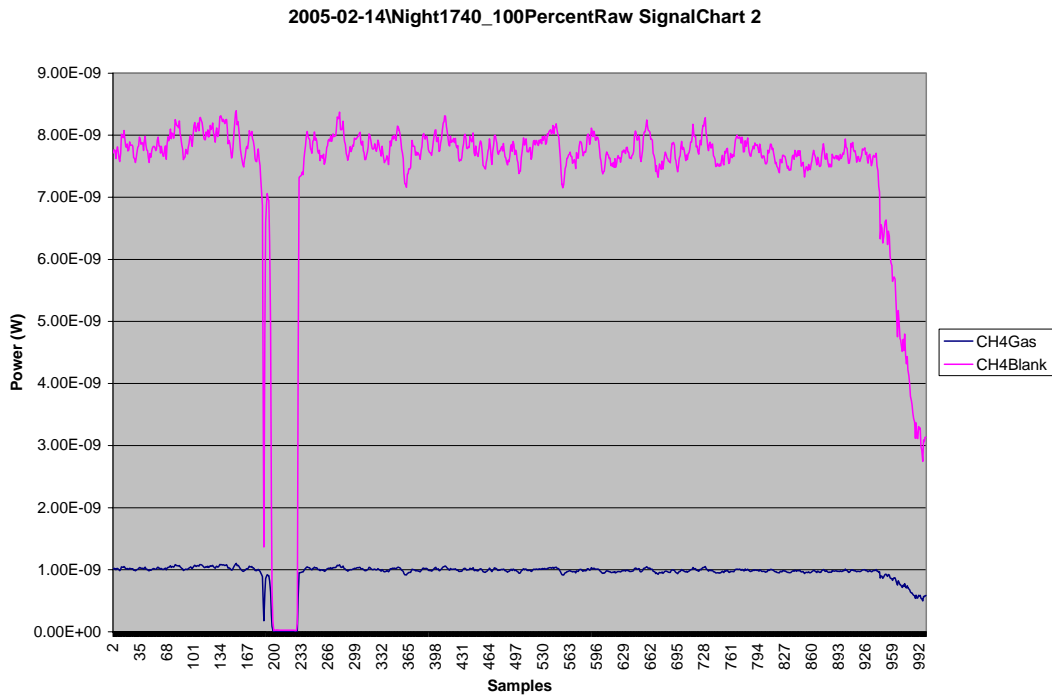
Figure 35. Outdoor Evening Test on February 14th Showing Gas and Blank Detector Changes Due to Injected 99.9% Methane into Optical Path

2005-02-14\Night1740_100PercentRatioChart 3
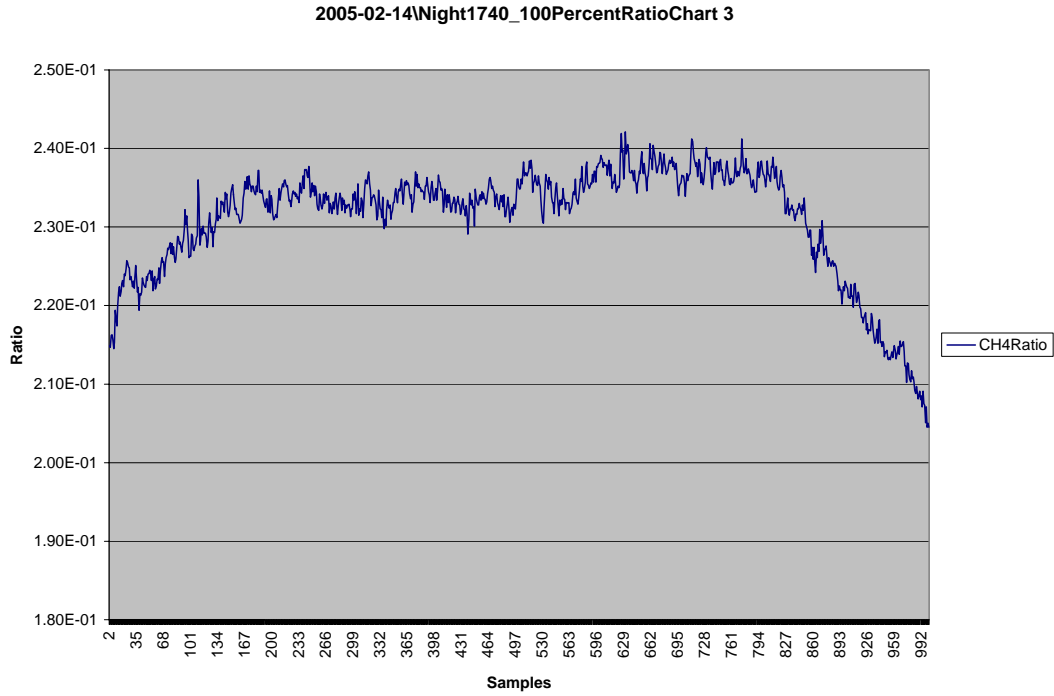
Figure 36. Next Data Snapshot of Gas Correlation Ratio for February 14th Outdoor Test Looking Through Injected 99.9% Methane

2005-02-14\Night1740_100PercentRaw SignalChart 3
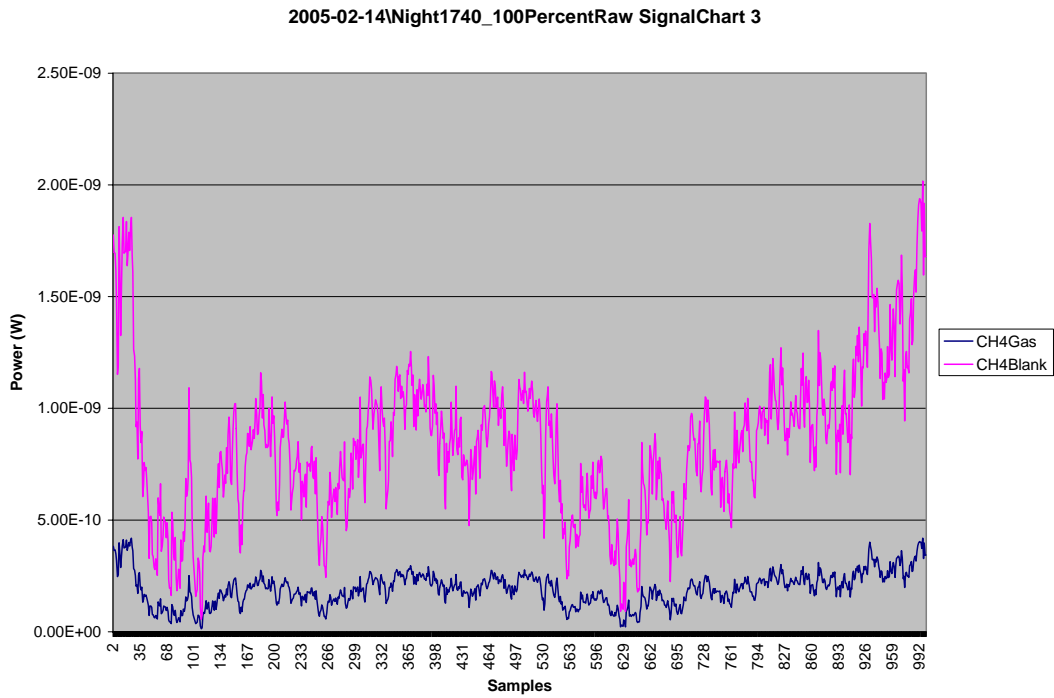
Figure 37. Next Data Snapshot of Gas and Blank Detector Changes for February 14th Outdoor Test Looking Through Injected 99.9% Methane

2005-02-14\Night1740_100PercentRatioChart 13
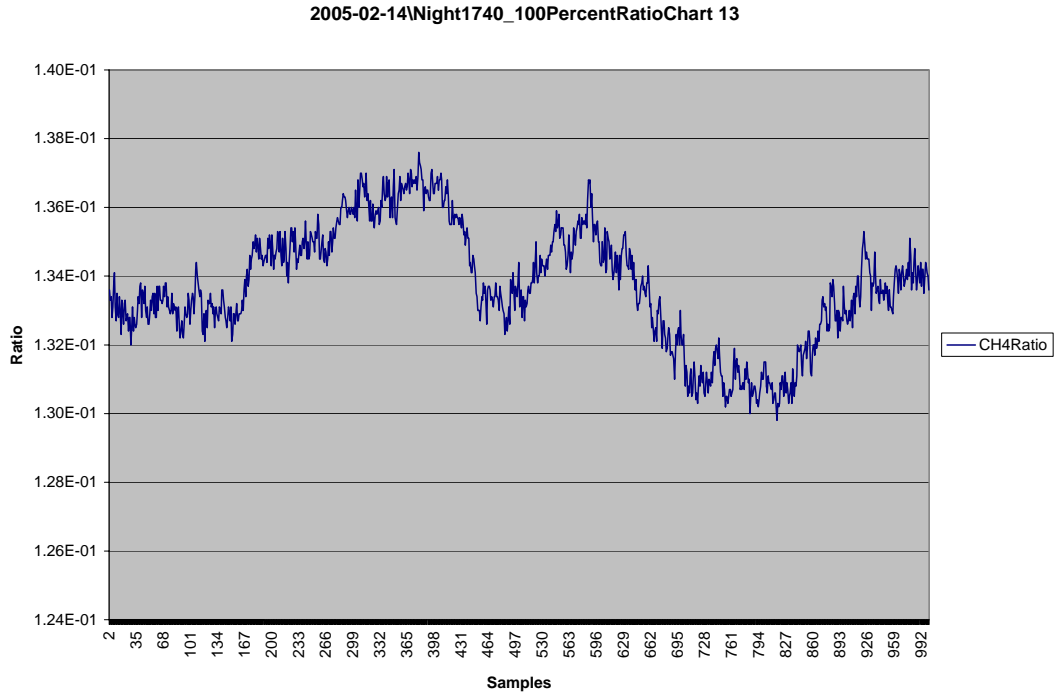
Figure 38. Gas Correlation Ratio for February 14th Outdoor Test Following Closing of the 99.9% Methane Gas Cylinder

**2005-02-14\Night1740_100PercentRaw SignalChart 13**
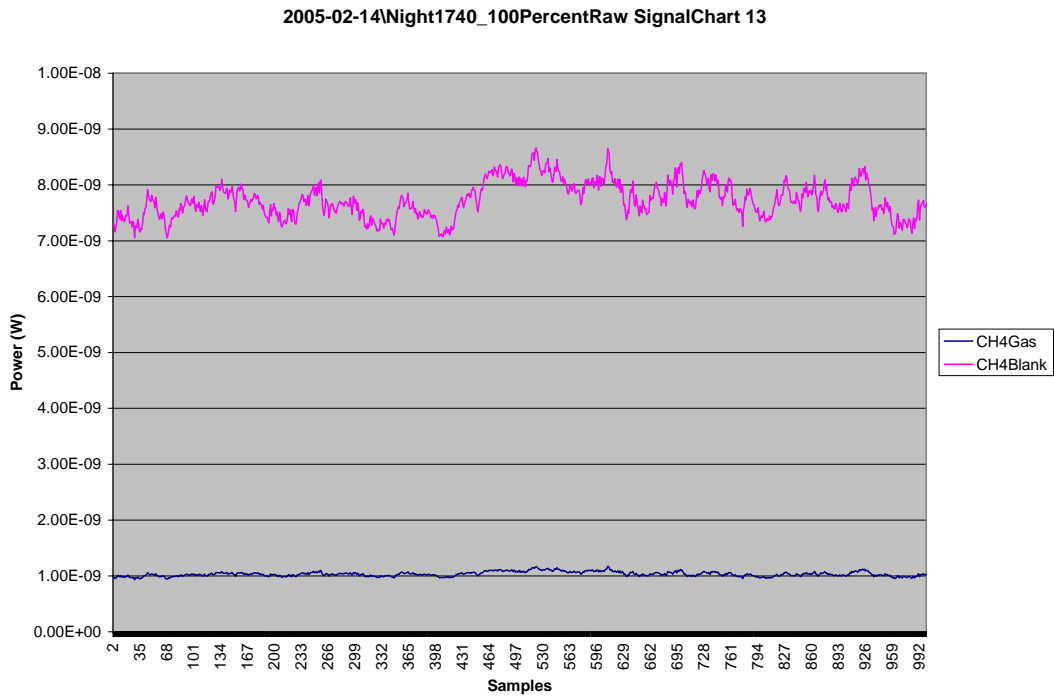
Figure 39. Gas and Blank Detector Signals for February 14th Outdoor Test Following Closing of the 99.9% Methane Gas Cylinder

From Figure 38 it was evident that there was some background noise associated with the ratio data, as evidenced both by the "hair" on the waveform and the longer term drift. This type of ratio signature was apparent in all the remaining signal and ratio plots and was an important discriminator of system noise versus actual methane absorption.

Ophir conducted the same open tube tests using lower concentration methane releases of 10% and 1%. The gas correlation ratio and signal data for the 10% methane release is shown in Figures 40 and 41. The chart showed a similar ratio and signal change when the bottle was opened, only smaller in magnitude. This result was evident in all of the data snapshots taken for the 10% release. The data taken during the 1% methane release showed less defined but nonetheless smaller levels of increased gas correlation ratios. Lesser methane release concentrations below 1% did not show any ratio changes.

2005-02-14\Night1740_10PercentRatioChart 3
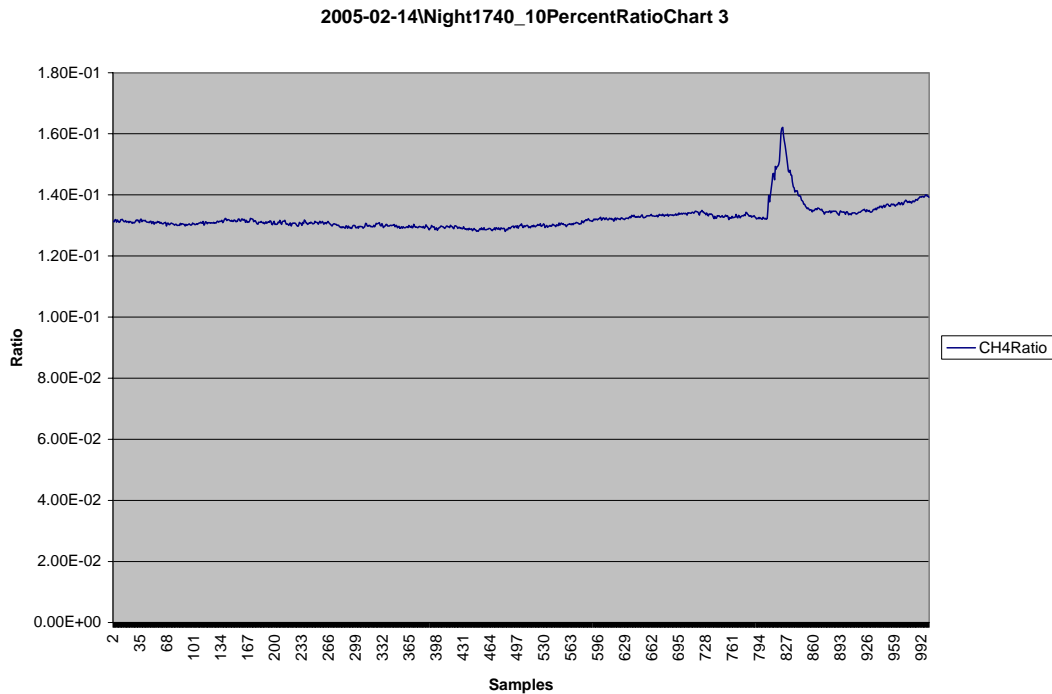
Figure 40. Gas Correlation Ratio for February 14th Outdoor Test with 10% Methane Release into PVC Tube

2005-02-14\Night1740_10PercentRaw SignalChart 3
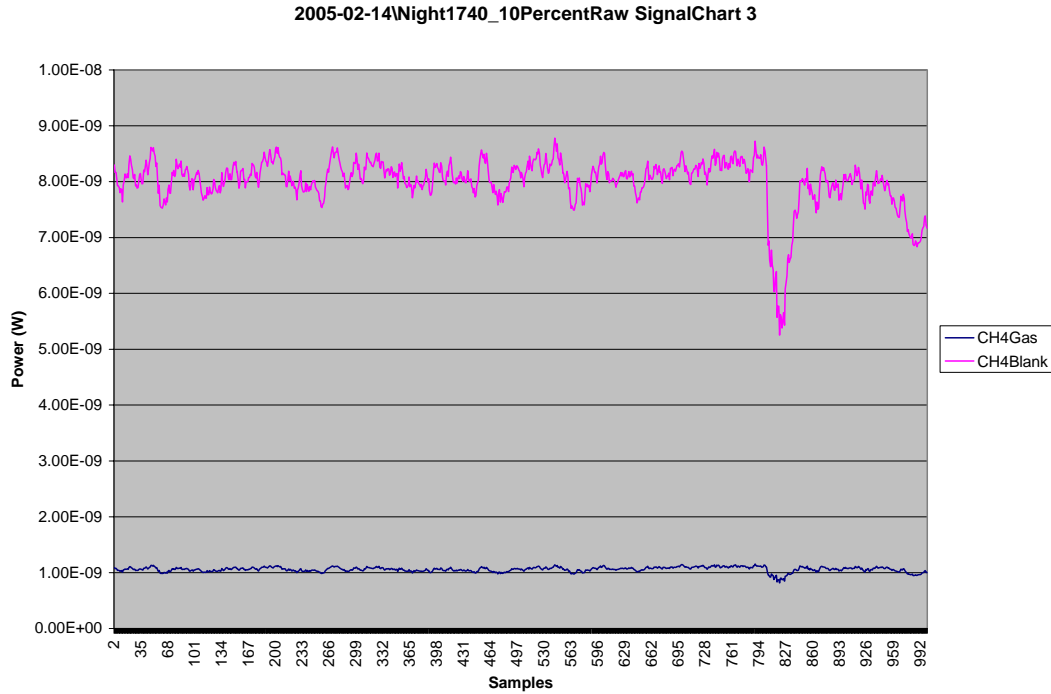
Figure 41. Gas and Blank Detector Signals for February 14th Outdoor Test with 10% Methane Release into PVC Tube

3.12.3   Flight Test Results Using Airborne System with HNLF Methane and Ethane Light Source

3.12.3.1   Aircraft Installation of Airborne System with HNLF Light Source

Based upon the ground test results gathered on February 14th, Ophir decided to next mount the equipment onto the Cessna Model 207 to measure gas absorption from an airborne platform over controlled methane releases on the ground. The installation of the airborne system took place on February 17th and 18th. Ophir had already been in the air several times with this aircraft, so the installation was done pretty quickly. The only installation differences dealt with the mounting of the HNLF amplifier into the 19-in equipment rack and converting the optical breadboard into a methane-only configuration.

A thick aluminum plate with four aircraft elastomer shock mounts was hard mounted to a fixed tray within the rack. The HNLF amplifier was next placed onto the aluminum plate with foam padding in between the amplifier and the plate. Four securing bolts were attached through the front panel ears on the amplifier into the rack. The bolts were also foam isolated from the rack and only loosely tightened to allow for the amplifier to rest on the shock mounted plate, not on the panel ears. A photograph showing the amplifier installation is shown in Figure 42. The system laptop computer is also shown on an extruded aluminum tray, facing the test operator seat.

Figure 42. Photograph of Installation of the HNLF Amplifier within the 19-inch Electronics Rack

Figure 43. Photograph of Optical Breadboard in the Methane Detection Configuration

The optical breadboard, shown in Figure 43, consisted of 1000-µm diameter fiber coupled components including the narrowband 1666-nm centered optical filter, 1:2 non-polarization sensitive optical beam splitter, pure methane gas cell (optical depth = 10 cm), and two Agilent large-area optical detectors sensitive out to 1700 nm. The optical

interconnects between the components were accomplished through the use of short, variable length 1000 μm diameter, FC/PC terminated, NA = 0.22 optical fibers. The framework for the optical breadboard was built with extruded aluminum railing, slotted for adjustable positioning of the components. This structure proved to be strong and lightweight, and saved considerable time when repositioning of the components.

3.12.3.2   Site Selection for Controlled Methane Leak Release

The primary goal of the airborne, remote sensing project was to detect the presence of methane and ethane from a ground leak source from an airborne platform. With the delays in receiving the fiber amplifier, it was decided to concentrate on measuring methane only from the air. It is hoped that follow-on testing later in the year will prove the system capable of sensing ethane, as well. Short of a real working pipeline, a well-controlled release using bottled methane was determined to yield the most useful test results. The site selection process for locating the leak source was based upon the following criteria:

- Flight pattern over release point must be clear of tall structures, which might impede the pilot from flying at the desired altitude of 150 m (500 ft) above the ground.
- The flight pattern must be clear of dwellings related to residential homes and businesses.
- The site must have minimal terrain features that might impact flying over the release point or impact the release of the methane gas. Flat unimpeded terrain absent of large areas of trees was determined to be the ideal test site.
- Ready vehicle access to the release site is required.
- The site must be within 30 minutes flight time from the base airport located near Erie, Colorado.
- The release site requires entry permission from landowner or leasing entity.

The site selection was narrowed down to two locations, one near Platteville, Colorado and the other within the Pawnee Prairie National Grasslands in Northeast Colorado. While the National Grassland site was remote and free of structures, the Platteville site was chosen due to its close proximity to the base airport (within 15 minutes flight time). A topographical map showing the site proximity to Platteville and the contour gradients is shown in Figure 44. The GPS-located position labeled as DITCH corresponds to the release point. The terrain relief was relatively flat with a slight upward gradient on a line from northeast to southwest through the site. Although there were several of houses withione-half mile of the release site, they were not in the direct path of the anticipated test flights. Interesting surrounding features included a large chicken farm due east of the site, across from the nearest road represented by thin black lines, a small pond within 100 m (333 ft) to the east, and several active gas wells within 400 m (1330 ft). Immediately surrounding the site were either plowed or fallow fields. The fields contained loose dirt in the plowed sections and hay stubble (some tall weeds) elsewhere. A site survey using a flame ionizer device (FID) was performed on the site following the first flight, identifying any sources of leaking natural gas such as the active gas wells. A FID analysis was also performed around the perimeter of the chicken farm and two cattle feedlots, located one to two miles northeast of the site. The chicken farm did not show

any elevated levels of methane, but the largest cattle feedlot did show levels of 20-30 ppm above the background methane. This measurement would prove to be an important detail during flight testing. A detailed photograph of the DITCH site looking to the north along the 130-m-long axis is shown in Figure 45. A close-up photograph of the DITCH site showing the vegetation and relief of the depression is shown in Figure 46. There was no snow present in the DITCH site during any time of the flight testing.
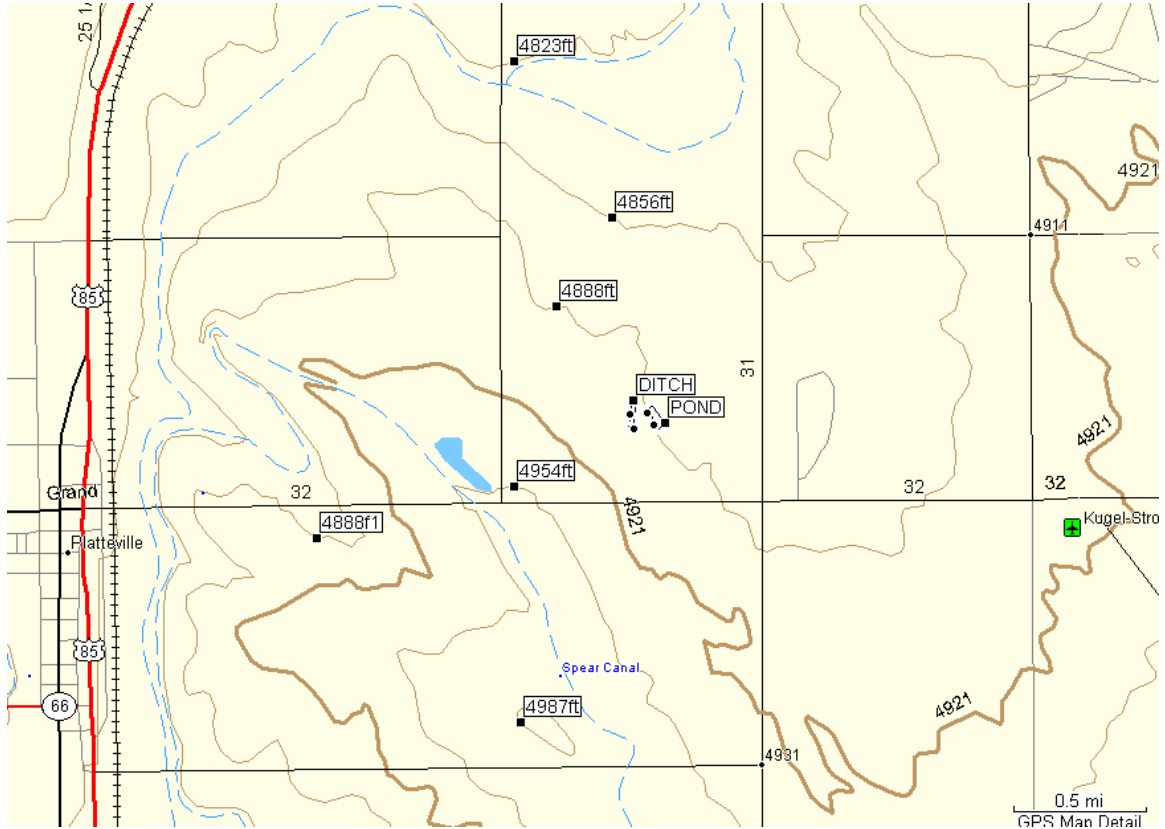
Figure 44. Topographical Map of Methane Release Site near Platteville, Colorado

Figure 45. Photograph of DITCH Methane Release Site Looking North

Figure 46. Detailed Photograph of DITCH Methane Release Site Showing Terrain and Vegetation

3.12.3.3   Flight Test Performed on February 19, 2005

The first flight tests using the complete airborne system, including the HNLF methane-sensing light source was completed on February 19th. The flight scenario consisted of a flight in the morning, which turned out to be more of a system checkout turning up several problems, and a second flight in the afternoon that included numerous passes over

the release site. Weather data was collected from a surface station shown in a photograph in Figure 47. The methane bottle release rate on the ground for both flights was measured by a flow meter to be 75 standard cubic feet per hour (scf/h). A photograph of the methane cylinder release is shown in Figure 48. Plastic tubing carried the methane to a copper tube lying horizontally on the ground surface with numerous small slits to allow for vertical dispersion of the methane. This rate was considerably lower than what previous airborne methane measurement systems have been able to detect.[2]

Figure 47. Photograph of Weather Station used during Flight Testing

---

[2] "Field Testing of Remote Sensor Leak Detection Systems", Final Report Submitted by: U.S. DOE Rocky Mountain Oilfield Testing Center under DOE Contract No. DE-AC01-04WR01058, SwRI® Project No. 18.10485, December 2004, Southwest Research Institute®

Figure 48. Photograph of Methane Cylinder Release for Flights on February 19th

The first flight indicated a data collection problem with both the detector signals and the GPS data coordinates. The computer display of the detector and GPS data (delayed in real time by 40 seconds) showed bogus or out-of-range values for the detector and a display of all zeros for the GPS coordinates. The out-of-range values for the detectors were traced to the auto ranging function of the optical mainframe. The auto ranging function can only record detector power data that spans four orders of magnitude. Anything that falls outside of this range is displayed and recorded as a very large number, improperly skewing the power scale of the detector. This problem was seen before in previous flights, but was corrected in the software setup by overriding the auto ranging mode with the correct manual range setting. Unfortunately, at the last minute a new version was loaded onto the computer that did not have this feature. The computer operator did not debug the problem until well into the flight. The GPS data coordinate problem was thought to be isolated to a boot-up problem with the system, where the RS-232 to USB communication hub was not recognized by the computer. Rebooting of the system in the air did not correct the problem and it was decided to scrub the flight at this point.

Some time was spent on the ground to isolate the GPS problem, with some success. The communication between the computer and the hub was reestablished and the correct GPS data was recorded and displayed. The new detector acquisition software was loaded onto the computer, correcting the ranging problem and a second flight was performed later in the morning. Figure 49 showed certain selected flight paths over the methane release site. The ditch is shown as a brown-shaded region within the GPS waypoints surrounding the ditch interior. The length of the ditch is oriented along a south-north

line, with north towards the top of the page. The methane release was measured by a flow meter to be 75 scfh and was located within 20 m of the southern tip of the ditch.
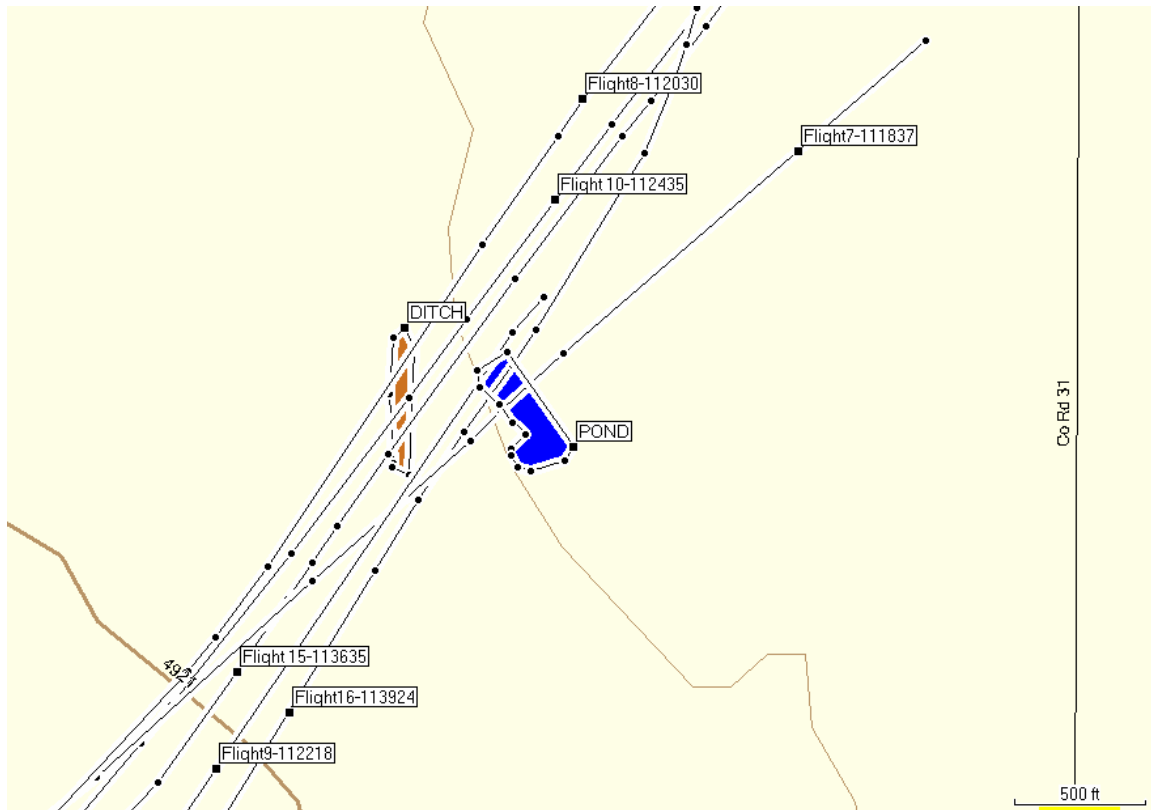
Figure 49. Flights Paths for Second Flight on February 19th

Flight paths 7, 9, and 16 clearly missed the ditch to the south, and passed over the pond to the east of the release point. The water signature (typically very low signal return and high ratio) was clearly evident in the raw signal and the ratio data towards the end of flight # 9 as shown in Figures 50 and 51, and indicated no methane-induced ratio change near time 11:27:03 (time of flight over southern end of ditch). It should be noted that there was a time difference of + 4 minutes and 35 seconds between the GPS-collected flight path data and the computer generated signal display data. This time difference was due to the fact that the computer was not synchronized to the recorded GPS clock. At time stamp 11:26:52, a slight ratio change and a large signal change was seen in the data. This did not correspond to any known sources of methane, although there were numerous gas wells and pipelines in the area. A flame ionizer device (FID) ground analysis was performed several days later to determine the presence of flammable gases near this location, but none were found. Flights # 7 and 16 showed similar water signatures without any unusual ditch release induced ratio or signal changes.

Flight paths #8, 10 and 15 passed over the ditch release site with path #15 being the closest. Direction of these flights was from the northeast to the southwest. The wind direction and wind speed at the time of these flights can be seen in Attachment 2, Table 4. Time of day measurements were based upon the computer clock (not the GPS clock),

the same as shown on the horizontal scale of the ratio and signal data display. The winds were generally from the northeast at speeds near 5 mph. Raw signal and ratio plots for these three flights are shown in Figures 52-57. It should be noted that the vertical scales were autoscaling and were, therefore, not the same for all plots. A general analysis of the plots showed a noise level consistent with that seen in the laboratory. The background noise was seen as higher frequency noise, and as longer term noise drifts (several second drift seen in Flight #8 ratio data near time 11:24:45). This noise was likely associated with the wavelength drift of the amplifier. Tighter wavelength control specifications in the future should yield better overall sensitivity. The real items of interest are those peaks associated with sudden noticeable ratio changes above the noise level for example, at time 11:25:13 of the ratio plot for Flight #8. These excursions from the noise level indicated some sort of ratio change, either associated with the presence of methane or due to some other external affecting the ratio. This same ratio peak was seen in other plots at about the same location on the flight path. Unfortunately, the peak did not appear to be correlated well with the location of the ditch methane release point. The smaller ratio peak seen near the center of the plot for flight #10 (time 11:29:06) actually correlated to the approximate location of the ditch release point. These peaks were smaller and closer to the background noise level on Flights # 8 and 15. It was theorized that the slight ratio change (2-4 %) associated with the ditch release point was maybe due to a terrain induced change rather than methane. The raw signal levels certainly dropped off coincident with the ratio change, indicating significantly less return (maybe gas absorption). The overall gradual decrease in raw signal towards the back end of these flights was probably due to a slight ground elevation increase along this geographical line, which decreased the optical path from the plane to the ground. Previous testing proved that the signal back through the telescope decreased as the optical path decreased below 150 m (500 ft). This altitude impact on the signal was actually worse than when the airplane went above the 500-ft ground adjusted altitude. Previous flight testing indicated that acceptable signal returns were seen by the system up to a ground adjusted altitude of 300 m (1000 ft).

As stated before, Ophir conducted an exhaustive FID survey following these flights on February 19th. Several days later, the goal was to help isolate the source of the large peak excursion towards the end of flights #8, 10 and 15. The location of the peak was ascertained from the GPS coordinates for that time. Repeated attempts to measure elevated gas levels near the flight paths proved futile. There were several gas wells in the area that showed levels of methane above the ambient, with the highest level over 50 ppm, but these wells were not directly in the flight path. Conclusions based upon the flight test results of February 19th were as follows:

- Inconclusive results were obtained when trying to detect methane leaks of 75 scf/h. Some evidence of elevated ratios near the ditch release site was seen, but it was not obvious that these were due to the slight terrain change or to methane.
- When flying over any water, the signal returns decreased drastically and the gas to blank ratio increased just as dramatically. This indicated absorption of the light either by the presence of water vapor or through penetration beneath the surface.
- Some areas of elevated ratios could not be explained by the presence of methane. These appear as false alarms and need to be studied in more detail to determine

whether certain terrain features were impacting the signal return through the blank and gas cells differently.

- It was difficult to consistently hold the flight path directly over the release point. Drift of the airplane, even with low wind speeds, caused some flight paths to miss the release point. Ultimately, a single axis scanning system may be required.
- Two flights over large cattle feedlots consistently yielded higher gas correlation ratios, perhaps indicating the presence of methane.
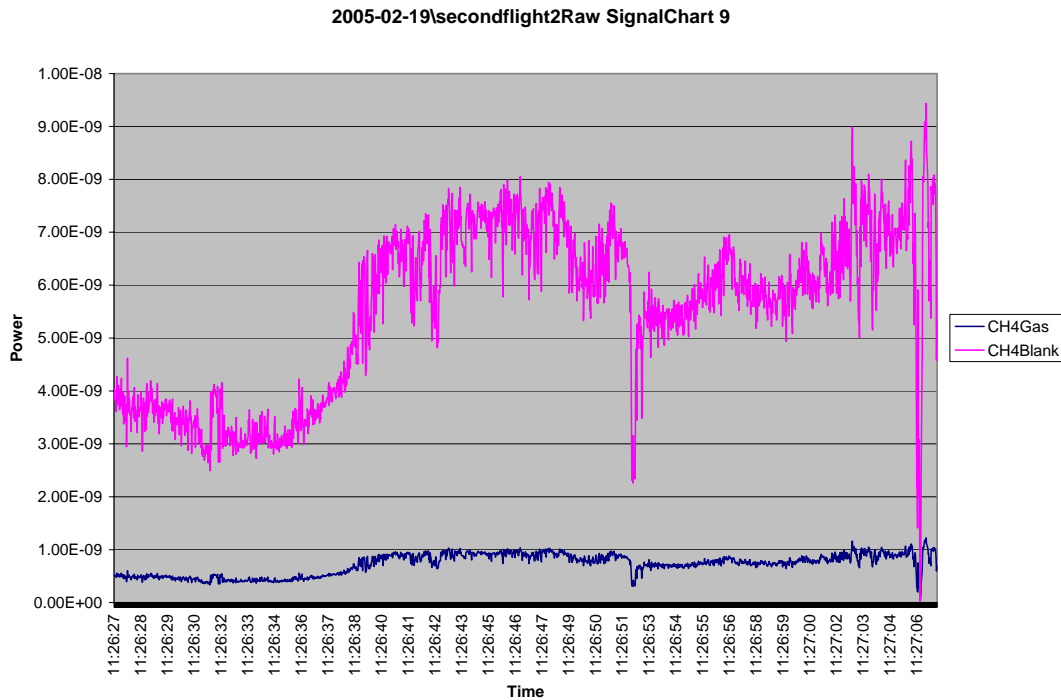
Figure 50.   Raw Detector Signals for Gas and Blank Channels during Flight # 9 on February 19th

2005-02-19\secondflight2RatioChart 9
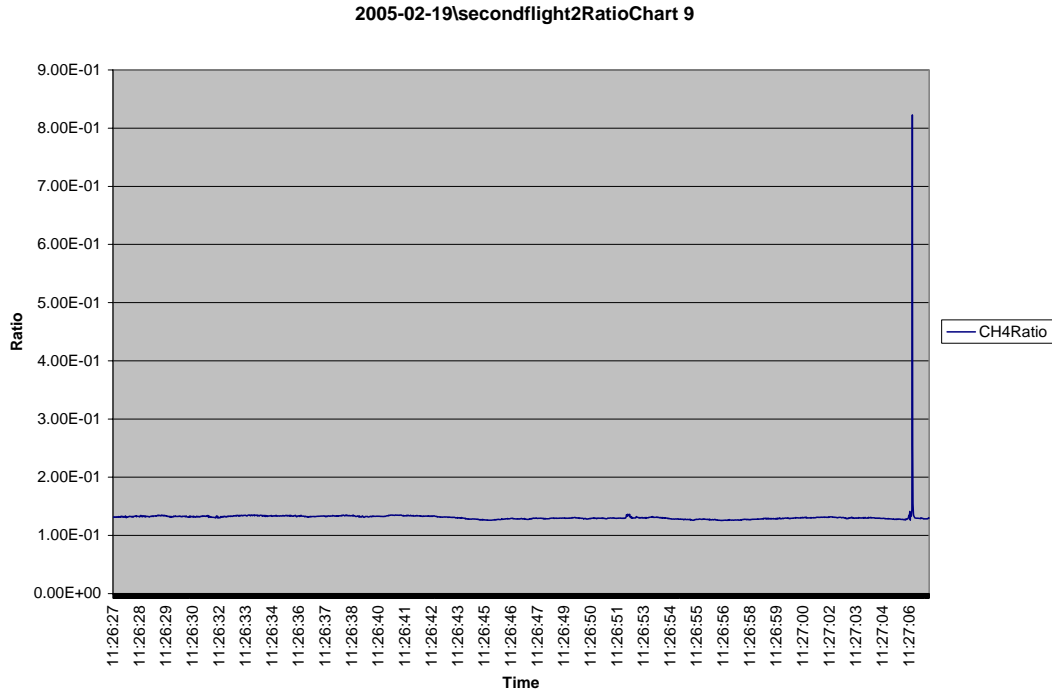
Figure 51. Gas Correlation Ratio for Flight # 9 on February 19th

2005-02-19\secondflight2Raw SignalChart 8
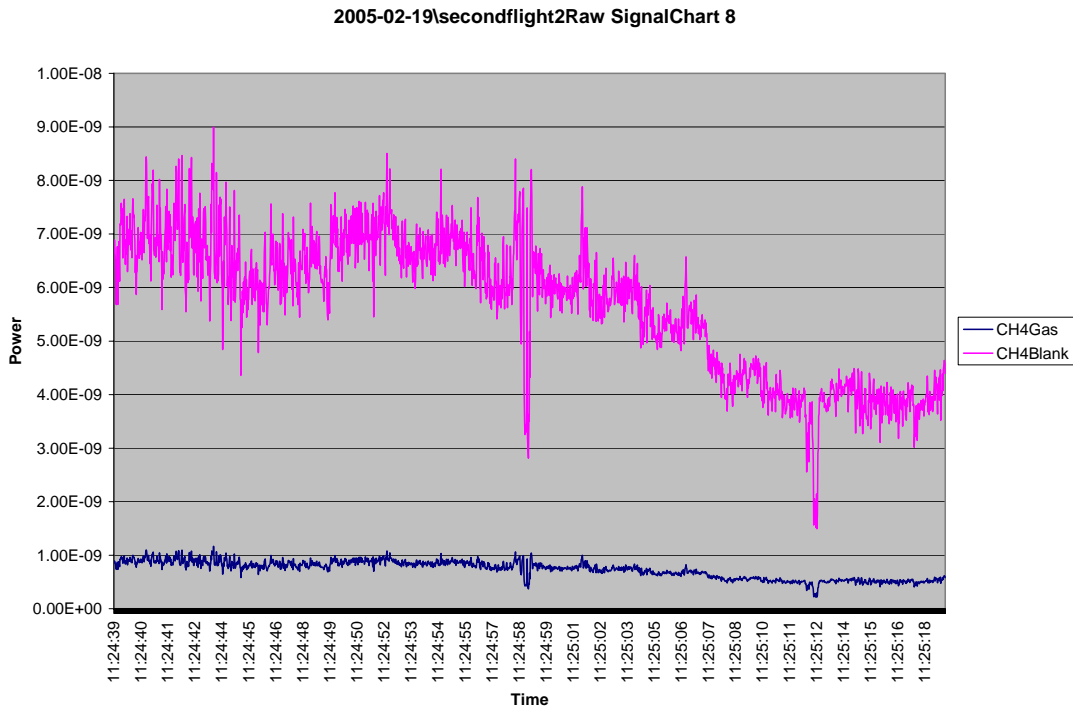
Figure 52. Raw Detector Signals for Gas and Blank Channels during Flight # 8 on February 19th

2005-02-19\secondflight2RatioChart 8
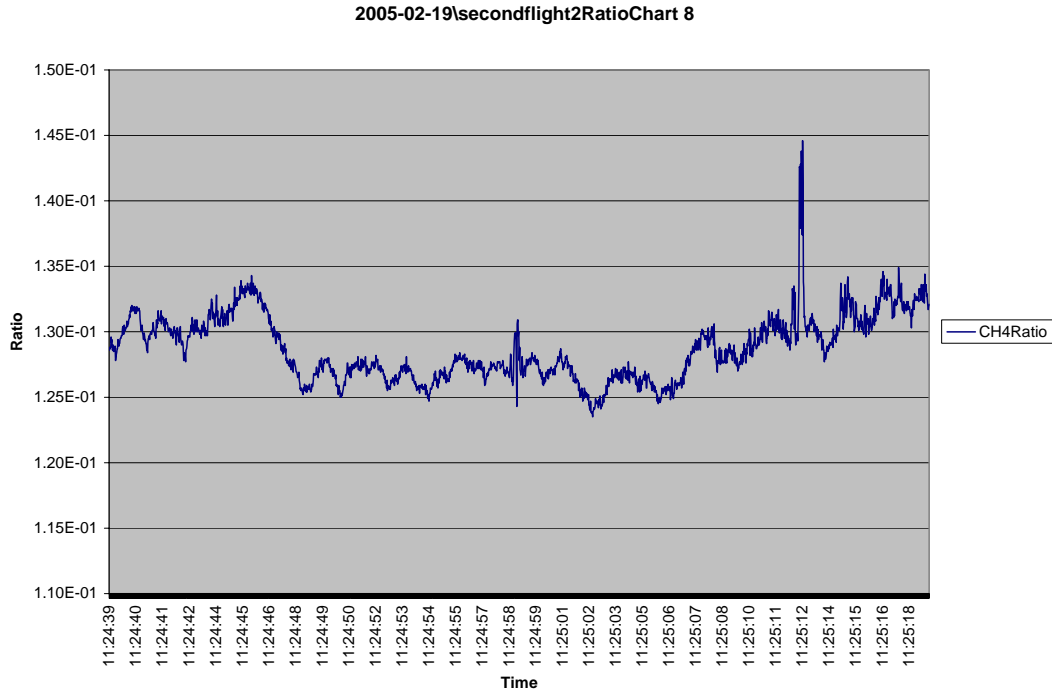
Figure 53. Gas Correlation Ratio for Flight # 8 on February 19th

2005-02-19\secondflight2Raw SignalChart 10
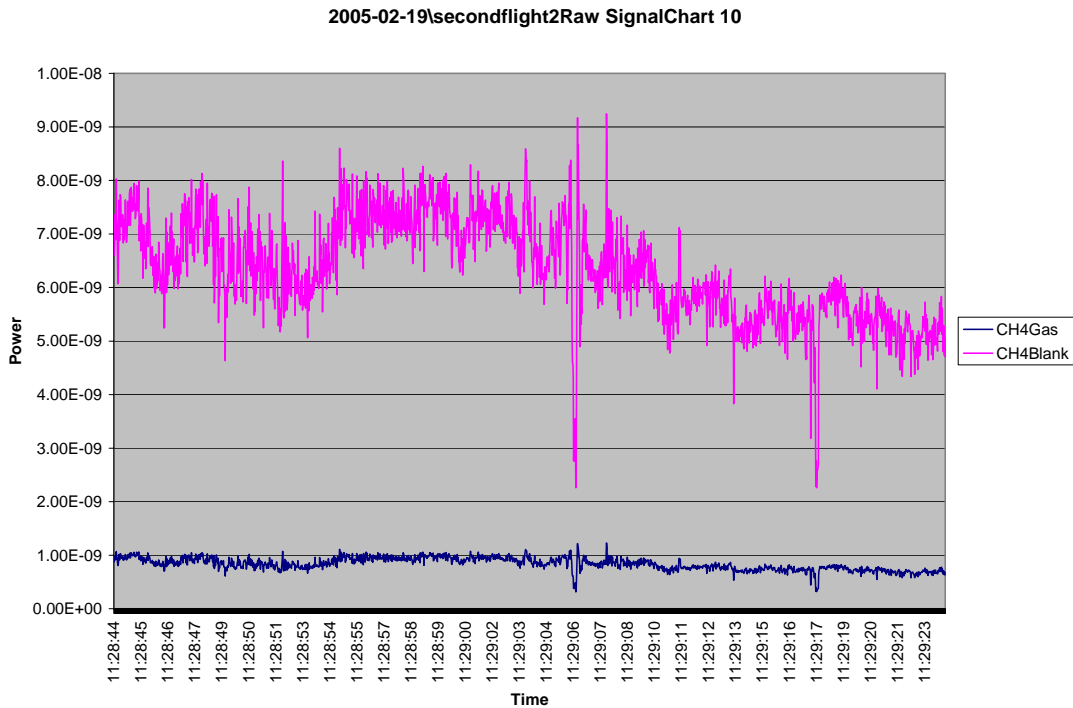
Figure 54. Raw Detector Signals for Gas and Blank Channels during Flight #10 on February 19th

2005-02-19\secondflight2RatioChart 10
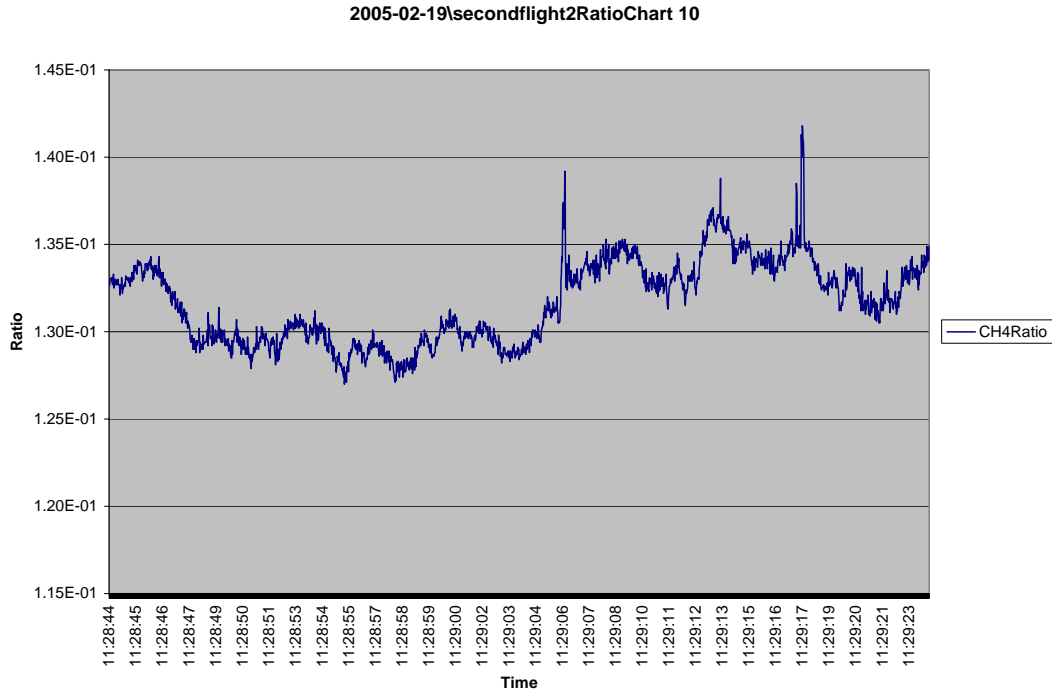
Figure 55. Gas Correlation Ratio for Flight #10 on February 19th

2005-02-19\secondflight2Raw SignalChart 15
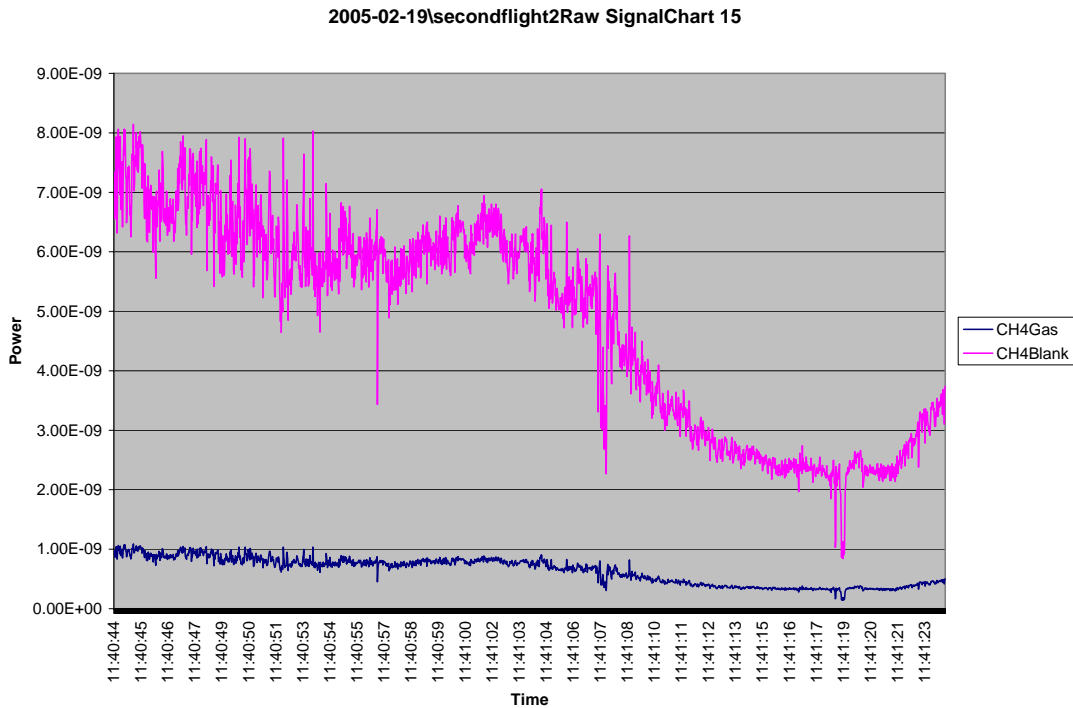
Figure 56. Raw Detector Signal for Gas and Blank Channels during Flight #15 on February 19th

2005-02-19\secondflight2RatioChart 15
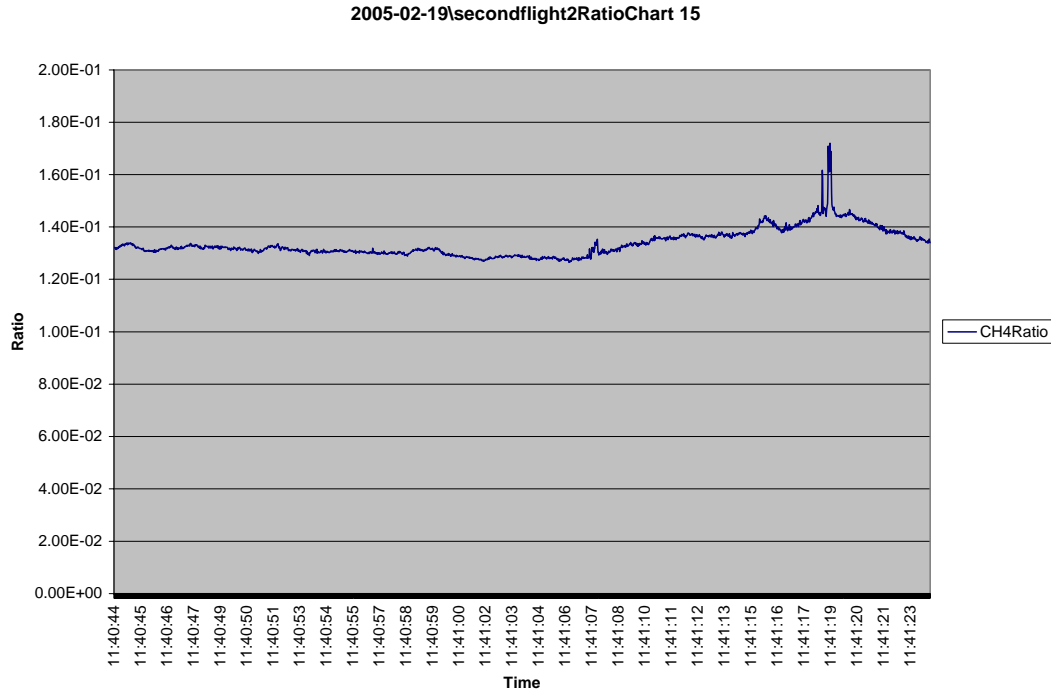
Figure 57. Gas Correlation Ratio for Flight #15 on February 19th

3.12.3.4   Flight Test Performed on February 25, 2005

The second day of flight testing with the methane-sensing light source was performed on February 25th. The purpose of these flights was to continue increasing the methane release to a level where Ophir could correlate the GPS coordinates of the release site to a definite increase in the gas correlation ratio.

3.12.3.4.1   First Flight Looking for Methane Gas Release of 150 scf/h

For the first flight of the day, the ditch site was again chosen as the release point, as the slight depression aided in the confinement of the released methane (especially in light winds). The methane flow was increased to 150 scf/h by using two methane cylinders of 99.9% purity. For safety reasons, the methane cylinders were located remotely from the actual release point as shown in the photograph in Figure 58. The long neon-green strip of cloth just to the north of the cylinder was used as a ground locator to indicate the position of the release point in the ditch. A second piece of cloth was located in a line on the opposing side of the ditch, as well. Each of the cylinders had a gas regulator and a flowmeter (shown in photograph in Figure 59) used to quantify the amount of methane released. Long sections of plastic tubing was used to pipe the methane gas down the incline of the ditch to a central release point in the ditch approximately 30 m (100 ft) from the southern end of the ditch, as shown in the photograph in Figure 60. The release nozzle end of the tubing was left open this time, instead of connecting it to copper tubing with numerous holes. This allowed for a less restricted flow, enabling Ophir to release

larger amounts of methane. The gas flow was initiated approximately 20 minutes prior to the first flight pass over the site.

Figure 58. Photograph Showing Positioning of Methane Release Cylinders used for Morning Flight on February 25th


Figure 59. Photograph of Methane Release Cylinder, Gas Regulator, Flowmeter, and Release Plastic Tubing

Figure 60. Photograph Showing Methane Release Point at Bottom of Ditch

The flight direction was setup to traverse the methane release point closer to right angles, taking the airplane directly over the small pond. During the previous flight on February 19th, the flight path was chosen to avoid crossing the pond. At that time it was thought that the pond provided no useful data due to the absence of reflected signal. With the problems encountered when reading the GPS data over the serial communications bus, the strategy was changed to use the definite pond ratio change as a locator for the methane release point. Even when failures occurred when reading the GPS data, the pond edge could always be located on the data and the release point could be ascertained. It became apparent that the GPS data stored on the GPS device as route information was far more reliable than the data read off of the serial bus. The GPS device had enough onboard memory to store second by second data for every flight route conducted during the entire day. This route information was downloaded following the flights onto the flight computer and the manufacturer-supplied software was used to create flight path maps over the release site. Time-of-flight comparisons of the raw signal and ratio plots could be made using the route waypoints generated by the GPS device (remembering the + 4 minute and 35 second separation). Using this type of analysis, the map shown in Figure 61 was created showing certain key flight paths and times of significant gas correlation ratio increases (normally associated with the presence of methane).
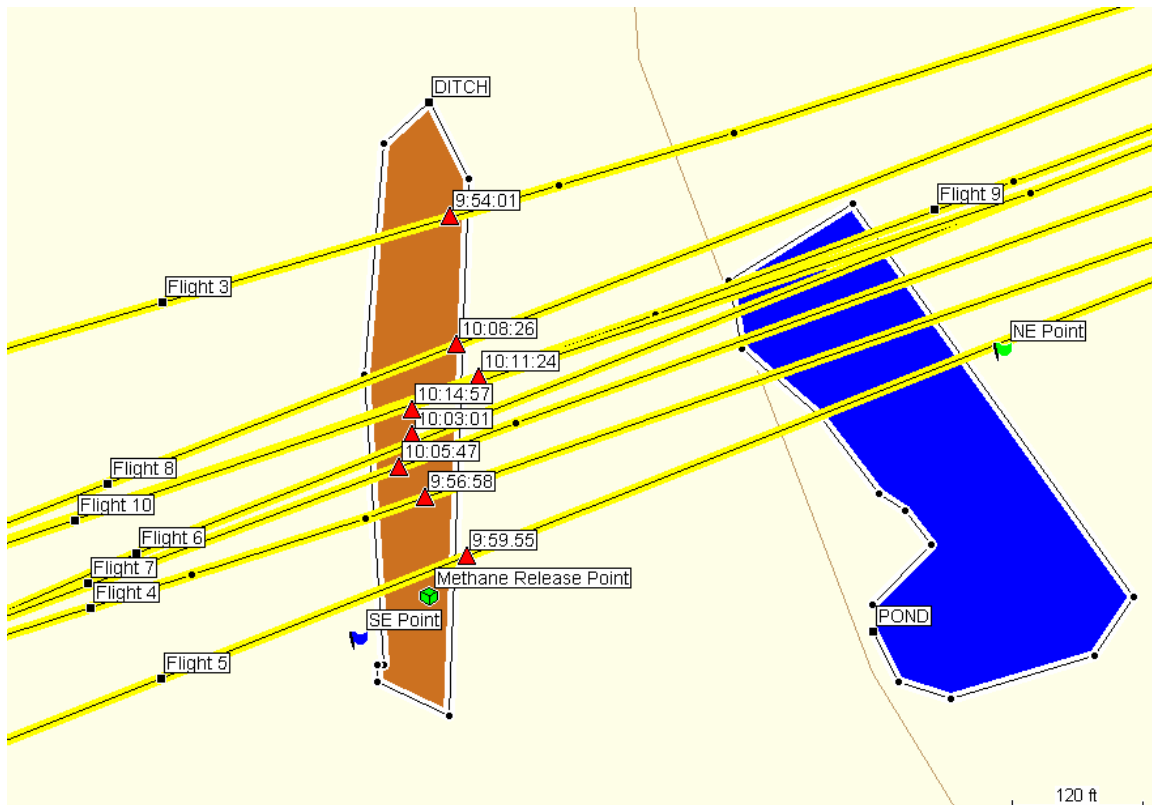
Figure 61. Map of Selected Flight Paths on Morning of February 25th Showing Significant Gas Correlation Ratio Changes

The morning flight headings were all from the northeast to the southwest, in an attempt to standardize the approach to the release site. The red triangles indicated the time heading of the GPS route data, which was offset from the computer generated plots by four minutes and 35 seconds that showed the greatest short term gas correlation increase. All of the noticeable gas correlation increases for these flights were seen to fall within the general boundary of the ditch. The wind direction was generally from the northeast with wind speeds below 4 mph. More details on minute to minute variations of the wind speed and direction are shown in Attachment 2, Table 5.   The skies were clear throughout the day.

Collecting ratio data over water normally skewed the data such that the smaller ratio values associated with the ditch site could not be accurately determined, without expanding the flight section after the water crossing.   Improvements to the analysis software will be made in the future to eliminate the misleading ratios from water crossing. Flights paths #3 and 8 did not cross over the small pond, therefore the entire 40-second data snapshot of raw signal and ratio plots can be analyzed as collected and are shown in Figures 62-65. The following interesting observations can be made from these plots:

- In both ratio plots the large spike in ratio at times 9:58:36 of flight #3 and 10:13:00 of flight #8 correlated closely with the GPS coordinates of the ditch release site. The percentage increase over the baseline ratio (> 15 %) near the ditch release was

substantially higher than was seen for the lower concentration release flights on February 19th. The raw signal at these points indicated a signal decrease in both the gas and blank channels.

- The longer time scale changes in ratio seen throughout the flight #3 and at the end of flight #8 seemed to be related to wavelength shifts in the fiber amplifier source. There was a fundamental change in the ratio for flight #3 at time 09:58:20 from 0.130 to 0.160. The noise level of the ratio also increased pretty dramatically, signaling that the amplifier was having a harder time holding the output wavelength. Towards the end of the flight #3 ratio plot, the ratio again reverted to 0.130 and smoothed out. It was important to note the drop in the gas channel at this point was not seen in the blank channel, indicating a wavelength shift (not a power shift) away from the primary methane absorption line of the gas cell. Ophir believed that the larger long term shifts in ratio throughout the flight testing was due almost entirely to the inability of the amplifier to hold a tight enough output wavelength.

Plots of the correlation gas ratios for flights #4-7, 9, and 10 have been zoomed in to the flight path just following the water crossing and are shown in Figures 66-71. The first ratio data point shown in these figures represented the edge of the water boundary, plus or minus a few points. Interestingly enough, the water to mud transition was seen in the ratio data as a fairly sharp but discernable slope. It should be noted that flight #4, 5, and 7 indicated that the amplifier was having a hard time controlling the output wavelength, as seen by the large baseline level ratio shifts. But the small time scale ratio spike was still discernable. The horizontal scale for these figures was shown as # of 20 ms samples. Each sample represented roughly 0.9 m of integrated flight path ratio data based upon airspeed of 100 mph. The distance between the pond edge and the release point was approximately 95 - 100 m, or 105 - 111 data samples. These numbers were approximations and may be slightly off due to changing airspeed. Nonetheless, it was clear that the 15-25 % ratio spike seen in the ratio data correlated closely to the location of the ditch. The spike in the ratio data appeared to be much higher than what was seen during the lower release tests. The moisture in the ditch soil was less for these later flight tests, lending more evidence to a methane-induced spike.

Ophir evaluated the flight data immediately following the flights and decided that during the next flight test would make a single pass from northeast to southwest over the ditch without any methane release to use as a baseline for the earlier flights. An absence of a ratio spike for this benign test would offer conclusive evidence that the large spike was due mostly to the presence of methane. The flight path and the associated ratio data are shown in Figures 72 and 73 for the first flight pass of the second flight with the methane cylinders turned off. The data clearly showed the absence of any large ratio spike near the sample points (105-110) associated with the ditch location. There was a slight (1-2 %) ratio rise, but when it was compared to the remainder of the flight it appeared to be imbedded within the ratio noise. Other outdoor ground testing was performed, following these flights, using grass sod samples of different moisture content and at different incident angles to the laser. None of these variations caused any change in the calculated gas correlation ratio, further bolstering the view that similar terrain anomalies were not responsible for any ratio step changes.
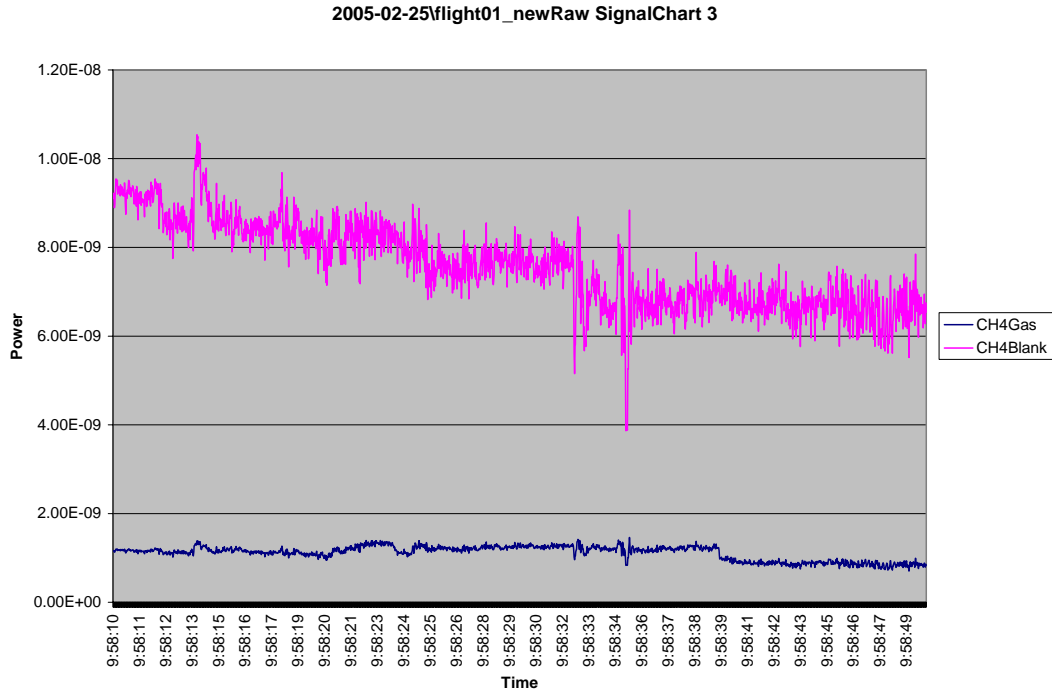
2005-02-25\flight01_newRaw SignalChart 3

Figure 62. Raw Detector Signal for Gas and Blank Channels for Flight # 3 on Morning of February 25th

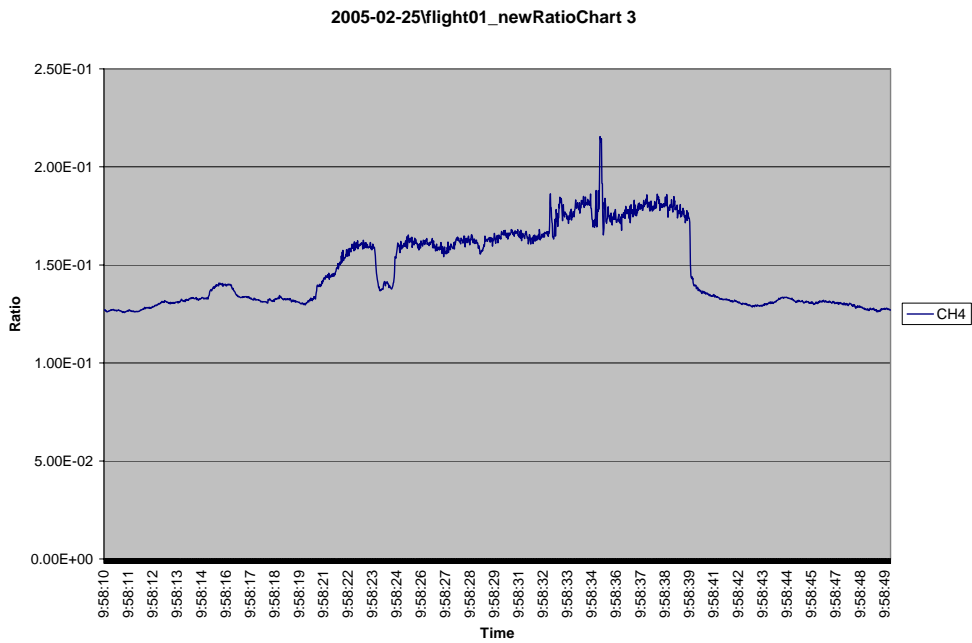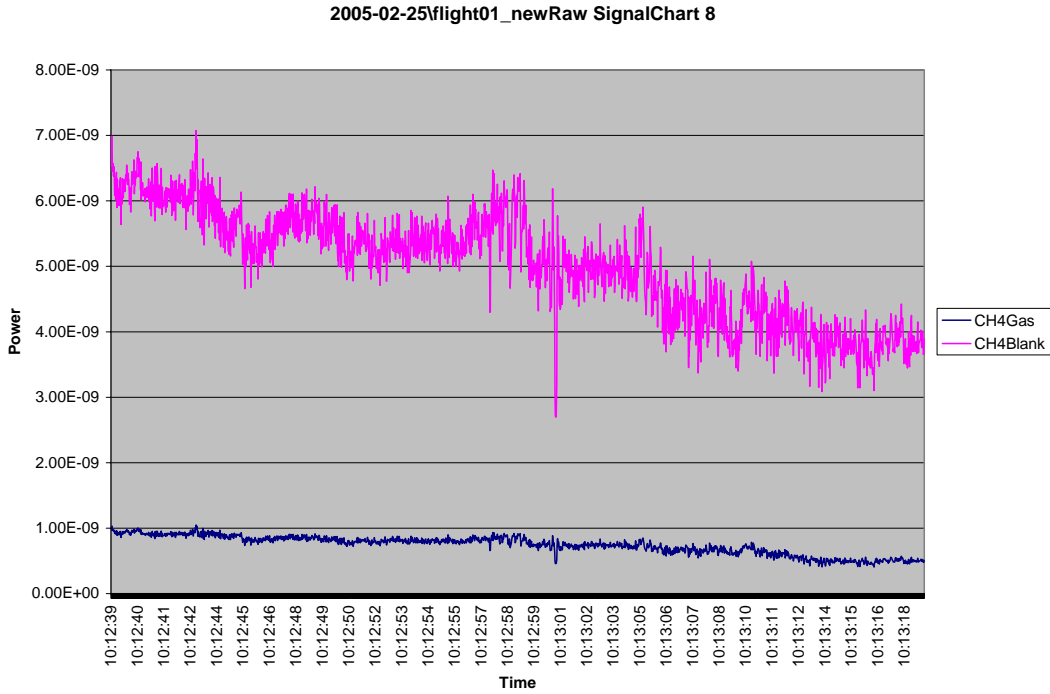**2005-02-25\flight01_newRatioChart 3**

Figure 63. Gas Correlation Ratio for Flight # 3 on Morning of February 25th

Figure 64. Raw Detector Signal for Gas and Blank Channels for Flight # 8 on Morning of February 25th
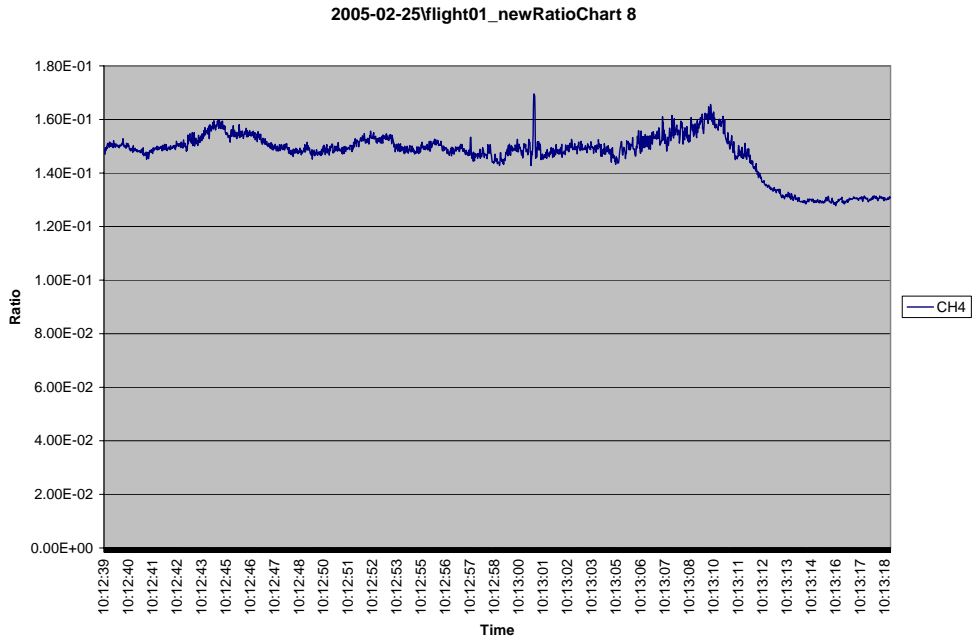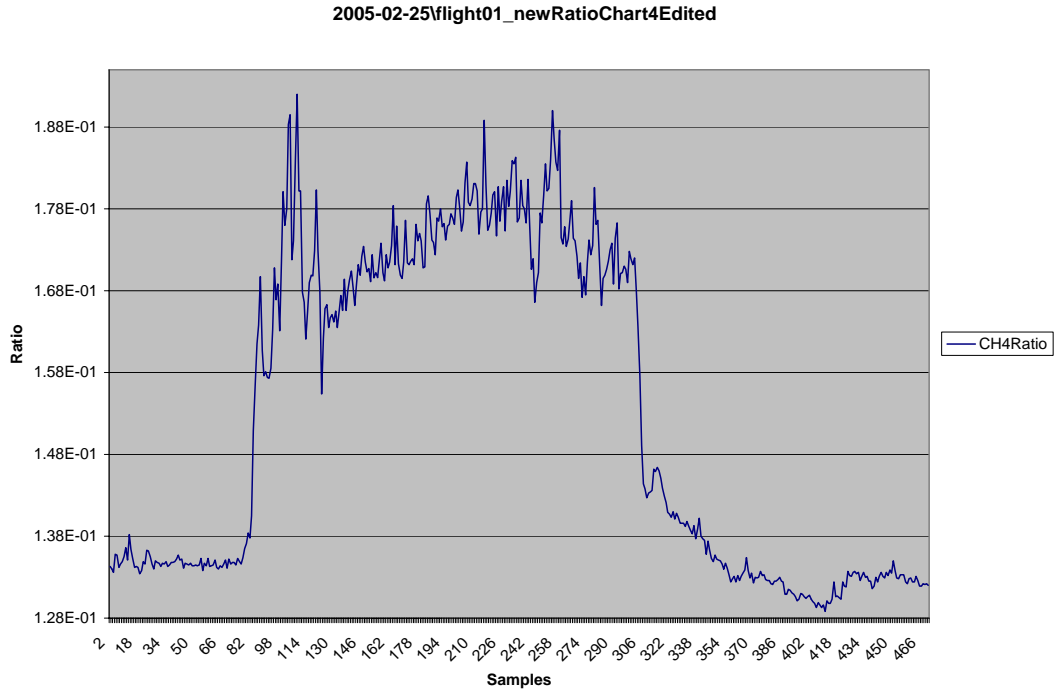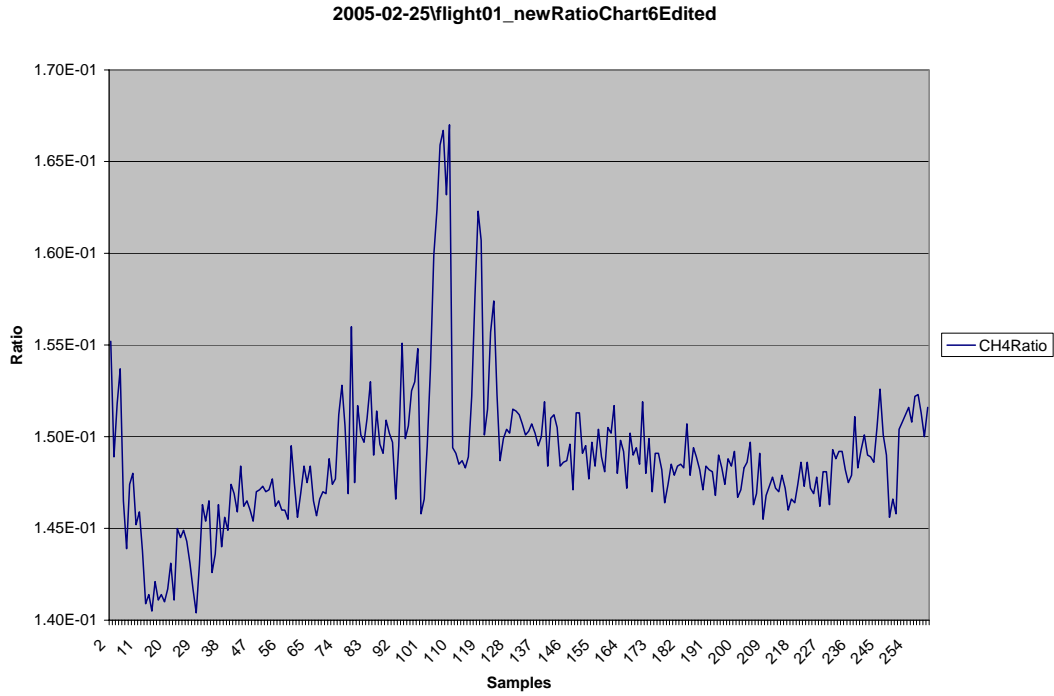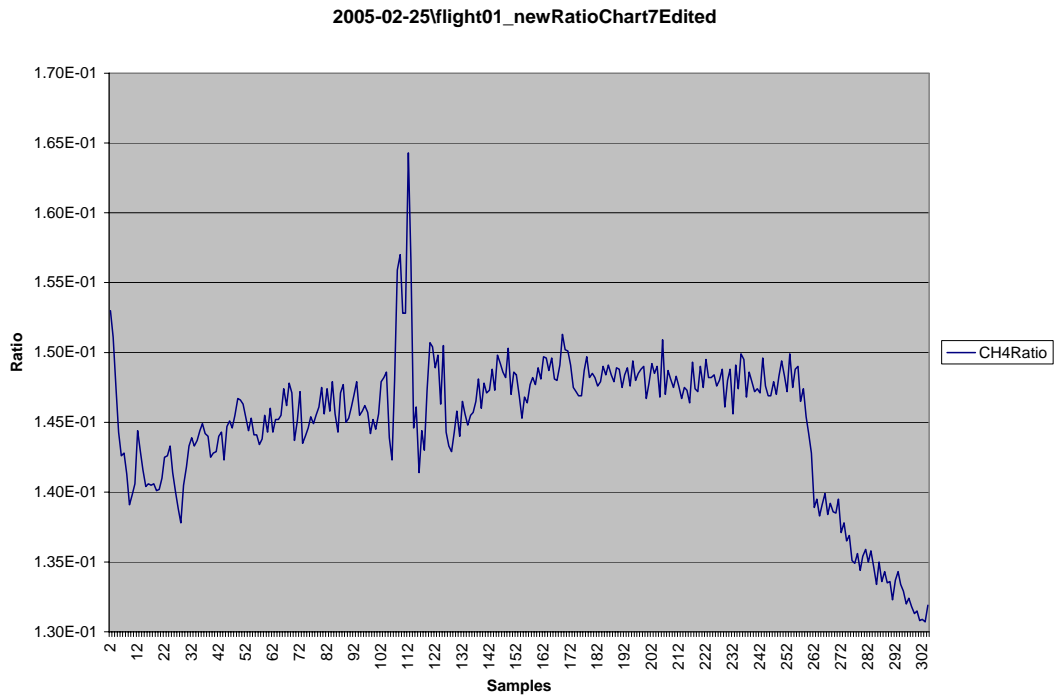

Figure 65. Gas Correlation Ratio for Flight # 8 on February 25th

2005-02-25\flight01_newRatioChart4Edited

Figure 66. Gas Correlation Ratio for Flight # 4 on February 25th Showing Flight Region Following Small Pond

2005-02-25\flight01_newRatioChart5Edited
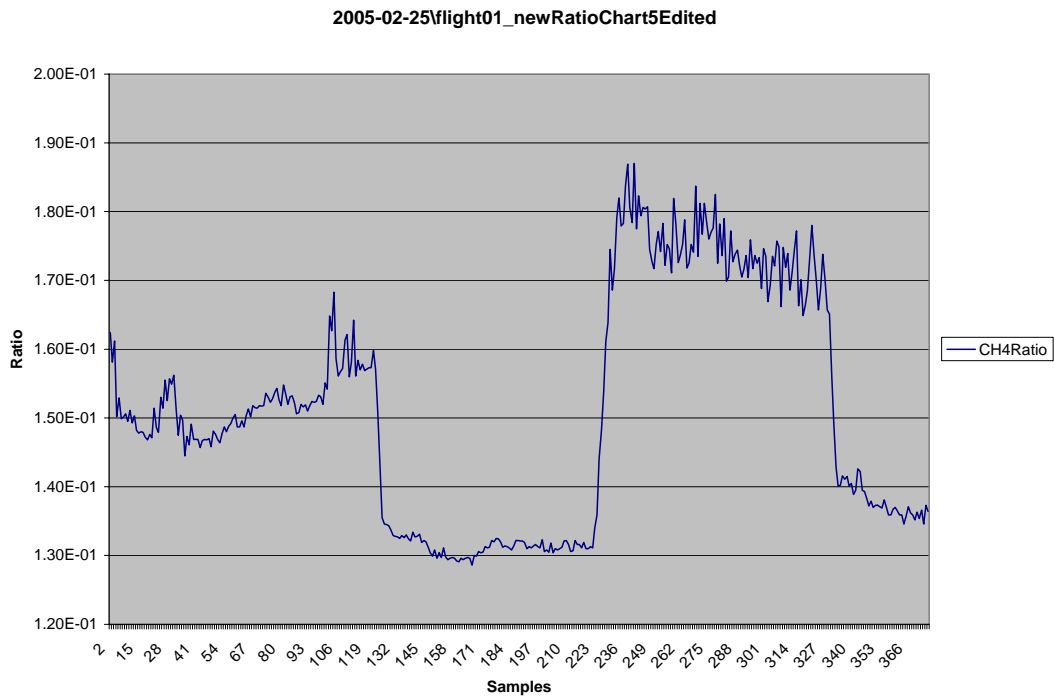
Figure 67. Gas Correlation Ratio for Flight # 5 on February 25th Showing Flight Region Following Small Pond

2005-02-25\flight01_newRatioChart6Edited

Figure 68. Gas Correlation Ratio for Flight # 6 on February 25th Showing Flight Region Following Small Pond

2005-02-25\flight01_newRatioChart7Edited

Figure 69. Gas Correlation Ratio for Flight # 7 on February 25th Showing Flight Region Following Small Pond

2005-02-25\flight01_newRatioChart9Edited
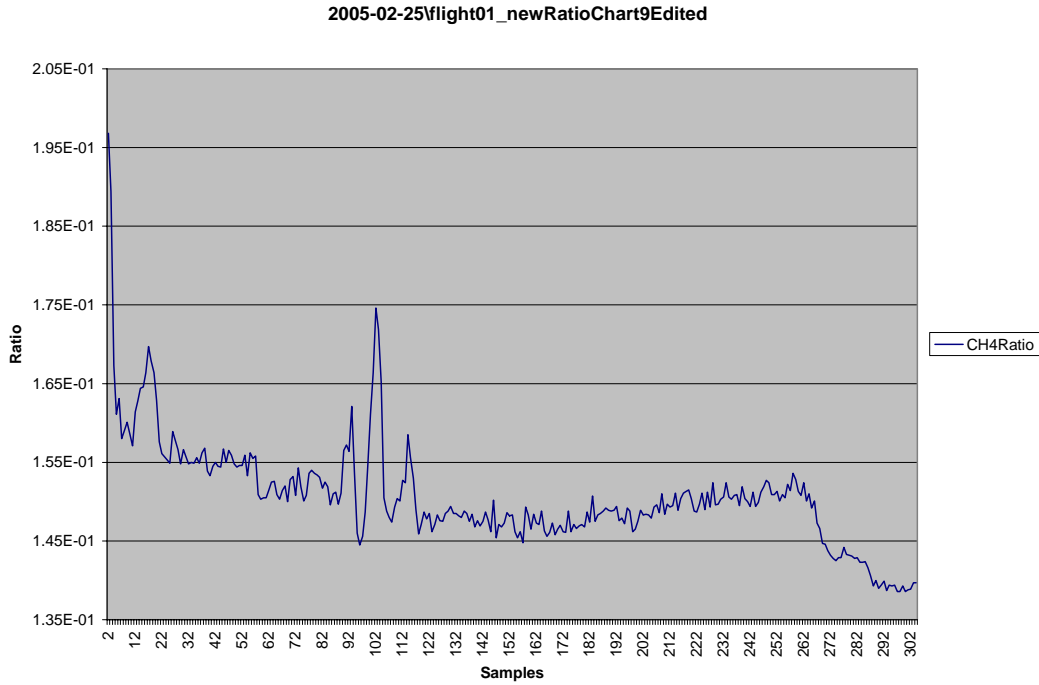
Figure 70. Gas Correlation Ratio for Flight # 9 on February 25th Showing Flight Region Following Small Pond

2005-02-25\flight01_RatioChart10
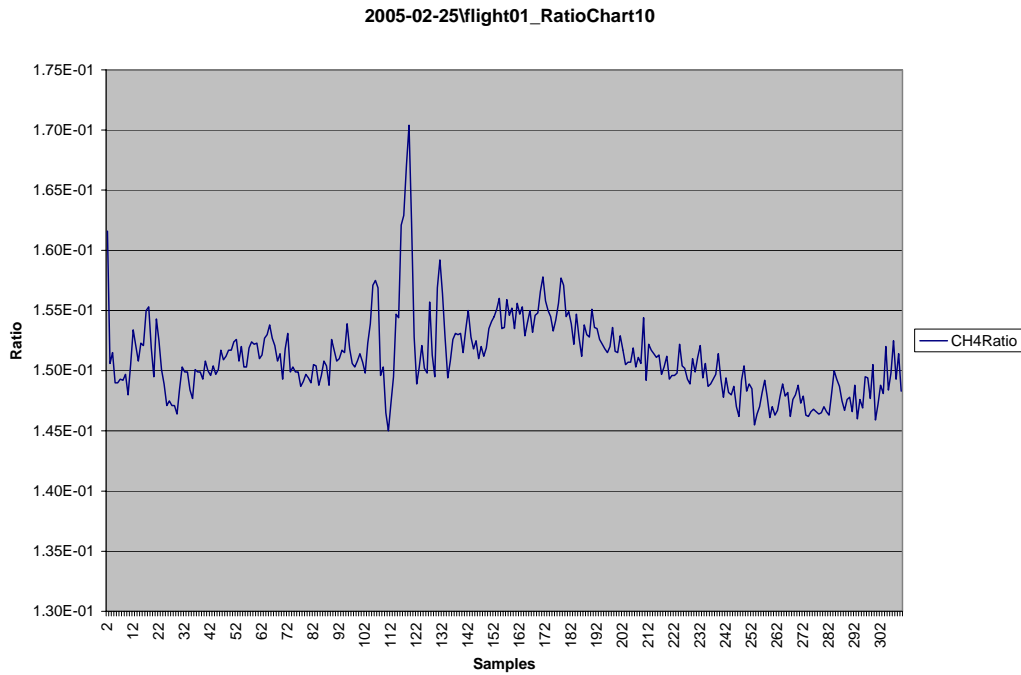
Figure 71. Gas Correlation Ratio for Flight # 10 on February 25th Showing Flight Region Following Small Pond
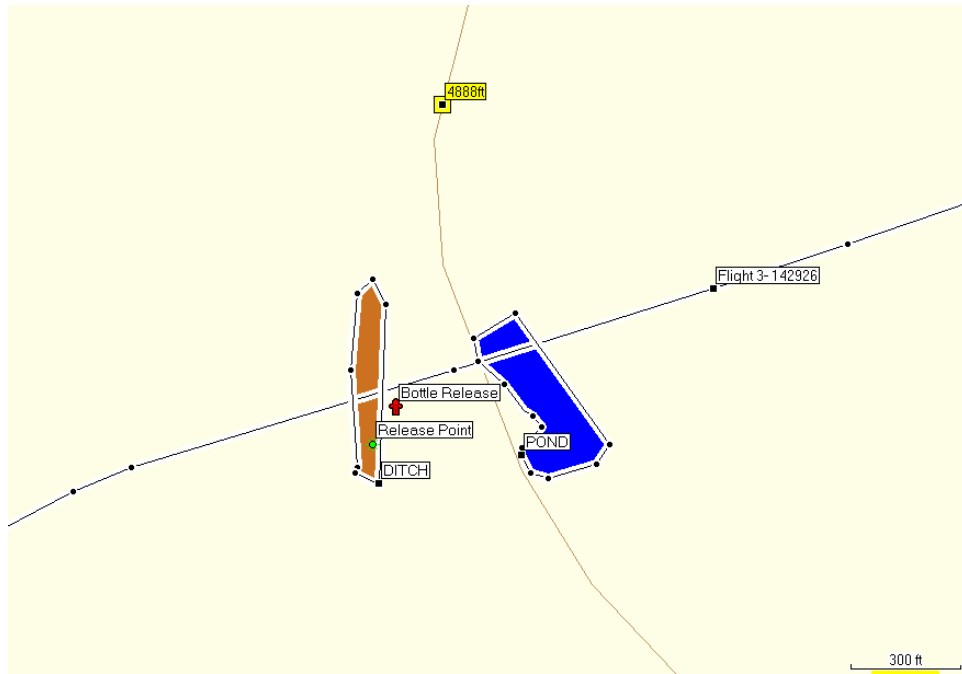
Figure 72. Map Showing Flight Path of First Pass (Afternoon Flight on February 25th) over Release Site with Leak Source Turned Off
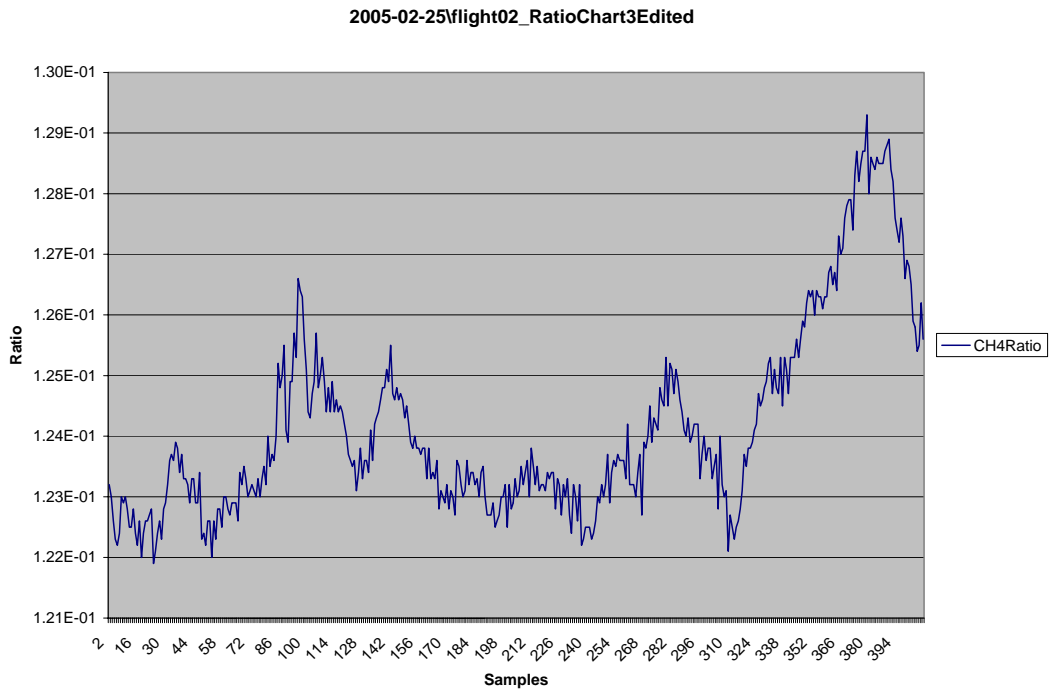
Figure 73. Expanded (After Water Crossing) Gas Correlation Ratio of Second Flight over Release Site with Leak Source Turned Off

3.12.3.4.2   *Flight Test Sensing of Large Uncontrolled Methane Release*

During the afternoon of February 25th, Ophir attempted to simulate a larger methane leak by using four methane cylinders opened simultaneously. Unfortunately, Ophir did not possess enough regulator and flowmeter hardware to monitor and quantify the output from the cylinders. As a result, the cylinders (without any regulating hardware) were placed side by side on the flat ground between the small pond and the ditch, pointing towards the ditch in a southwesterly direction, and the valves were slightly opened, dispersing the methane to the north along the ditch, just immediately prior to the fly-overs (no pre-soaking of the site). It would have been preferable to have the release within the ditch, but the cylinders were much too heavy to physically locate them on the bottom of the ditch. A photograph of this setup is shown in Figure 74.

Figure 74. Photograph of Large Uncontrolled Methane Release for Afternoon Flight on February 25th

The second flight test of the day started shortly after 02:00 PM and lasted until 02:50 PM. GPS routes of the individual flight paths over the release site are shown in Figure 75. The bottle-release site is shown on the figure as a red cross. The green release marker within the brown-shaded region was only shown for reference and was not used during this flight scenario. The wind speed and direction data for the time of the afternoon flight on February 25th is shown in Attachment 2, Table 6. Surface winds were generally from the southeast at between 5-10 mph. Figures 76 and 77 show the gas correlation ratio calculated for flights 4 and 7 expanded for the region following the water crossing. These flights were the closest to the actual release site. A small (1-2 %) spike in the data

was apparent near sample 105, which correlated to the ditch site. The sample region between 80 and 100 represented the new release site, and from the data no noticeable correlation ratio shift occurred. The ratio data for flight 5 revealed similar findings with no noticeable spike in the data. The flight 5 GPS data indicated a severe bank of the airplane just prior to crossing the release site. This caused the airplane to miss the release site by a fair amount. Finally, the raw signal and ratio data is shown for flights 8 and 9 in Figures 78 and 81. These flights were the farthest away from the release point and showed the same relatively small spike in the data related to the ditch terrain.

Unfortunately, the lack of quantified release data for this test limited the usefulness of the test results. Other test variables such as higher wind speeds, shorter duration turn on of the methane cylinders and the methane leak location outside the ditch may have contributed as well to the lack of methane detection. The inclusion of large methane leak (> 500 scf/h) detection using the airborne sensor would be a useful metric, but is only practical when large volumes of gas are available such as from a large working natural gas pipeline.
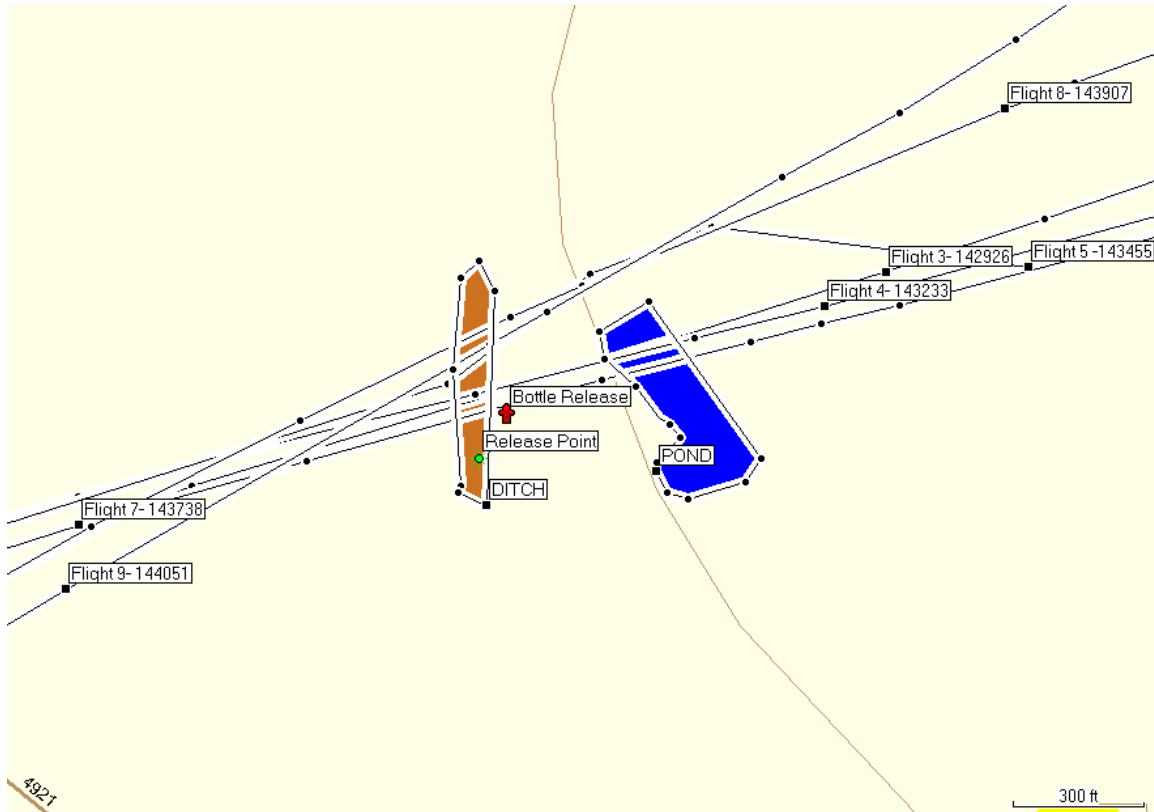
Figure 75. Map of Flight Paths over Large Simulated Leak on February 25th

2005-02-25\flight02_RatioChart4Edited
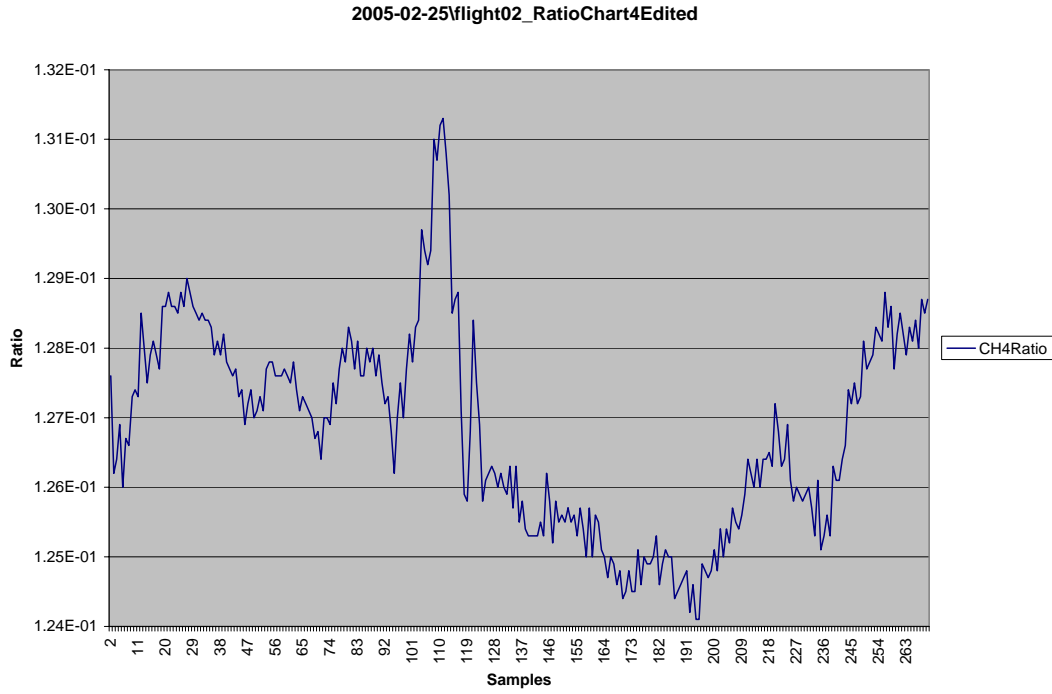
Figure 76. Gas Correlation Ratio for Flight # 4 Second Flight February 25th Showing Flight Region Following Small Pond

2005-02-25\flight02_RatioChart7EditedVer2
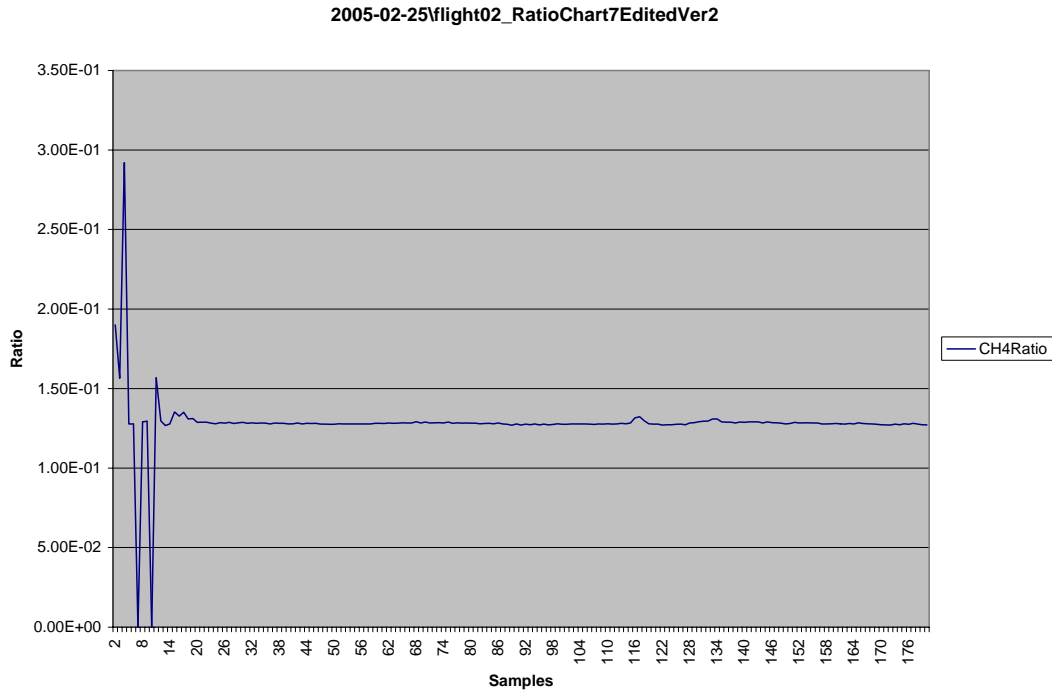
Figure 77. Gas Correlation Ratio for Flight # 7 Second Flight February 25th Showing Flight Region Following Small Pond

2005-02-25\flight02Raw SignalEdited.txtChart 8
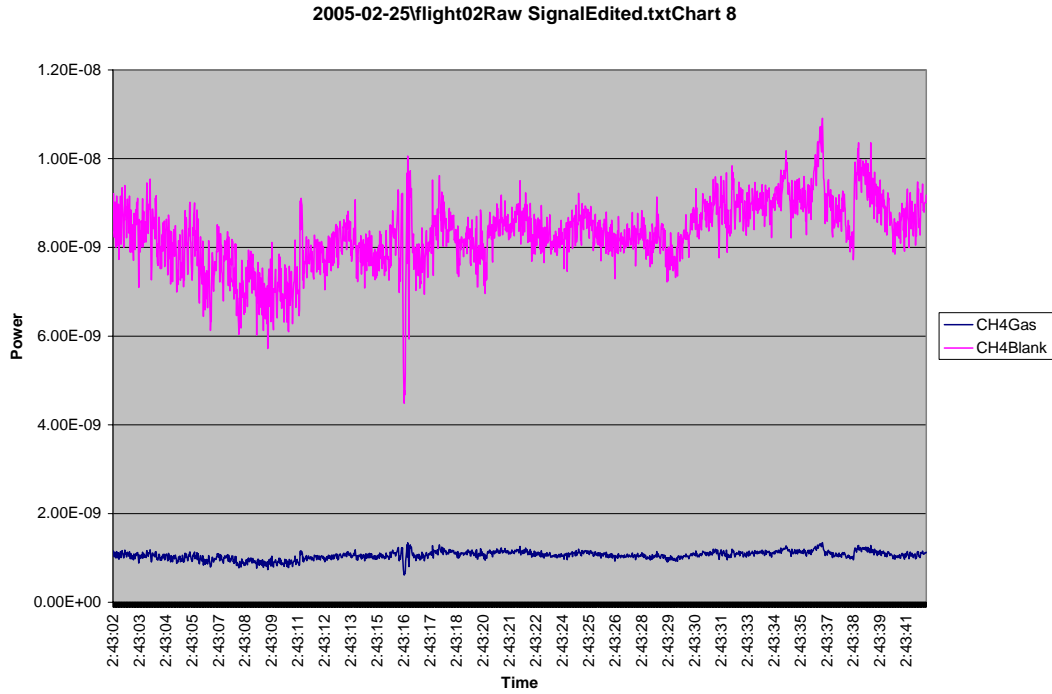
Figure 78. Raw Detector Signal for Gas and Blank Channels for Flight # 8 on Afternoon Flight of February 25th

2005-02-25\flight02RatioChart 8

Figure 79. Gas Correlation Ratio for Flight # 8 on Afternoon Flight of February 25th

2005-02-25\flight02Raw SignalEdited.txtChart 9
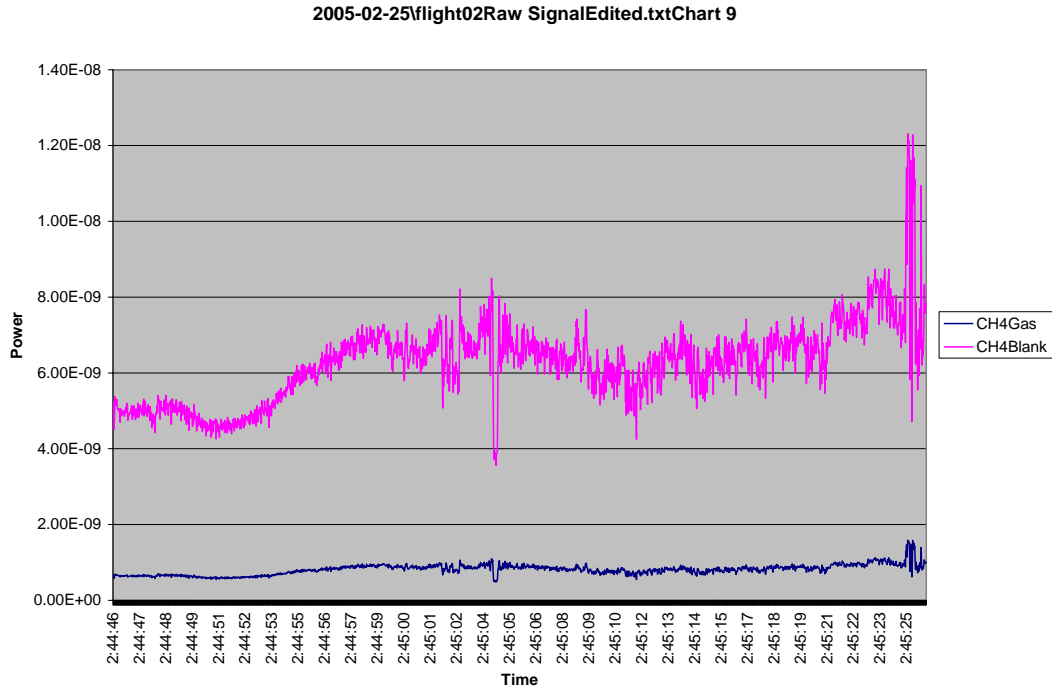
Figure 80. Raw Detector Signal for Gas and Blank Channels for Flight # 9 on Afternoon Flight of February 25th

2005-02-25\flight02RatioChart 9
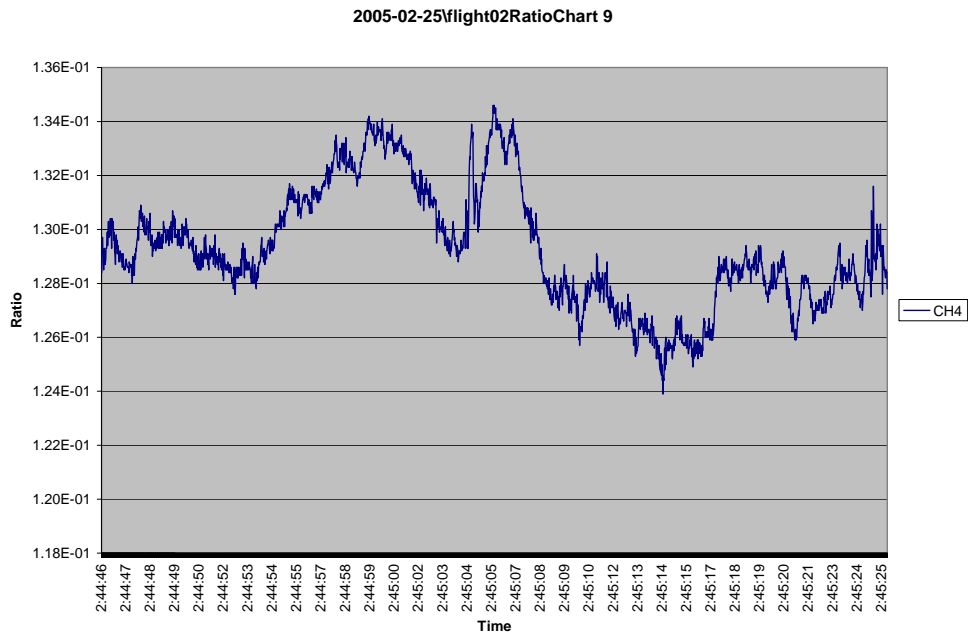
Figure 81. Gas Correlation Ratio for Flight # 9 on Afternoon Flight of February 25th

3.12.3.4.3   *Flight Testing over Cattle and Chicken Feedlots*

Naturally occurring sources of methane are known to exist in and around cattle feedlots and to a lesser extent chicken feedlots. During the flight testing over the simulated natural gas leak site, Ophir was able to locate and survey two nearby cattle feedlots and two chicken feedlots. The largest chicken feedlot was located a little more than one-half mile to the east of the release site, across from the north-south road just to the east of the site, and is located near the light grey-colored oval road shown in Figure 44. The second smaller chicken feedlot was located on the way to the ditch leak site. The cattle feedlots were located between 2-4 miles northeast of the site. A flight was performed over the larger chicken farm east of the ditch release site as shown in Figure 82. Normal ambient background methane was measured with the exception of one small spike, as shown by ratio data collected on February 19th in Figure 83 (the second spike towards the end of the plot occurred at the edge of the farm and may have been due to the paved highway road surface).   It was not clear what the small spike was from, but given the large piles of chicken manure present at the site it would have been expected to have found more methane ratio signatures. Speculations were that the minor ratio spike was due to some surface feature such as a building rooftop. Similar methane ratio data was found when flying over the larger chicken farm on February 25th.
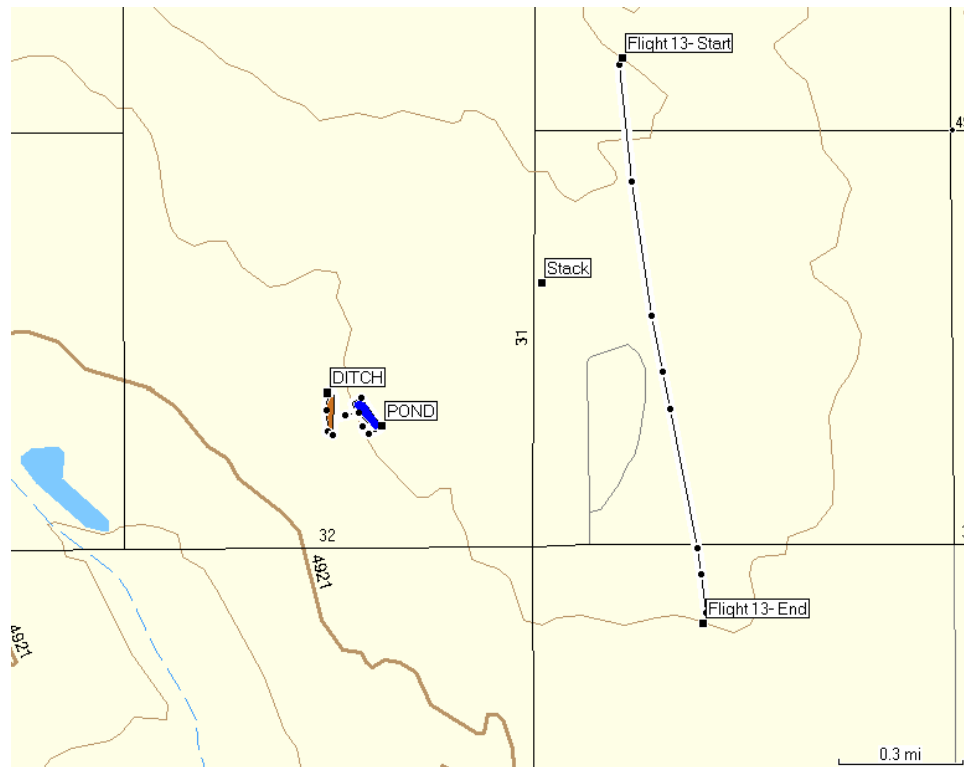
Figure 82. Flight Path # 13 over Large Chicken Farm on Afternoon of February 19th
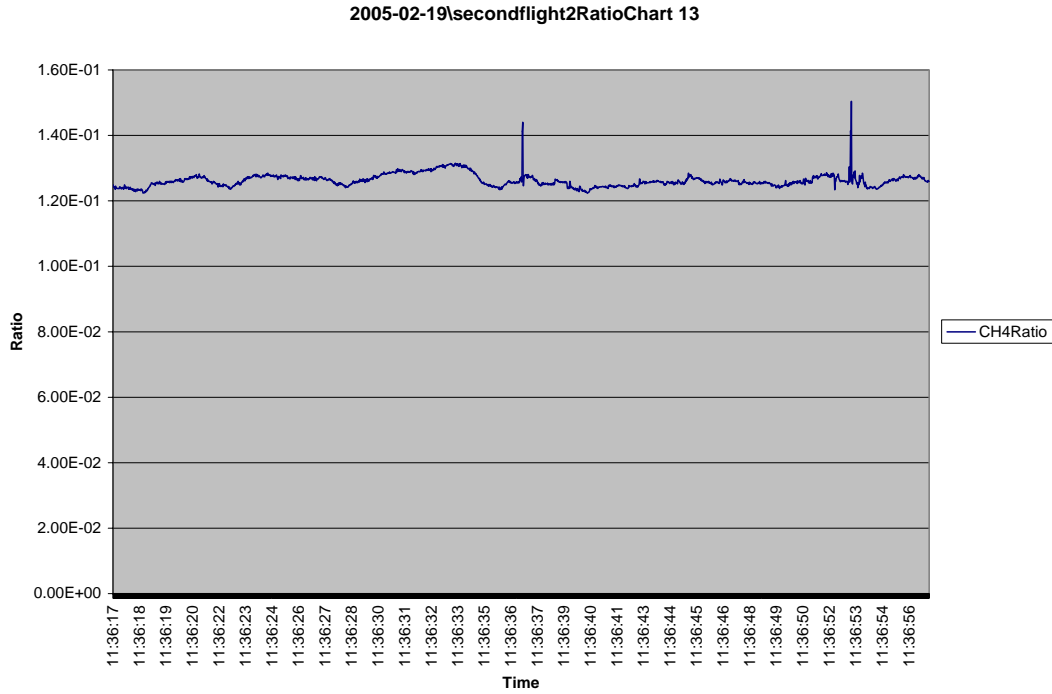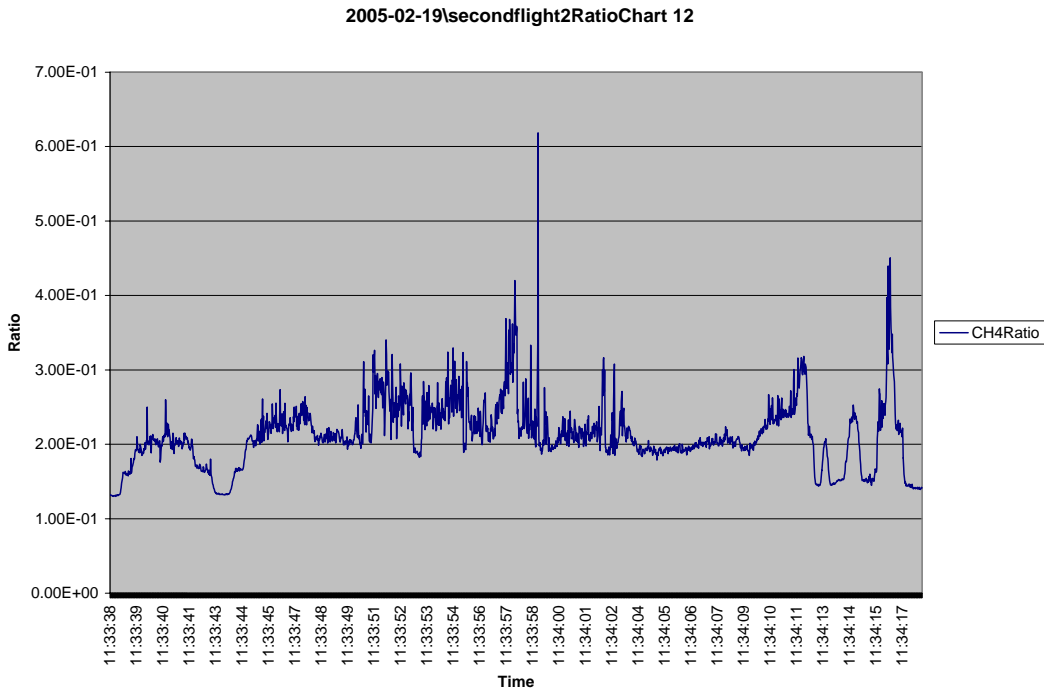
Figure 83. Gas Correlation Ratio for Methane over Chicken Feedlot on Afternoon Flight of February 19th

The cattle feedlot ratio plots were much more interesting, and may have revealed much higher background levels of methane. The flights over the smaller of the feedlots on February 19th and 25th are shown in Figures 84-86. The feedlot boundaries were typically associated with the regions of highest peak-to-peak variability towards the middle of the plot in Figure 85 and the later half of the plot in Figure 86. The baselines of the entire 40 second plots were actually above what was normally seen when flying over pasture and grassland (typically ratio of 0.130). Some of this baseline and multiple second step changes may have been due to what has been described previously as the inability of the amplifier to maintain a stable wavelength. This conclusion seems bolstered by the ratio signature near time 11:34:11 of Figure 84, where the gas channel magnitude change was greater than the blank channel (an unlikely scenario). Certainly the large spikes over the feedlot were unusual in that they had never been seen before at this magnitude. It should be noted that this noisy region was also closely associated with a strong odor in the airplane.

2005-02-19\secondflight2Raw SignalChart 12
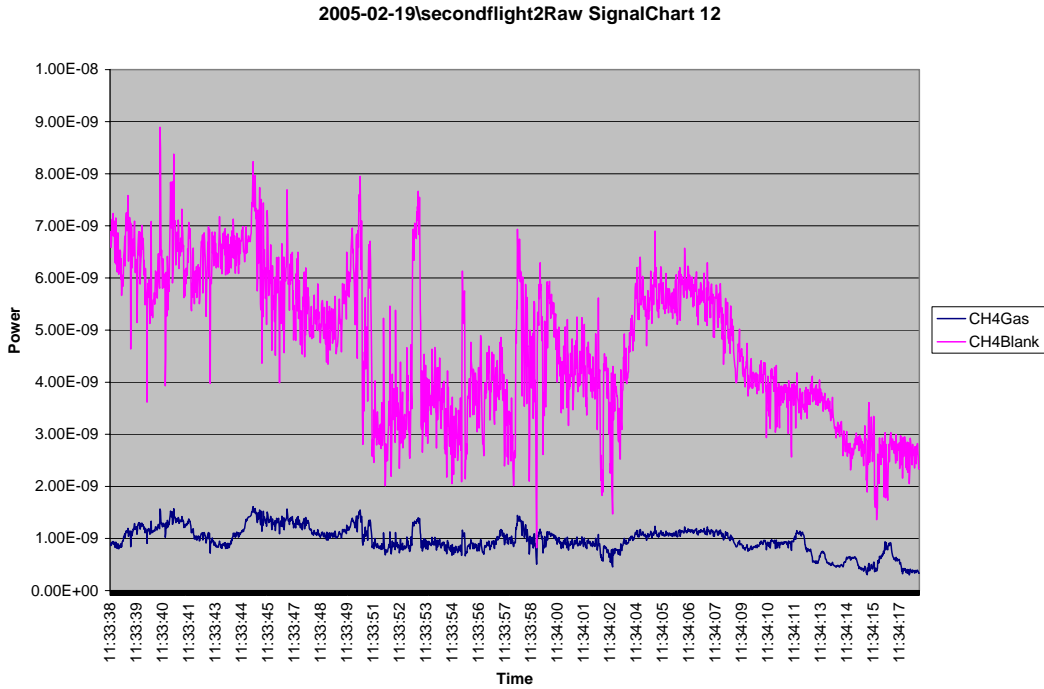
Figure 84. Detector Signal Plots for Gas and Blank Channels over Small Feedlot on February 19th

2005-02-19\secondflight2RatioChart 12

Figure 85. Gas Correlation Ratio of Methane over Smaller Cattle Feedlot on February 19th
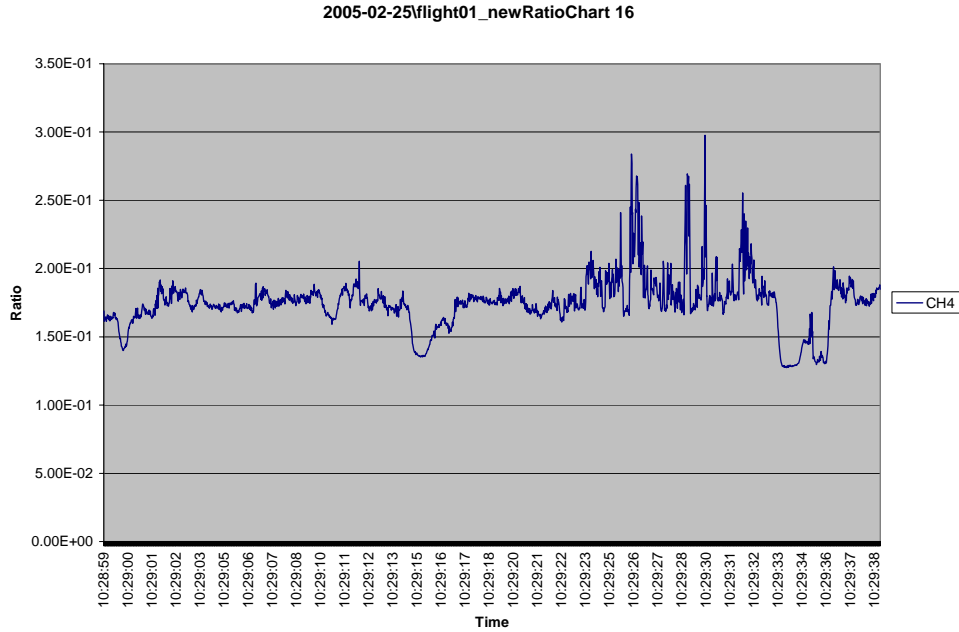
Figure 86. Flight over Smaller Feedlot on Morning of February 25th showing Gas Correlation Ratio

On the second day of flying, the pilot notified Ophir of a much larger feedlot about 4 miles away from the release site. He had indicated that it was a much more "odorous" feedlot and continued to be a sore spot with the community. This particular site appeared to have a cross section of between a half-mile and a mile, which would have taken most of a 40-second snapshot to traverse. Interestingly enough the ratio signature for this feedlot, shown in Figure 87, showed significantly less ratio variability and a lower baseline than that for the smaller feedlot flight passes (noting the smaller ratio scale for this plot). Clearly, more research is required on what impacted the ratio over the smaller feedlot, and a working relationship would have to be established with the feedlot owners allowing Ophir permission to survey the site terrain features.

2005-02-25\flight01_newRatioChart 17
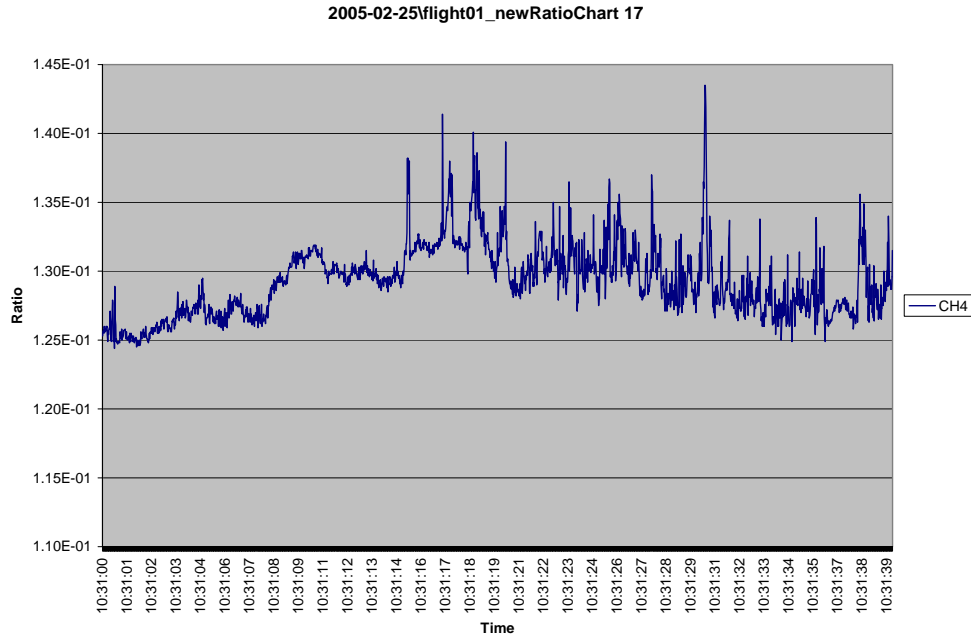
Figure 87. Gas Correlation Ratio for Large Feedlot Flyover on February 25th

4 Project Issues

4.1 Performance Issues Related to the Highly Non-Linear Fiber Amplifier

4.1.1   Lack of Ruggedization of the HNLF Amplifier

It was hoped that the amplifier would be capable of performing over a wide temperature region. Unfortunately, the amplifier actually had a very narrow operational temperature range of between 15 – 30 ºC. Ophir had to develop methods to counter the colder temperatures typically encountered with the airborne testing. At times, it took several hours to reach an acceptable operating temperature for the amplifier. There were also problems with operating the amplifier in too warm an environment. These problems manifested themselves in the form of a software control shutdown. Normally, the laser diodes would exceed the preset operating maximum temperature and the system would remove power from the pump diodes. This problem did not show itself on the airplane, although it is likely that it would appear on a hot summer day.   The amplifier was also not mechanically rugged, and was damaged in shipment due to inadequate securing bolts within the unit. Once this problem was diagnosed and corrected, the unit seemed to perform adequately within the shock and vibration environment of the airplane.

4.1.2 Wavelength and Power Stability

The operational temperature issues for the HNLF amplifier continued to plague the system throughout the project. The amplifier actually had a very narrow operational temperature range of between 15 – 30 ºC. When operating at colder temperatures, the amplifier went into an unstable wavelength output mode, where the wavelength on an optical spectrum analyzer looked like a sawtooth waveform. At very cold temperatures (under 5 ºC), the unit basically quit working. The front panel mounted displays began to fade out and some of the C-Band laser pump diodes began to fail. In order to work around this problem, Ophir utilized a heating blanket wrapped around the unit both on the ground and in the air. Still, some of the wavelength instability problems seen in the signal and ratio data may have been a result of being on the performance edge of the amplifier.

A second problem with the amplifier centered on the output power drift. The amplifier specifications were originally set to allow only 5% output power drift. The manufacturer asked for and was granted a larger output drift specification of 10% towards the end of the design effort. Actual performance of the amplifier showed a drift of a couple of dBs or 30-40 %. The source of the problem dealt with the polarization dependence of the non-linear fiber. The varying input polarization of the light into the non-linear stage produced a widely changing power output. The manufacturer tried to correct this problem by adding a polarization adjuster onto the output stage of the L-Band amplifier. This did allow the operator to maximize the power output by changing the input polarization, but the power drift was still present. While the power drift was readily apparent in the raw signal plots, it was reasoned that the ratio data would be independent of the source output power. Late in the project, the vendor replaced the non-linear fiber with new supposedly polarization independent fiber, but achieved only mediocre results. In future amplifier designs, the power drift will be corrected through the use of improved polarization independent non-linear fiber.

4.2 Gas/Blank Ratio Excursions from Baseline Level Resulting in False Alarms

The gas-to-blank ratio excursions along the baseline levels could severely impact the ability of the system to discriminate methane from the background and could produce false alarms within the output data. The in-line optical filter removed all unwanted wavelengths that might change the transmission split ratio through the splitters (the splitters were wavelength dependent). Unfortunately, the split ratio appeared to also change with different types of light sources *i.e.* narrowband versus broadband. In several ratio snapshots, the fiber amplifier was turned off and the background solar light was collected. The calculated ratio for just the background solar light was quite a bit higher (between 0.5 and 1.0) than what was seen with the greater amplifier contribution. Normally the amplifier return dominated the calculated ratio, but it became obvious that in some cases the ratio was significantly impacted by the solar contribution. In several instances, banking the airplane mounted transceiver towards the sun revealed a temporary increase in the calculated ratio. This did not totally explain some of the baseline shifts that were seen in the calculated ratio, especially in the flights performed on February 25th

where the sky was typically clear. The background ratio with constant sun should have yielded a somewhat constant ratio with the exception of areas where methane was present.

The short term spikes above the baseline were not always obvious as to the origin. Some ratio spikes appeared to be correlated in space to certain types of road surfaces such as highly reflective asphalt. Surfaces with highly specular reflections such as metallic surfaces may also have contributed to ratio changes. The light source was focused down to a spot size of approximately 5-7 cm (2-3 in) on the ground surface and the signals were integrated over about 1-m surface, so it was fairly likely that occasional highly reflective surfaces on the order of several feet in diameter could have influenced the calculated ratio. More ratio testing with different types of surfaces, other than dull asphalt, sod and Spectralon, is in order to determine the exact impact on the ratio.

4.3 Gas Correlation Technique versus Differential Absorption Laser Radar (DIAL)

Ophir developed the airborne methane and ethane detector using our patented active gas correlation technique. Gas correlation depends upon comparing the collected detector returns through a known gas sample and a blank sample. Any return deviations due to terrain, atmospheric perturbations, water content will be seen in both channels and will be absent in the calculated ratio. In order to utilize gas correlation, Ophir had to specify a light source that was much more broadband in nature than a typical laser diode source. The spectral width of the light source had to be great enough to detect both on and off band. Typical methane absorption lines are on the order of several hundredths of a nanometer wide, and as a result, a light source of spectral width near 0.1 nm was specified. While this source worked well enough for determining gas correlation ratios, it was less than optimal in the signal-to-noise area. Since part of the energy fell outside the absorption band, the return power to the detectors did not yield maximum detection efficiency. The technique known as differential absorption laser radar (DIAL) is the better method for maximizing the signal-to-noise ratio of the return signal. The light source developed by Ophir had some interesting possibilities for use in a DIAL system. Several out-of-band wavelengths existed at the amplifier output that could or could not be filtered out. With some slight modifications to the optical breadboard and lower frequency modulation of the light source, it would be possible to configure the airborne sensor as a DIAL system. An especially intriguing aspect of the fiber amplifier is that the output wavelengths happen at the same time and can be used simultaneously to detect on and off band detector returns. This will possibly eliminate the problem of time-separated gas sampling commonly associated with most DIAL techniques. Ophir believes that the DIAL technique may aid in the detection of ethane, which has a much smaller absorption line than methane.

4.4 Future Flights over Real Natural Gas Pipelines

Ophir was able to discriminate small methane leaks on the order of 150 scf/h, from the background methane over a simulated natural gas pipeline leak. Larger leaks proved to be impossible to create using gas cylinders obtained locally from gas suppliers. Without

the ability to create larger leaks, Ophir was unable to accurately determine concentration pathlengths of surface methane leaks. In addition, Ophir was unable to determine the impact of increased wind speeds on the methane plume due to the rapid dispersion of the small quantity of released gas. The small quantity of gas available from the cylinders also would have made it next to impossible to detect the presence of ethane. As a result, Ophir hopes to continue testing of the airborne system at a remote site that has the capabilities of releasing large amounts of natural gas. A likely site for these later tests is the Rocky Mountain Oilfield Test Facility (RMOTC) located near Casper, Wyoming; operated by the DOE. Ophir has been in discussion with RMOTC personnel to determine the cost associated with conducting airborne surveys of an existing simulated natural gas pipeline that was created for a previous DOE and DOT-sponsored test.

5 Conclusions

Ophir Corporation has demonstrated the feasibility of using an airborne, optical remote sensor to detect natural gas leaks from simulated leak sources. Highlights of the airborne sensor development and test effort can be summarized as follows:

- An airborne system has been designed and developed that is capable of detecting methane. The light source used in the project has a dual output wavelength, theoretically capable of detecting both methane and ethane gases.
- Methane was detected, using an Ophir-patented approach known as active gas correlation, from an airborne platform flying at an altitude of 150 m (150 ft) and at an air speed of 43 m/s (100 mph) during multiple flight passes over above-ground, point source leaks of 150 scf/h.
- The airborne sensor is capable of flying during daylight and nighttime conditions, and has sufficient signal-to-noise to fly at altitudes of 400 - 1000 ft.
- The optical breadboard used in the airborne platform is made up entirely of fiber optics and fiber optics connected components. Optical alignments problems, commonly associated with optical transmitters and receivers, have been largely eliminated.
- A custom fiber-coupled, high-power (1-Watt output) light source was designed and developed for this project. This light source is capable of performing either gas correlation spectroscopy or active DIAL spectroscopy. Possible light source wavelength output instability has produced some drift in the ratio technique, producing some false positive methane indications.
- The calculated gas-to-blank ratios during the flight surveys occasionally produced spikes in the data, sometimes from methane and sometimes from unknown sources. More work is required to ascertain the impact of all types of surface terrain on the ratio calculation.
- Ophir hopes to continue testing of the airborne system at a remote site that has the capabilities of releasing large amounts of natural gas. A likely site for these later tests is the Rocky Mountain Oilfield Test Facility (RMOTC) located near Casper, Wyoming and operated by the DOE. Ophir has been in discussion with RMOTC personnel to determine the cost associated with conducting airborne surveys of an existing simulated natural gas pipeline that was created for a previous DOE and DOT sponsored test.

6 References

N. Gopalsami, D. B. Kanareykin, V. Asanov, S. Bakhtiari and A. C. Raptis "Microwave Radar Detection of Gas Pipeline Leaks", Energy Technology Division, Argonne National Laboratory, Argonne, Il 60439 and AOZT Finn-Trade, St Petersburg, Russia, 2002

Thomas A. Reichardt, Sanjay Devdas, Thomas J. Kulp, and Wayne Einfeld "Evaluation of Active and Passive Gas Imagers for Transmission Pipeline Remote Leak Detection: Quarterly Report", Sandia National Laboratory, April 2002

7 Attachment 1 – Gas Industry Data Survey Results

Ophir sent the following list of informational questions to WBI Holdings, Inc. in Bismarck, ND and El Paso Pipeline Group in El Paso, TX:

1.) Recently, Ophir took some data with the fence-line monitoring sensor next to a pipeline near Glendive, Montana. Gas distribution company personnel simulated some typical Class 1, 2 and 3 natural gas leaks. Do you have any information on what the Flame Ionization Detector (FID) gas concentration is of these leaks (Class 1, 2 and 3) at the source?

2.) Do you have any data or information illustrating the quantitative impact of wind on pipeline natural gas leak leaks (gas plume movement and concentration)? This will impact the pointing of the airborne optical sensor. Does the sensor need to be scanned over a broad region or can the sensor be pointed in just a single downwind position from the pipeline?

3.) Does the natural gas pipeline industry have any need for detecting gas concentrations smaller than class 1, 2 or 3 leaks?

4.) Do you have any input on the desired aircraft speed or flight altitude? This might depend upon your preferred airborne platform *i.e.* helicopter or small propeller driven airplane.

5.) What kind of ground surface resolution do you require for the location of the natural gas leaks? How would you like these gas leak locations to be specified? We envision the flight path of the air vehicle to be monitored and recorded by saving appropriate GPS coordinates. How about other information that needs to be time tagged to the flight such as time of day, date, known weather conditions, etc.? Ultimately, how would you like the final flight survey to look and what kind of data should it contain?

6.) A related question is how do we determine the location of the pipeline from the air? Are there any visual features that closely identify the pipeline location? This is important since the sensor beam size may be as small as a few feet hitting the ground. Do we know the exact GPS coordinates along the pipeline, so that they could be pre-programmed into the computer? Perhaps a computer display of flight path vs. pipeline location would be useful for both real time and post-flight analysis. Finally, do you think that having a visual recording of the ground terrain would be helpful during the post-processing of the data? Does this add any useful information to the pipeline leak surveys?

7.)   Do you have any input as to the desired size, weight, and cost of the airborne sensor? Would you purchase airborne sensors or would you more likely hire service bureaus to perform the inspections? What target cost per mile for pipeline inspection would the industry support?

8.)   Would you be interested in accessing airborne pipeline leak reports via the Internet? One method of delivering and reporting airborne pipeline surveys would be to download the survey results to a central website. Each customer would have a secure and company-specific series of web pages that show the current survey status (which pipeline sections were surveyed, which were still scheduled for survey, leak detection results, etc.) Would this be beneficial for your company's operations?

9.)   A significant fraction of the U.S. pipeline network is available on Global Positioning System/Geographical Information System (GPS/GIS) databases. Would you be interested in receiving pipeline survey results overlaid on a GPS/GIS map of their pipelines? (This could be provided either via the Internet or on a CD deliverable with the survey final report).

10.) Currently, Ophir plans to provide the measured methane and ethane concentrations along the length of the pipeline section surveyed as the primary data product. These measurements could also be roughly classified as zero, low, medium, and high, providing a general indication of the probability of a leak occurring at a reported location. Is this the best format and method for reporting of the survey data? Is there additional information or an alternate format that your company would prefer?

Table 3 summarizes the responses from these companies to the questionnaire.

Ophir Directed Question	WBI Holdings, Inc. Response	El Paso Pipeline Group Response	Design Impacts for System
Any known gas concentrations of Class 1, 2 and 3 leaks?	Leaks are not classified by concentration but by potential danger	Leaks are not classified by concentrations but by potential danger, detect smallest leak possible	It seems as if Ophir should design system to detect minimal or ambient levels of methane and ethane gases
Are you aware of any wind impact data on natural gas leak dispersion?	WBI has no data on this	They know of no data. Most companies have max. wind speed limits when performing surveys.	No help here in determining the minimal detectable concentration in the presence of wind
Does the natural gas industry have any need for detecting gas leaks smaller than Class 1, 2 or 3?	They would like to know whenever there is a leak of any size	A leak is a leak. They have detected leaks once the pipes are exposed.	Design goals here are to detect at least Class 3 leaks and let companies decide what to do with the data.
Do you have any input on the desired aircraft speed or flight altitude?	Whatever works the best	Best answered by the pilots. Company has flight restrictions on aircraft. Helicopters might disrupt the gas plume.	Design around existing airspace rules and regulations. Helicopter designs need to take into account the rotor downdrafts.
What kind of ground location resolution do you require for the location of natural gas leaks?	No input on resolution. Person will go out to confirm leak and then classify it for potential danger.	Leaks are currently specified by mileposts. Time, date tagging, and weather conditions would be useful. Progressing towards GPS in future.	Design of system around GPS coordinates with location specified as to nearest milepost marker.
How do we determine location of the pipeline for aerial survey? Is visual recording of the pipeline useful?	Some pipelines have visible markers but not all. Pipeline database moving towards GPS. Visual recording would be useful.	Visually locating pipelines is tough. Location in future with GPS is a solution. One solution is to have an employee present with surveyors.	This is going to be a problem since there are no standardized GPS coordinates for most pipelines. Can't see some pipelines visually from air.
Input as to the desired weight, size, and cost of the sensor? Would you purchase a unit or hire out to bureau?	No input on this subject.	Smaller the better. They would hire a service bureau before purchasing the sensor (less capital and maintenance).	Basically, no input on size, weight and cost. They would rather not purchase the sensors.
Would you be interested in accessing the airborne leak reports via the Internet?	Yes	This sounds like a great idea. The data should be at least Internet capable, possibly on CDs.	They like the accessibility of the Internet.
Would you be interested in receiving pipeline survey data overlaid on a GPS/GIS map of their pipelines?	This would be helpful in that we are in the process of inputting data to GIS now.	This might be useful for trend analysis, seasonal leak analysis, verifying fixed leaks.	Everyone seems to like this although the GIS data available on pipelines is minimal.
Do you want classification of leaks? Any additional info required for leak data?	No classification of leaks, they will determine upon site survey the amount and type of leak.	They don't want classification label put on leaks. They would classify by percent gas or ppm.	We would just give them leak in ppm-m.

Table 3. Response to Ophir Corporation Questionnaire Requesting Input on the Design Requirements for an Airborne, Optical Remote Sensor from WBI Holdings, Inc. and El Paso Pipeline Group

8   Attachment 2 – Weather Data for Methane Survey Flight Testing Performed on February 19th and 25th

Table 4. Weather Data for Flight Testing on February 19th

Date	Time	Wind Direction	Wind Speed (MPH)	Temperature	Humidity	Pressure
Sat 19 Feb	11:10:03	20	2.8	42.5	61	25.254
Sat 19 Feb	11:11:03	34	6.5	41.8	62	25.255
Sat 19 Feb	11:12:03	34	5	41.6	62	25.257
Sat 19 Feb	11:13:03	27	4.6	41.5	62	25.257
Sat 19 Feb	11:14:03	18	3.8	42.5	68	25.262
Sat 19 Feb	11:15:03	35	3.6	42.1	62	25.254
Sat 19 Feb	11:16:03	83	4.5	41.9	62	25.25
Sat 19 Feb	11:17:03	41	5.6	42.4	63	25.255
Sat 19 Feb	11:18:03	4	2.8	43.1	64	25.257
Sat 19 Feb	11:19:03	34	6.1	42	63	25.253
Sat 19 Feb	11:20:03	39	6.1	41.9	64	25.252
Sat 19 Feb	11:21:03	34	5	42.6	65	25.255
Sat 19 Feb	11:22:03	11	3.2	42.6	64	25.253
Sat 19 Feb	11:23:03	51	5.6	41.9	64	25.257
Sat 19 Feb	11:24:03	49	4.6	42	64	25.255
Sat 19 Feb	11:25:03	58	4.4	42.2	64	25.255
Sat 19 Feb	11:26:03	42	5.4	42.4	64	25.253
Sat 19 Feb	11:27:03	15	4.4	42.6	64	25.255
Sat 19 Feb	11:28:03	46	4.5	43.1	64	25.252
Sat 19 Feb	11:29:03	24	3.7	42.8	62	25.255
Sat 19 Feb	11:30:03	41	6.1	42.8	62	25.256
Sat 19 Feb	11:31:03	20	6.4	43.3	62	25.253
Sat 19 Feb	11:32:03	21	4.9	43.5	61	25.253
Sat 19 Feb	11:33:03	35	4.3	43.9	61	25.25
Sat 19 Feb	11:34:03	25	6	43.9	60	25.247
Sat 19 Feb	11:35:03	45	5.8	43.5	60	25.249
Sat 19 Feb	11:36:03	14	4.7	44.4	60	25.248
Sat 19 Feb	11:37:03	18	4.6	44.5	58	25.247
Sat 19 Feb	11:38:03	13	4.3	44.5	58	25.249
Sat 19 Feb	11:39:03	18	5.5	44.1	58	25.248
Sat 19 Feb	11:40:03	14	4.2	44.3	58	25.248
Sat 19 Feb	11:41:03	23	5.7	44.7	58	25.25
Sat 19 Feb	11:42:03	6	4.5	44.8	57	25.247
Sat 19 Feb	11:43:03	24	4.5	45.4	58	25.245
Sat 19 Feb	11:44:03	6	5.7	45	56	25.248
Sat 19 Feb	11:45:03	14	5.9	45.1	57	25.246
Sat 19 Feb	11:46:03	15	4.2	45	57	25.245
Sat 19 Feb	11:47:03	15	2.9	45.4	57	25.248
Sat 19 Feb	11:48:03	7	2.7	45.7	57	25.245
Sat 19 Feb	11:49:03	10	4.9	45.7	56	25.246

| Sat 19 Feb | 11:50:03 | 4 | 3.4 | 46.4 | 56 | 25.25 |

Table 5. Weather Data for the Morning Flight on February 25th

Date	Time	Wind Direction	Wind Speed (MPH)	Temperature	Humidity	Pressure
Fri 25 Feb	9:54:57	96	0.6	45.5	35	25.602
Fri 25 Feb	9:55:57	211	0.5	45.7	35	25.602
Fri 25 Feb	9:56:57	225	0.7	45.9	35	25.604
Fri 25 Feb	9:57:57	84	1.2	46.5	35	25.602
Fri 25 Feb	9:58:57	172	0.5	47.1	35	25.603
Fri 25 Feb	9:59:57	179	1	47.2	34	25.603
Fri 25 Feb	10:00:57	165	0.9	47.6	34	25.601
Fri 25 Feb	10:01:57	256	0.6	47.4	34	25.603
Fri 25 Feb	10:02:57	229	0.6	47.5	33	25.602
Fri 25 Feb	10:03:57	228	0.4	47.8	33	25.603
Fri 25 Feb	10:04:57	205	0.7	47.1	33	25.601
Fri 25 Feb	10:05:57	239	2	46.1	33	25.601
Fri 25 Feb	10:06:57	238	1.7	45.5	34	25.604
Fri 25 Feb	10:07:57	302	0.5	46.1	34	25.602
Fri 25 Feb	10:08:57	290	0.8	46.4	34	25.6
Fri 25 Feb	10:09:57	297	1	46.3	33	25.602
Fri 25 Feb	10:10:57	246	0.9	46	33	25.601
Fri 25 Feb	10:11:57	214	2.4	45.5	34	25.603
Fri 25 Feb	10:12:57	226	2.5	45.2	34	25.605
Fri 25 Feb	10:13:57	233	1.6	46.1	35	25.605
Fri 25 Feb	10:14:57	280	2	45.9	35	25.606
Fri 25 Feb	10:15:57	290	2	46.3	34	25.609
Fri 25 Feb	10:16:57	300	0.5	46.6	34	25.605
Fri 25 Feb	10:17:57	291	0.1	46.7	34	25.605
Fri 25 Feb	10:18:57	260	2.3	46.2	34	25.608
Fri 25 Feb	10:19:57	285	2.6	47.4	34	25.606
Fri 25 Feb	10:20:57	336	1.6	47.7	34	25.607
Fri 25 Feb	10:21:57	274	1.1	48	33	25.61
Fri 25 Feb	10:22:57	195	1.7	48.2	32	25.608
Fri 25 Feb	10:23:57	158	0.9	48.4	32	25.61
Fri 25 Feb	10:24:57	80	0.5	48.8	32	25.614
Fri 25 Feb	10:25:57	158	1.4	48.8	32	25.613
Fri 25 Feb	10:26:57	201	3.2	47.5	31	25.613
Fri 25 Feb	10:27:57	239	0.7	47.6	31	25.615
Fri 25 Feb	10:28:57	203	0.9	48.2	31	25.612
Fri 25 Feb	10:29:57	129	0.3	48.9	31	25.615
Fri 25 Feb	10:30:57	215	3.4	49.1	32	25.615
Fri 25 Feb	10:31:57	197	3.3	48.2	30	25.615
Fri 25 Feb	10:32:57	201	2.6	47.9	31	25.615
Fri 25 Feb	10:33:57	184	3.3	48	30	25.618
Fri 25 Feb	10:34:57	184	2.2	48.7	31	25.614
Fri 25 Feb	10:35:57	150	2.9	49.4	30	25.615

Fri 25 Feb	10:36:57	114	2.1	49.4	30	25.618
Fri 25 Feb	10:37:57	108	2.7	48.8	30	25.613
Fri 25 Feb	10:38:57	83	1.7	49.7	31	25.616

Table 6. Weather Data for Afternoon Flight on February 25th

Date	Time	Wind Direction	Wind Speed (MPH)	Temperature	Humidity	Pressure
Fri 25 Feb	14:09:16	113	2.1	58.6	21	25.483
Fri 25 Feb	14:10:16	125	5.1	59	21	25.483
Fri 25 Feb	14:11:16	114	4.1	58.7	21	25.482
Fri 25 Feb	14:12:16	127	7.6	58.8	21	25.487
Fri 25 Feb	14:13:16	122	8.6	58.7	21	25.485
Fri 25 Feb	14:14:16	121	9.8	57.9	21	25.482
Fri 25 Feb	14:15:16	121	6.2	58.2	21	25.484
Fri 25 Feb	14:16:16	118	3.7	58.3	20	25.484
Fri 25 Feb	14:17:16	111	4.1	58.3	21	25.478
Fri 25 Feb	14:18:16	122	5.5	58.4	21	25.477
Fri 25 Feb	14:19:16	113	4.8	57.8	21	25.48
Fri 25 Feb	14:20:16	104	6.8	56.8	21	25.477
Fri 25 Feb	14:21:16	117	4.3	57.6	21	25.475
Fri 25 Feb	14:22:16	155	2.2	57.3	21	25.477
Fri 25 Feb	14:23:16	183	3.1	57	21	25.475
Fri 25 Feb	14:24:16	97	5.4	58	22	25.48
Fri 25 Feb	14:25:16	118	9.7	58.2	22	25.474
Fri 25 Feb	14:26:16	124	6.3	58.1	21	25.477
Fri 25 Feb	14:27:16	121	4.5	58.6	21	25.476
Fri 25 Feb	14:28:16	124	4.1	58.6	21	25.473
Fri 25 Feb	14:29:16	135	3.9	57.5	21	25.472
Fri 25 Feb	14:30:16	76	3.8	57.9	21	25.474
Fri 25 Feb	14:32:47	131	3.1	58	21	25.471
Fri 25 Feb	14:33:47	162	2.6	58.5	21	25.473
Fri 25 Feb	14:34:47	113	2.7	58.8	22	25.477
Fri 25 Feb	14:35:47	105	5.2	59.4	21	25.475
Fri 25 Feb	14:36:47	134	5.2	59.7	21	25.475
Fri 25 Feb	14:37:47	117	4.8	59	21	25.472
Fri 25 Feb	14:38:47	93	9	57.4	21	25.475
Fri 25 Feb	14:39:47	53	6.8	56.2	21	25.472
Fri 25 Feb	14:40:47	56	6.9	55.8	22	25.471
Fri 25 Feb	14:41:47	108	8.6	57.4	23	25.472
Fri 25 Feb	14:42:47	136	7.5	58.4	22	25.476
Fri 25 Feb	14:43:47	125	8.1	58.8	22	25.475
Fri 25 Feb	14:44:47	129	9	58.8	21	25.473
Fri 25 Feb	14:45:47	134	8.1	58.9	21	25.475
Fri 25 Feb	14:46:47	136	6	59	21	25.472
Fri 25 Feb	14:47:47	136	6.9	58.9	20	25.472
Fri 25 Feb	14:48:47	122	6.1	58.6	21	25.472
Fri 25 Feb	14:49:47	100	6.4	57.2	21	25.474
Fri 25 Feb	14:50:47	80	4.9	57.4	21	25.472
Fri 25 Feb	14:51:47	121	3.6	58.5	22	25.468

This page is intentionally left blank.